

7-1-2000

Results of Field Instrumentation and Testing of the Newark Monorail Guideway Structure

Robert J. Connor

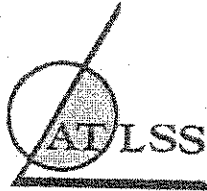
Frank E. Stokes

Follow this and additional works at: <http://preserve.lehigh.edu/engr-civil-environmental-atlss-reports>

Recommended Citation

Connor, Robert J. and Stokes, Frank E., "Results of Field Instrumentation and Testing of the Newark Monorail Guideway Structure" (2000). ATLSS Reports. ATLSS report number 00-06.
<http://preserve.lehigh.edu/engr-civil-environmental-atlss-reports/6>

This Technical Report is brought to you for free and open access by the Civil and Environmental Engineering at Lehigh Preserve. It has been accepted for inclusion in ATLSS Reports by an authorized administrator of Lehigh Preserve. For more information, please contact preserve@lehigh.edu.



LEHIGH
University

**Results of
Field Instrumentation and Testing
of the
Newark Monorail Guideway Structure
Final Report**

By

Robert J. Connor

Frank E. Stokes

ATLSS Report No. 00-06

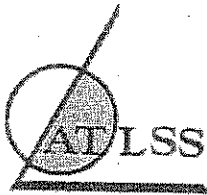
Prepared for:
Adtranz NA - Newark, NJ
July 2000

**ATLSS is a National Center for Engineering Research
on Advanced Technology for Large Structural Systems**

117 ATLSS Drive
Bethlehem, PA 18015

Phone: (610)758-3525
Fax (610)758-5902

www.lehigh.edu/~inatl/default.htm
Email: inatl@lehigh.edu



LEHIGH
University

Results of Field Instrumentation and Testing of the Newark Monorail Guideway Structure

Final Report

By

Robert J. Connor
Research Engineer

Frank E. Stokes
Manager
ATLSS Structural Testing Laboratory

ATLSS Report No. 00-06

Prepared for:
Adtranz NA - Newark, NJ
July 2000

**ATLSS is a National Center for Engineering Research
on Advanced Technology for Large Structural Systems**

117 ATLSS Drive
Bethlehem, PA 18015

Phone: (610)758-3525
Fax (610)758-5902

www.lehigh.edu/~inatl/default.htm
Email: inatl@lehigh.edu

TABLE OF CONTENTS

	<i>Page</i>
EXECUTIVE SUMMARY	1
1. INTRODUCTION	2
2. TEST PROGRAM	3
2.1. <i>Controlled Load Tests</i>	3
2.1.1. <i>Crawl Tests</i>	3
2.1.2. <i>Dynamic Tests</i>	5
2.1.3. <i>Test Train for Controlled Load Tests</i>	6
2.2. <i>Uncontrolled Monitoring</i>	7
2.2.1. <i>Time Histories</i>	7
2.2.2. <i>Stress-Range Histograms</i>	7
2.2.3. <i>Triggered Time Histories</i>	8
3. INSTRUMENTATION PLAN AND DATA ACQUISITION SYSTEM	9
3.1. <i>Instrumentation Plan</i>	9
3.1.1. <i>Sensors and Signal Wire</i>	18
3.2. <i>Data Acquisition System</i>	20
4. RESULTS OF CONTROLLED LOAD TESTS	22
4.1. <i>Column 07 – Air Side Girders 209/211</i>	22
4.1.1. <i>Crawl and Dynamic Tests</i>	22
4.1.2. <i>Calculation of Forces</i>	28
4.2. <i>Column DLT-10 – Land Side Girders 218/220</i>	32
4.2.1. <i>Crawl and Dynamic Tests</i>	32
4.2.2. <i>Calculation of Forces</i>	35
4.3. <i>Column 12 – Air Side Girders 225/227</i>	37
4.3.1. <i>Crawl and Dynamic Tests</i>	37
4.3.2. <i>Calculation of Forces</i>	40
4.4. <i>Column 16 – Land Side Girders 234/236</i>	44
4.4.1. <i>Crawl and Dynamic Tests</i>	44
4.4.2. <i>Calculation of Forces</i>	46
4.5. <i>Column 26 – Land Side Girders 148/150</i>	48
4.5.1. <i>Crawl and Dynamic Tests</i>	48
4.5.2. <i>Calculation of Forces</i>	50
4.5.3. <i>Tri-axial Rosettes</i>	53

4.6. <i>Span 148 – Land Side Girder</i>	56
4.6.1. <i>Crawl and Dynamic Tests</i>	56
4.6.2. <i>Calculation of Forces</i>	59
4.6.3. <i>Tri-axial Rosettes</i>	61
5. RESULTS OF UNCONTROLLED MONITORING	64
5.1. <i>Results of 24 Hour Monitoring at Column 07</i>	64
5.2. <i>Results of 24 Hour Monitoring at Column DLT-10</i>	66
5.3. <i>Results of 24 Hour Monitoring at Column 12</i>	68
5.4. <i>Results of 24 Hour Monitoring at Column 16</i>	69
5.5. <i>Results of 24 Hour Monitoring at Column 26</i>	70
5.6. <i>Results of Week-Long Monitoring at Span 148 Mid-Span</i>	72
6. VARIABILITY IN MEASUREMENTS AND DEVELOPMENT OF STRESS-RANGE HISTOGRAMS	74
6.1. <i>Variability in Strain Gage Measurements</i>	74
6.2. <i>Development of the Stress-Range Histograms</i>	74
7. SUMMARY OF FIELD MEASUREMENTS MADE ON THE GUIDEWAY	76
REFERENCES	78
ACKNOWLEDGEMENTS	79

Executive Summary

Controlled load testing and uncontrolled monitoring were conducted at selected locations on the Newark Airport Mono Rail Guideway structure. Strain gages were installed on the edges of the box girder flanges at six different locations on the system. All instrumentation and testing was conducted between August and October of 1999 by personnel from Lehigh University's Center for Advanced Technology for Large Structural Systems (ATLSS) located in Bethlehem, PA.

The results of the measurements indicate the following:

1. Overall, the global behavior of the structure is as expected and no unusual behavior was observed during the controlled tests or uncontrolled monitoring.
2. Each train produces one dominant stress-range cycle in the box girder at the areas of instrumentation.
3. The maximum stress range observed during the "uncontrolled" or in-service monitoring was 6.5ksi at column 26 at a gage installed on the top flange.
4. It was shown that the individual wheels of the train apply concentrated loads to the top flange through the running plate/support bar assembly. Local bending of the top flange was observed at every location where instrumentation was installed. The individual wheels of trains each produce sub cycles of up to 1.3ksi in the top flange.
5. Tests were conducted at crawl and normal operating speed at all locations. Comparison of the crawl and dynamic test data revealed dynamic effects are not significant.
6. The measurements did not reveal any change in behavior with change in travel direction.
7. As the train travels around a curve, an overturning moment due to centrifugal forces is developed. This results in both increases and decreases in the vertical load applied by the wheels located on the outside and inside of the curve, respectively.
8. Stress-range histograms were developed at selected gages of the instrumented sections. The effective stress range and corresponding number of cycles per day were calculated.

It is important to note that the measurements are only representative of the immediate areas where strain gages were installed. Stress ranges could be higher or lower at other positions along the girder. Therefore, in order to more fully understand and characterize the behavior of the system, these measurements should be used to calibrate a detailed analytical model of selected portions of the guideway.

1.0 Introduction

This report discusses and summarizes the results of field testing performed on portions of the Newark Airport monorail structure. Approximately 18 months after being placed into service, cracks were reported at splices in the support bars, which are attached to the top flange of the box girder by fillet welds. At several locations these cracks have propagated into the top flange of the box girder through the fillet welds.

The structure consists of curved and straight continuous multi-span steel box girders. In-service stresses are not easily calculated due to the complex geometry of the girders. In addition, the extent to which the support bars and running plate participate in the overall behavior of the box girder is not clear or easily modeled. As a result, a comprehensive instrumentation and testing program was undertaken. Specifically, instrumentation was installed at several different locations in order to 1) develop stress-range histograms under normal or "uncontrolled" operating conditions; 2) collect data using a test train of known load and geometry to calibrate structural analysis models; 3) establish proportions of vertical bending, lateral bending, warping and axial stresses.

All field work was conducted August through October of 1999 by personnel from Lehigh University's Center for Advanced Technology for Large Structural Systems (ATLSS) located in Bethlehem, PA.

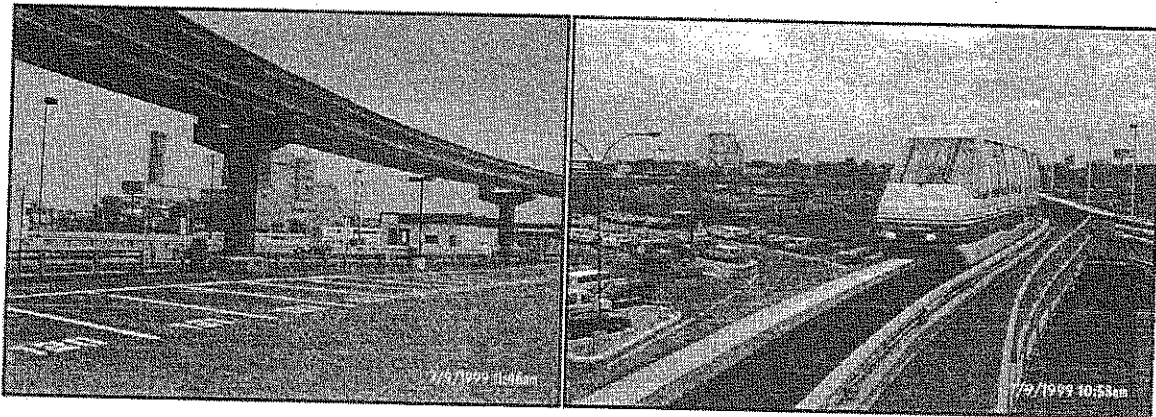


Figure 1 – Photographs Showing Typical Elevated Monorail Structure and Monorail Passenger Vehicle

2.0 Test Program

The test program included controlled and uncontrolled load tests. The controlled load tests utilized a standard, unloaded vehicle that traveled across the instrumented portion of the structure at predetermined speeds. During these tests, time history data were collected from all gages. Uncontrolled load tests involved collecting time history data and development of stress-range histograms during the passage of *random* trains as well as monitoring selected gages for extended periods.

2.1 Controlled Load Tests

2.1.1 Crawl Tests

A series of crawl tests were conducted at each location to establish the behavior of the structure to pseudo static loads. These tests are summarized in Table 2.1. During these tests, the test train traveled over the instrumented area at a crawl speed of about 4.5mph. Since there are no dynamic effects at this speed, these tests are useful for comparison and calibration to structural analysis models developed by others.

Several instrumented areas were located on horizontally curved portions of the guideway. As the vehicle travels on the box girder around these curves, centrifugal and other dynamic forces are produced in the box girder. These effects can be determined by comparing the results of the crawl tests to measurements made during the dynamic tests and normal operating conditions.

Each of the controlled-load crawl tests were repeated a minimum of three times. Data were collected as the train passed in both directions. However, the train traveled in the typical travel direction for a minimum of two crawl tests.

Test	Travel Direction	Girder	Speed (mph)	Comments
Column 26 and Midspan Girder 148 – Land Side				
CRWL26_1.dat	Southbound	Land Side	4.5	-
CRWL26_2.dat	Southbound	Land Side	4.5	-
CRWL26_3.dat	Northbound	Land Side	4.5	-
CRWL26_4.dat	Southbound	Land Side	4.5	Shuttle ¹ passed the test train on the air side girder headed south at the normal travel speed.
Column 16 - Land Side				
CRWL16_1.dat	Southbound	Land Side	4.5	Shuttle ¹ passed just ahead of the test train on the airside girder at the normal travel speed.
CRWL16_2.dat	Northbound	Land Side	4.5	Shuttle ¹ passed just after the test train on the air side girder at the normal travel speed.
CRWL16_3.dat	Southbound	Land Side	4.5	-
Column 12 - Air Side				
CRWL12_1.dat	Northbound	Air Side	4.5	-
CRWL12_2.dat	Southbound	Air Side	4.5	-
CRWL12_3.dat	Northbound	Air Side	4.5	-
CRWL12_4.dat	Southbound	Air Side	4.5	-
Column DLT 10 – Land Side				
CRL10_2.dat	Southbound	Land Side	4.5	-
CRL10_3.dat	Northbound	Land Side	4.5	-
CRL10_4.dat	Southbound	Land Side	4.5	Shuttle ¹ passed the test train on the air side girder headed south at the normal travel speed.
CRL10_5.dat	Northbound	Land Side	4.5	-
Column 07 - Air Side				
CRL07_1B.dat	Northbound	Air Side	4.5	-
CRL07_2B.dat	Southbound	Air Side	4.5	-
CRL07_3B.dat	Northbound	Air Side	4.5	-

Notes:

1. "Shuttle" refers to normal trains which are used during reduced operations in the late evening hours. The shuttle travels from one end of the system to the other, then returns on the same side of the guideway. The shuttle operated on girder which was not being tested on the given day.

Table 2.1 – Summary of controlled crawl tests using test train

2.1.2 Dynamic Tests

A series of dynamic tests were conducted at two different speeds. These tests are summarized in Table 2.2. At several locations, the test train traveled at an intermediate speed equivalent to 60% of the normal operating speed. The speed of the train was then increased to the "full" or "normal" travel speed for that section of the monorail track. At least three dynamic tests were conducted at each location as noted in Table 2.2. Data were collected for a minimum of two tests with the train headed in the typical travel direction and one test with the train reversed except at column DLT 10 land side. Controlled dynamic load tests were not performed at Column 26 and Midspan Girder 148 – Land Side due to lockout arrangements. Some baseline data was acquired for empty trains monitored under normal operating conditions. The sampling rate for all dynamic tests was 200Hz.

Test	Travel Direction	Girder	Speed (mph)	Comments
Column 26 and Midspan Girder 148 – Land Side				
Column 16 - Land Side				
INT16 1.dat	Southbound	Land Side	-	60% of normal operating speed
INT16 2.dat	Northbound	Land Side	-	60% normal of operating speed
INT16 3.dat	Southbound	Land Side	-	60% normal of operating speed
FULL16 1.dat	Northbound	Land Side		Normal operating speed
FULL16 2.dat	Southbound	Land Side		Normal operating speed
FULL16 3.dat	Northbound	Land Side		Normal operating speed
FULL16 4.dat	Southbound	Land Side		Normal operating speed
FULL16 5.dat	Northbound	Land Side		80% Normal operating speed
Column 12 - Air Side				
INT12 1.dat	Northbound	Air Side		60% of normal operating speed
INT12 2.dat	Southbound	Air Side		60% normal of operating speed
FULL12 1.dat	Northbound	Air Side		Normal operating speed
FULL12 2.dat	Southbound	Air Side		Normal operating speed
FULL12 3.dat	Northbound	Air Side		Normal operating speed
FULL12 4.dat	Southbound	Air Side		Normal operating speed
Column DLT 10 – Land Side				
FULL10 1.dat	Southbound	Land Side		Normal operating speed
FULL10 2.dat	Southbound	Land Side		Normal operating speed
Column 07 - Air Side				
INT07 1B.dat	Northbound	Air Side		60% of normal operating speed
INT07 2B.dat	Southbound	Air Side		60% normal of operating speed
INT07 3B.dat	Northbound	Air Side		60% normal of operating speed
INT07 4B.dat	Southbound	Air Side		60% normal of operating speed
FUL07 1B.dat	Northbound	Air Side		Normal operating speed
FUL07 2B.dat	Southbound	Air Side		Normal operating speed
FUL07 3B.dat	Northbound	Air Side		Normal operating speed

Table 2.2 – Summary of controlled dynamic tests using test train

2.1.3 Test Train for Controlled Load Tests

Table 2.3 summarizes the overall geometry and individual axle loads of the test train assumed for design. The geometry and the loads were taken directly from the *Newark Airport NEC Monorail Extension Design Criteria* design specifications. The actual axle loads and geometry of the test train were not measured.

Since the vehicle was empty during the controlled tests, it most closely resembles the AW-0 load case. The other two load cases, AW-1 and AW-2 are based on the above specification and are provided for information only. These load cases correspond to half and fully loaded conditions, respectively.

Train Designation	A (kips)	B (kips)	C (kips)	D (kips)	E (kips)	F (kips)	G (kips)	Total Load (kips)
AW-0 ¹	8.8	10.5	9.7	9.7	9.7	9.9	8.1	66.4 ¹
AW-1	10.5	12.5	11.5	11.5	11.5	11.7	9.4	78.6
AW-2	12.8	15.2	14.0	14.0	14.0	14.3	11.8	96.1

Notes:

¹ This load case most closely resembles the weight of the empty test train.

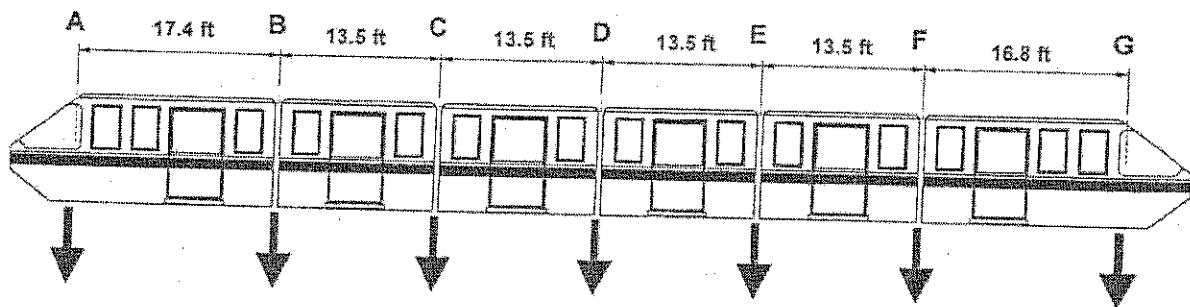


Table 2.3 - Individual Axle Loads of Trains

2.2 Uncontrolled Monitoring

Two types of data were collected during this phase of the testing program. Time history data were collected for several random trains, on each girder, for all gages. In addition, triggered time histories and stress-range histograms were developed for the gages located on the edges of the box girder flanges. The uncontrolled monitoring program is summarized in Table 2.4. The sampling rate was 200Hz during the uncontrolled monitoring.

Data were collected for a minimum of 24 hours at all locations except at columns 26 and midspan of span 148. Data were collected for one week at these two locations only.

2.2.1 Time Histories

Time history data were collected during the passage of several random trains. In some cases, the number of passengers was estimated or counted by visual inspection as the trains passed. Data were recorded for trains passing on either guideway.

2.2.2 Stress-Range Histograms

Stress-range histograms were developed concurrently, but independently of the triggered time histories, using the rainflow cycle counting method. The stress-range histograms were generated continuously and did not operate on triggers, thus all cycles were counted. Stress-range bins were divided into 0.5ksi intervals and stress cycles less than 0.2ksi were ignored. The stress-range bins were updated every 10 minutes.

Location/Girder	Channels Monitored for Time Histories and Stress-Range Histograms	Dates of Monitoring
Column 26 and Midspan Girder 148 Land Side	4 Gages on Edges of Top and Bottom Flanges at Both Locations	12:00AM 9/27/99 to 10:20AM 10/3/99
Column 16 Land Side	4 Gages on Edges of Top and Bottom Flanges	5:55AM 9/6/99 to 6:05AM 9/7/99 ¹
Column 12 Air Side	2 Gages on Edges of Top Flange	12AM 10/18/99 to 12:00 AM 10/19/99
Column DLT 10 Land Side	2 Gages on Edges of Top Flange	12AM 10/18/99 to 12:00 AM 10/19/99
Column 07 Air Side	4 Gages on Edges of Top and Bottom Flanges	12:00AM 9/27/99 to 12:00PM 9/27/99

Notes:

1. 24 hour monitoring occurred on Tuesday, September 7 due to Labor Day Holiday. According to the Port Authority, ridership was the same as a typical Monday.

Table 2.4 – Summary of Data Collected During the Uncontrolled Monitoring Program

2.2.3 Triggered Time Histories

During both the 24 hour and one week monitoring periods, triggered time histories were recorded when the stresses induced by live loads exceeded predetermined levels or triggers. As illustrated in Figure 2.1, the predetermined threshold stress levels had to be exceeded for a gage on the top flange *and* a gage on the bottom flange for the event to be recorded. For the event shown in Figure 2.1, the triggers were set at ± 1 ksi. In order to capture the entire event, data were recorded prior to the trigger event for a specified interval. In Figure 2.1, this time was set to 8 seconds, (i.e., an 8 second buffer was maintained). The data acquisition system recorded for 12 additional seconds and then stopped only if the triggers were no longer satisfied.

All gages were automatically re-zeroed on the whole and half hour using a digital balance algorithm. The appropriate intervals for the pre- and post-triggers and the trigger threshold stress magnitudes were based on the controlled load test data at each location. Thus, recording times and threshold stresses are not the same for all locations. Data sampling rates were 200Hz.

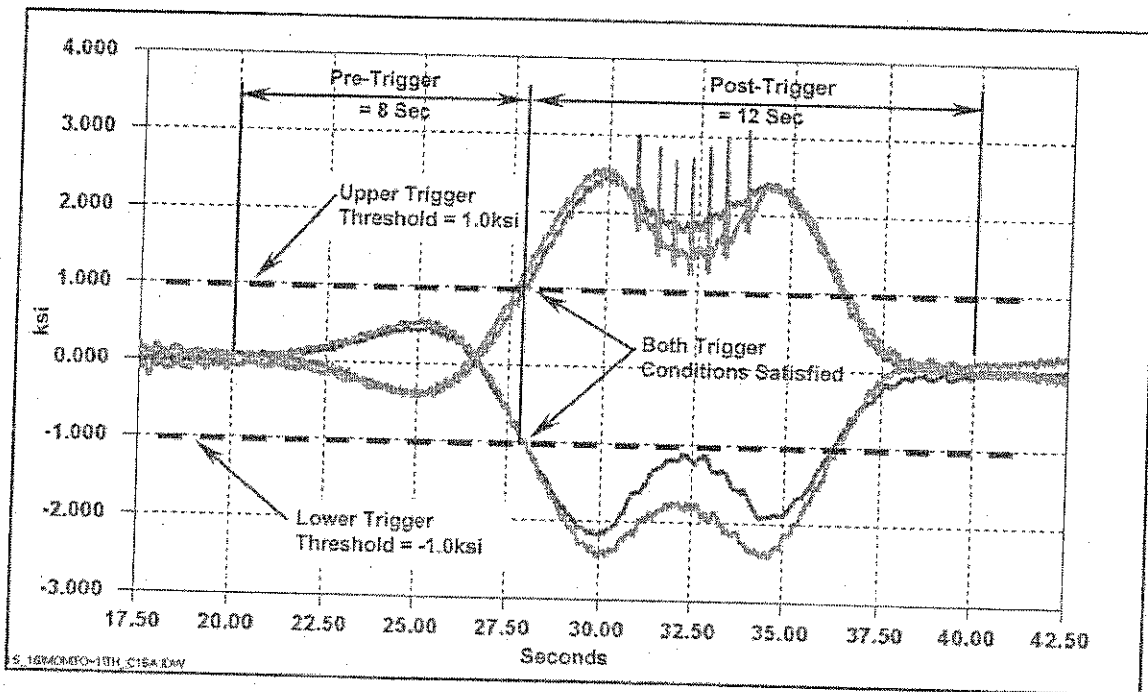


Figure 2.1 – Details of Typical Triggered Time History
(Data from Column 16)

3.0 Instrumentation Plan and Data Acquisition System

3.1 Instrumentation Plan

Uniaxial, weldable strain gages were installed on the edges of the top and bottom flanges, at the middle of the edge at all locations. Figure 3.1 is a photograph of a typical uniaxial strain gage installed on the edge of a bottom flange. Bondable triaxial rosettes were installed on the top flange at the midspan of Span 148 and near Column 26.

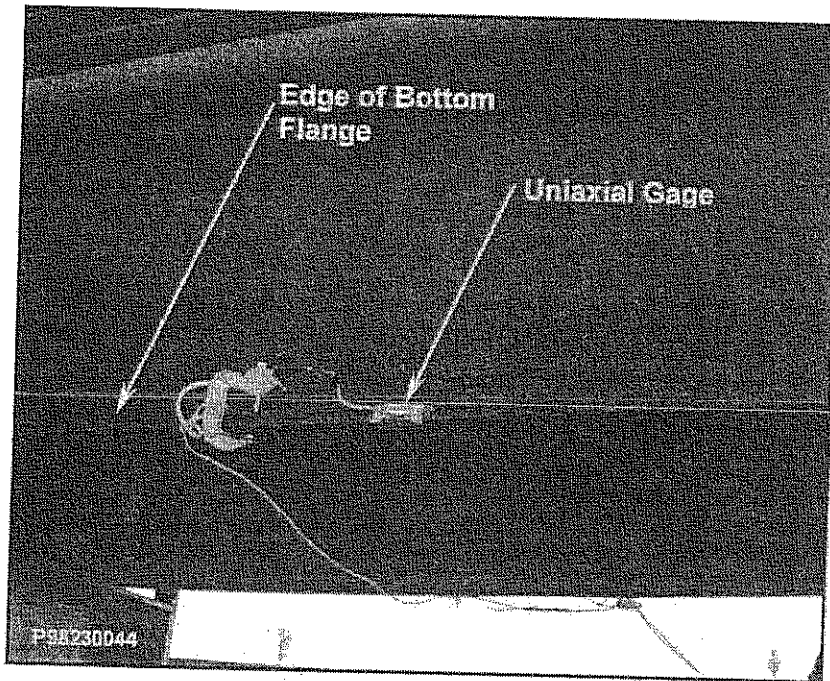


Figure 3.1 – Typical Uniaxial Strain Gage Installed on the Edge of a Flange
(Bottom Flange Shown, Top Flange Similar)

The locations of the strain gages are shown schematically in Figures 3.2 through 3.7 and summarized in Table 3.1. Figure 3.8 is plan view of the instrumented sections of the guideway. The label for each gage corresponds to the location of the gage. For example, channel DLT10_BFLS is located at column DLT 10 on the Bottom Flange on the Land Side girder. All gages are named in a similar format.

Gages located in the negative moment regions, adjacent to the columns, were positioned a minimum of one girder depth away from the centerline of bearing. This was done to avoid possible local effects, due to shear lag or bearing stresses and to avoid any physical conflicts with the bearings. The stress flow directly over a support is quite complex and would be difficult to interpret with the limited number of gages installed. In addition, the desired information could potentially be biased by these effects. The offset from centerline of bearing is shown in Figures 3.2 through 3.7.

Wire #	Channel Name	Location of Gages	Fig. #	Comments
1	C26_BFLS	B.F. Near Column 26 Land Side	3.7	1 Uniaxial Gage
2	C26_BFAS	B.F. Near Column 26 Air Side	3.7	1 Uniaxial Gage
3	C26_RLS 1	T.F. Near Column 26 Land Side	3.7	1 Rosette
4	C26_RLS 2	T.F. Near Column 26 Land Side	3.7	
5	C26_RLS 3	T.F. Near Column 26 Land Side	3.7	
6	C26_RAS 1	T.F. Near Column 26 Air Side	3.7	1 Rosette
7	C26_RAS 2	T.F. Near Column 26 Air Side	3.7	
8	C26_RAS 3	T.F. Near Column 26 Air Side	3.7	
9	C26_TFLS	T.F. Near Column 26 Land Side	3.7	1 Uniaxial Gage
10	C26_TFAS	T.F. Near Column 26 Air Side	3.7	1 Uniaxial Gage
11	S148_BFLS	B.F. Mid Span 148 Land Side	3.6	1 Uniaxial Gage
12	S148_BFAS	B.F. Mid Span 148 Air Side	3.6	1 Uniaxial Gage
13	S148_RLS 1	T.F. Mid Span 148 Land Side	3.6	1 Rosette
14	S148_RLS 2	T.F. Mid Span 148 Land Side	3.6	
15	S148_RLS 3	T.F. Mid Span 148 Land Side	3.6	
16	S148_RAS 1	T.F. Mid Span 148 Air Side	3.6	1 Rosette
17	S148_RAS 2	T.F. Mid Span 148 Air Side	3.6	
18	S148_RAS 3	T.F. Mid Span 148 Air Side	3.6	
19	S148_TFLS	T.F. Mid Span 148 Land Side	3.6	1 Uniaxial Gage
20	S148_TFAS	T.F. Mid Span 148 Air Side	3.6	1 Uniaxial Gage
21	C16_BFLS	B.F. Near Column 16 Land Side	3.5	1 Uniaxial Gage
22	C16_BFAS	B.F. Near Column 16 Air Side	3.5	1 Uniaxial Gage
23	C16_TFLS	T.F. Near Column 16 Land Side	3.5	1 Uniaxial Gage
24	C16_TFAS	T.F. Near Column 16 Air Side	3.5	1 Uniaxial Gage
25	C12_BFLS	B.F. Near Column 12 Land Side	3.4	1 Uniaxial Gage
26	C12_BFAS	B.F. Near Column 12 Air Side	3.4	1 Uniaxial Gage
27	C12_TFLS	T.F. Near Column 12 Land Side	3.4	1 Uniaxial Gage
28	C12_TFAS	T.F. Near Column 12 Air Side	3.4	1 Uniaxial Gage
29	DLT10_BFLS	B.F. Near Column DLT10 Land Side	3.3	1 Uniaxial Gage
30	DLT10_BFAS	B.F. Near Column DLT10 Air Side	3.3	1 Uniaxial Gage
31	DLT10_TFLS	T.F. Near Column DLT10 Land Side	3.3	1 Uniaxial Gage
32	DLT10_TFAS	T.F. Near Column DLT10 Air Side	3.3	1 Uniaxial Gage
33	C07_BFLS	B.F. Near Column 07 Land Side	3.2	1 Uniaxial Gage
34	C07_BFAS	B.F. Near Column 07 Air Side	3.2	1 Uniaxial Gage
35	C07_TFLS	T.F. Near Column 07 Land Side	3.2	1 Uniaxial Gage
36	C07_TFAS	T.F. Near Column 07 Air Side	3.2	1 Uniaxial Gage

Gage Name Key

C26_BFAS "C26" = Column or Span #
"BF" = Bottom Flange, "TF" = Top Flange
"AS" = Air Side, "LS" = Land Side

Table 3.1 – Summary of Strain Gage Locations

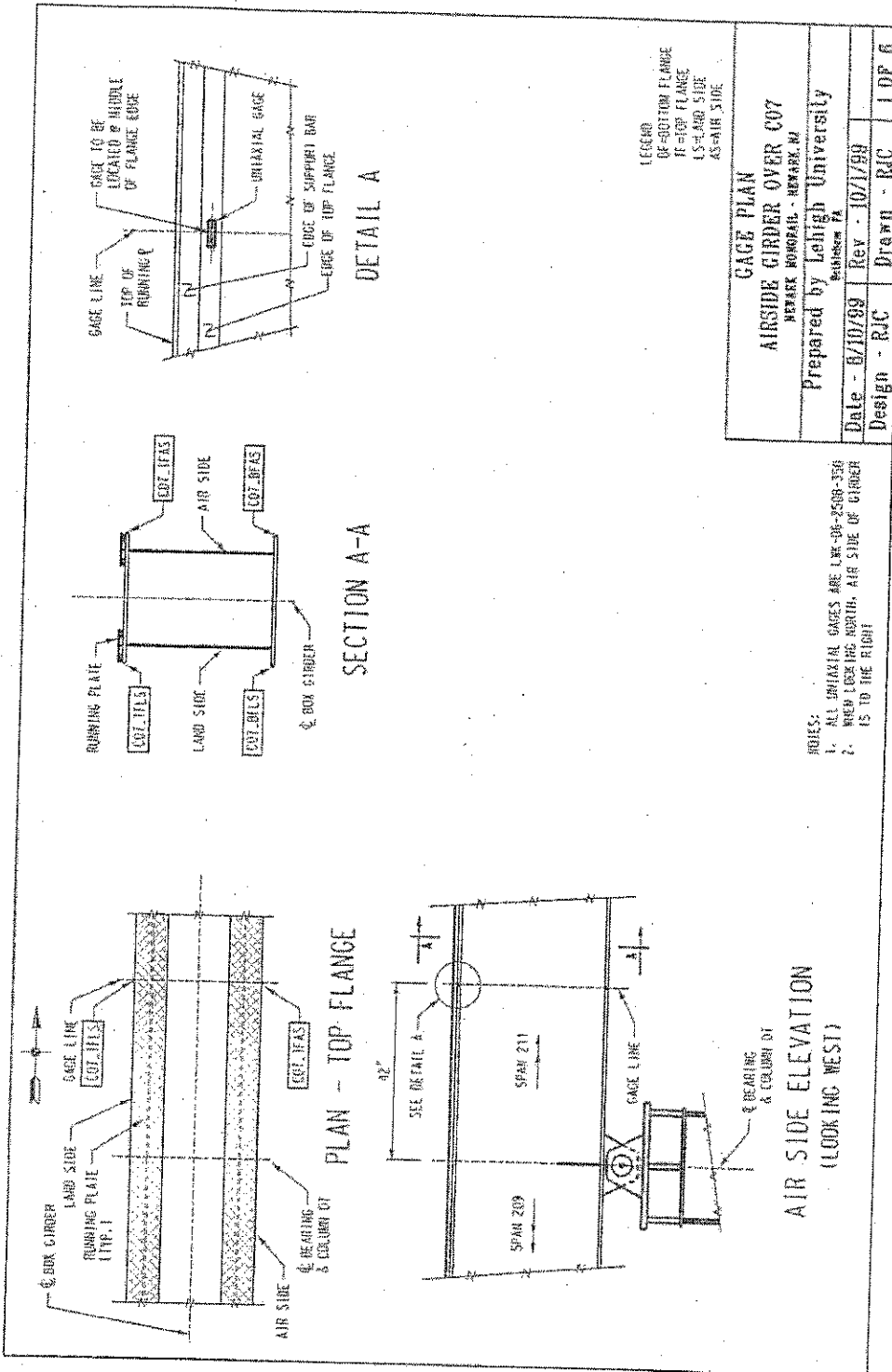


Figure 3.2 - Strain Gage Layout Adjacent to Column 07 - Air Side

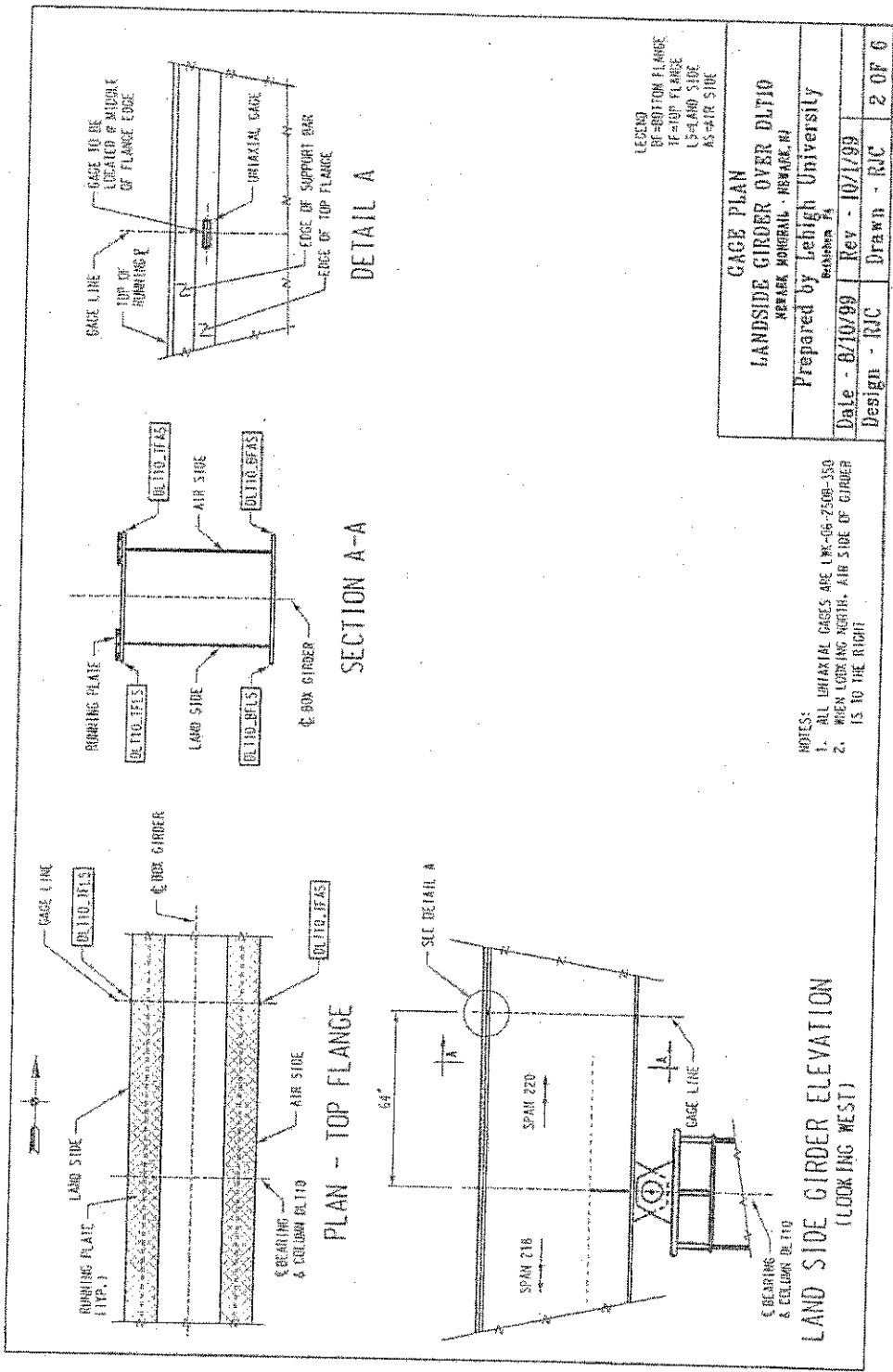


Figure 3.3 – Strain Gage Layout Adjacent to Column DLT-10 – Land Side

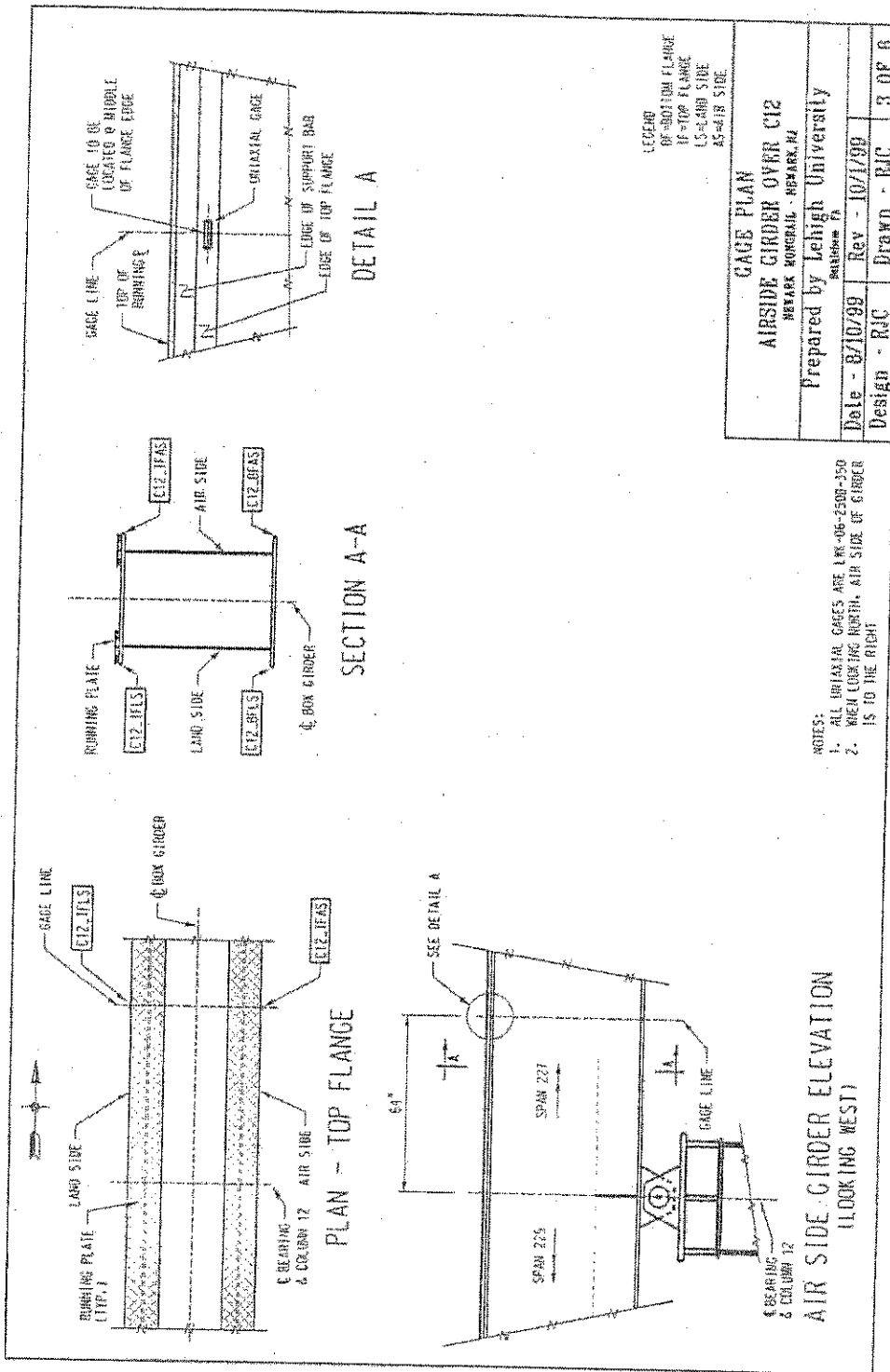


Figure 3.4 – Strain Gage Layout Adjacent to Column 12 – Air Side

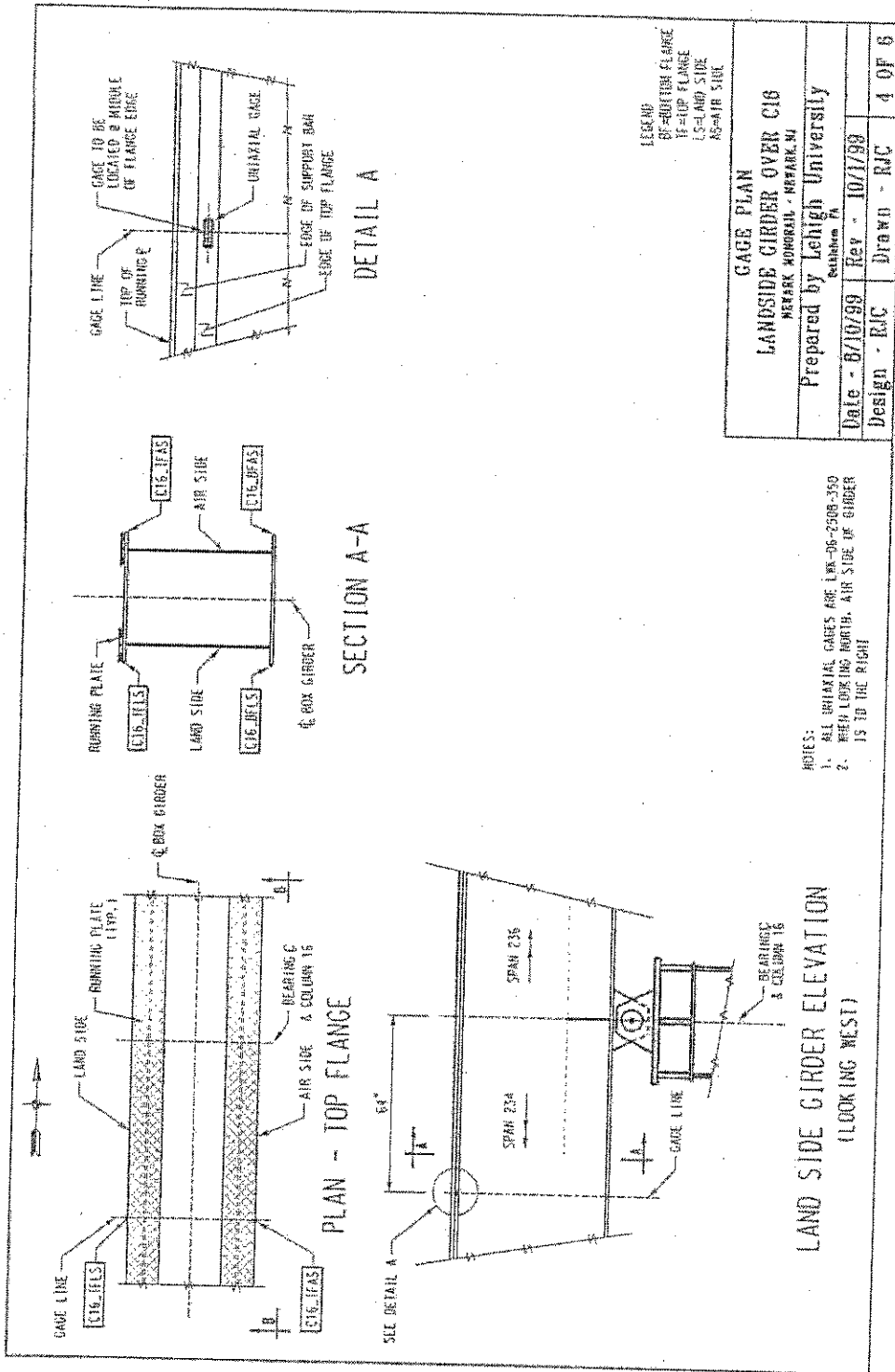


Figure 3.5 – Strain Gage Layout Adjacent to Column 16 – Land Side

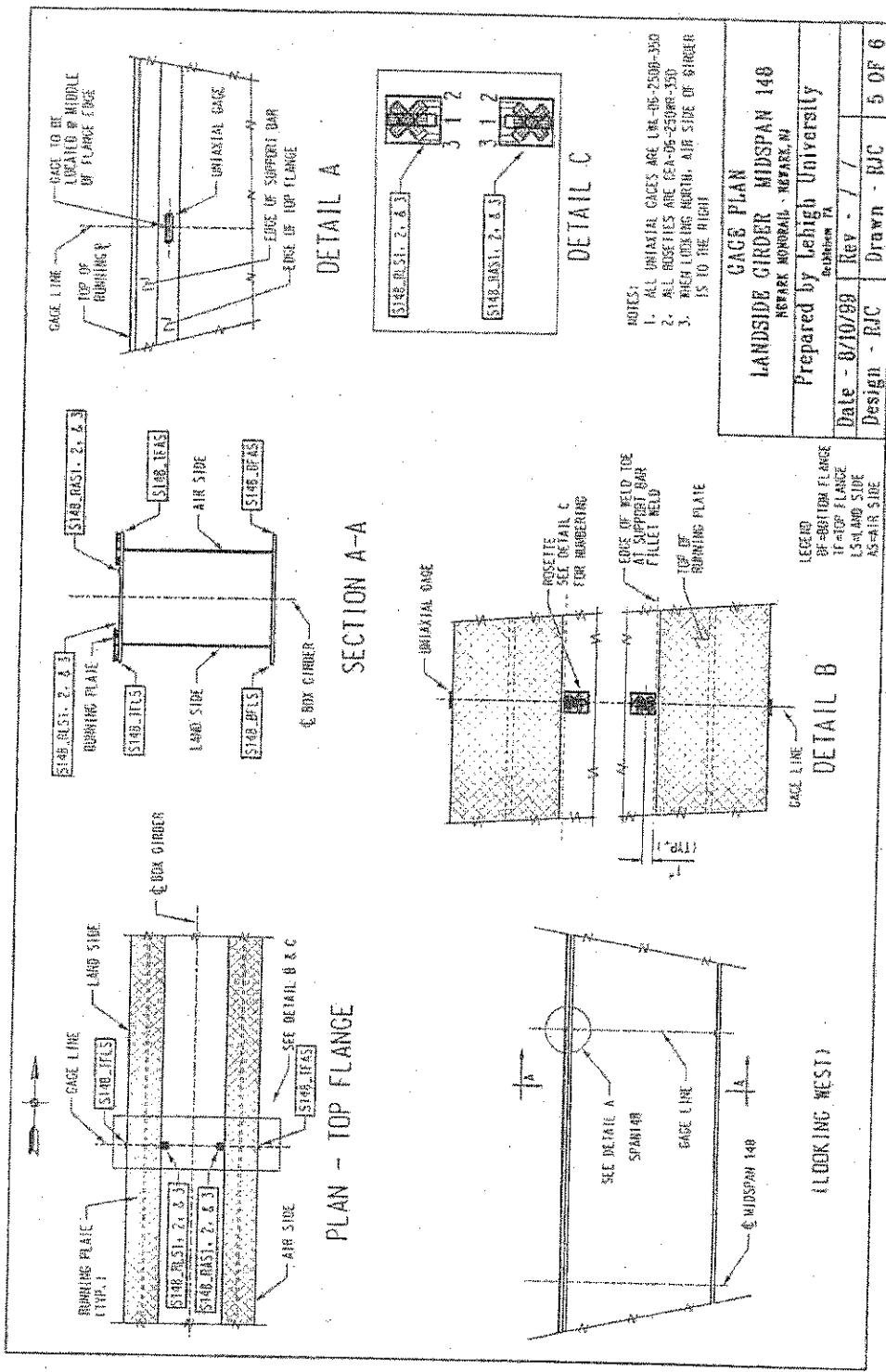


Figure 3.6 – Strain Gage Layout at Midspan Span 148 – Land Side

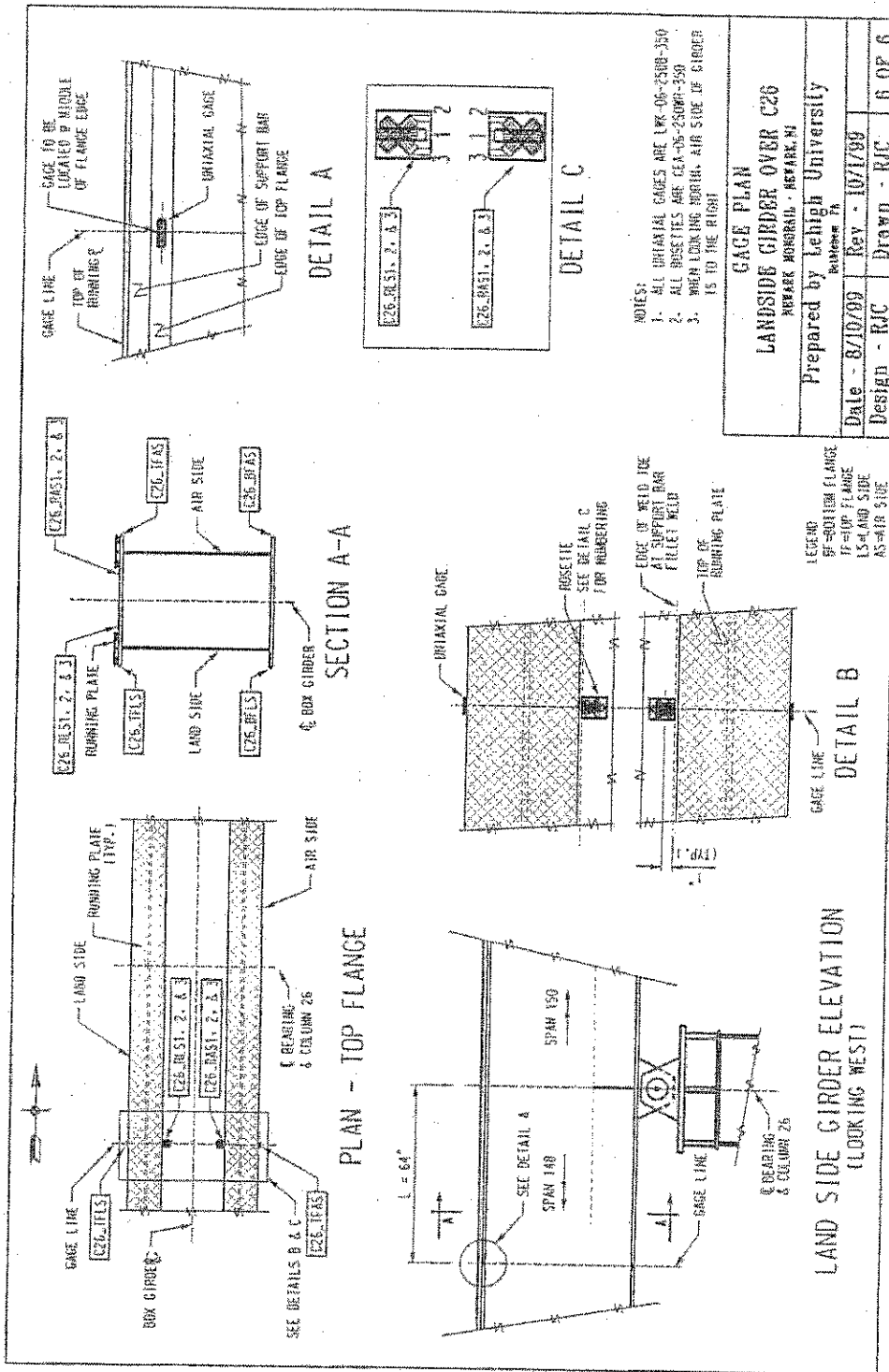


Figure 3.7 – Strain Gage Layout Adjacent to Column 26 – Land Side

STATION D

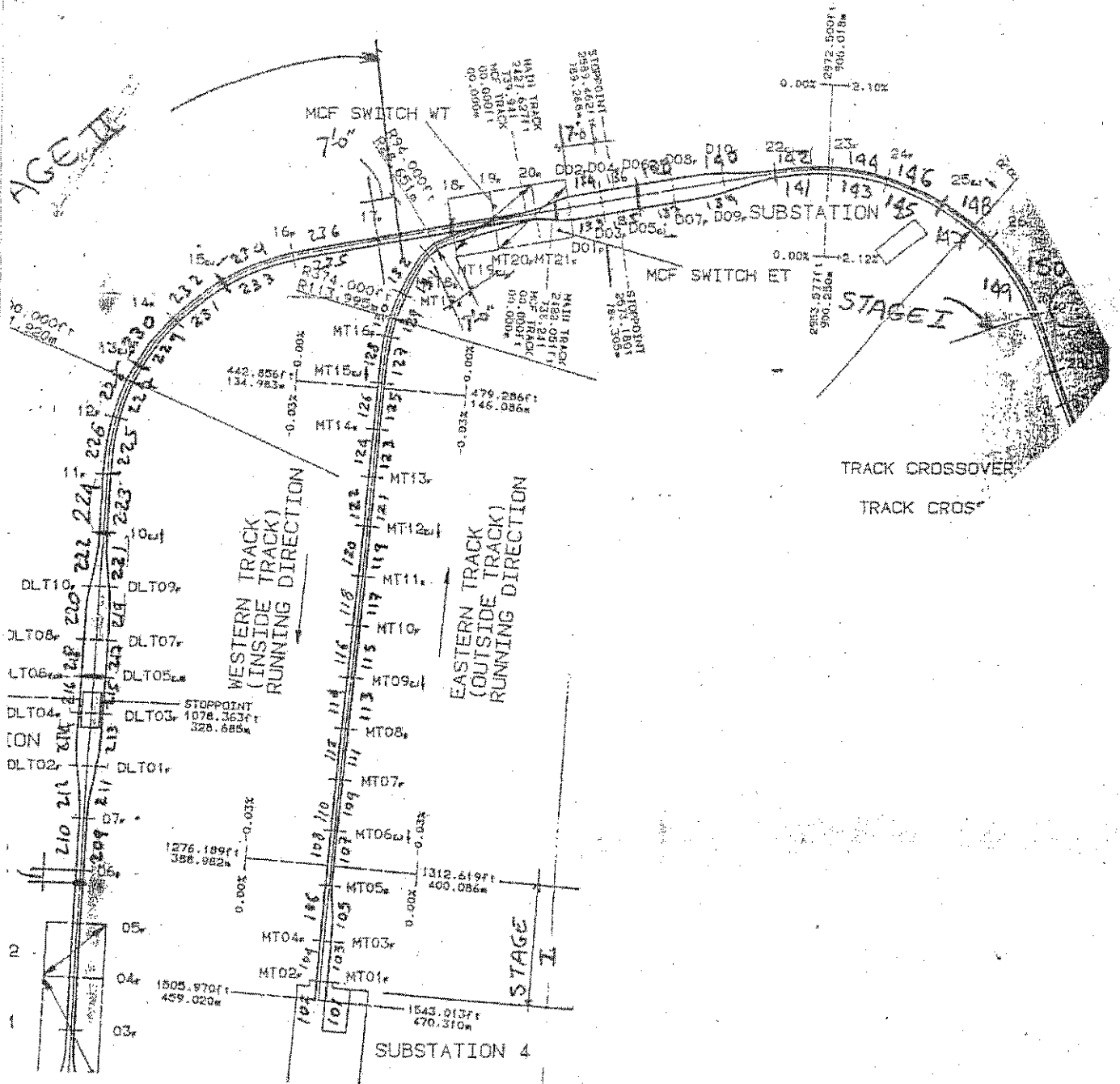


Figure 3.8 – Plan View of Monorail Guideway Showing Instrumentation Locations

3.1.1 Sensors and Signal Wire

Resistance strain gages, of both the bondable and weldable type, were installed on the top and bottom flanges of the box girder. All strain gages were wired as quarter-bridge circuits using a three-wire configuration and driven with an excitation voltage of 10 Volts. Both uniaxial and triaxial rosette gages were used.

All uniaxial gages were Measurements Group type LWK-06-W250B-350. These gages are a weldable, fully temperature-compensated uniaxial strain gage. The grid is composed of modified Karma (K-alloy), encapsulated in a fiberglass-reinforced epoxy-pheniloc. This strain gage exhibits good fatigue life ($>10^7$ cycles) and excellent stability. This type of gage is preferred for accurate strain measurements over long periods of time (months to years). Weldable type strain gages were selected due to ease of installation and durability. The gage resistance of 350 ohms and the excitation voltage of 10 Volts were selected for the following reasons:

1. Decreased lead wire effects, such as circuit desensitization due to lead wire resistance.
2. Decreases in unwanted signal variations caused by temperature induced lead wire resistance changes.
3. Improved signal to noise ratio, an important consideration in field instrumentation.

The triaxial rosettes were Measurements Group type CEA-06-250WR-350. These gages consist of three uniaxial gages which are "stacked" with the individual gages positioned on a 45° angle (See Figure 3.9). These type of rosettes are also referred to as "rectangular" rosettes. Using the data collected from these gages, principal strains and stresses can be calculated using well known relationships from mechanics of materials.

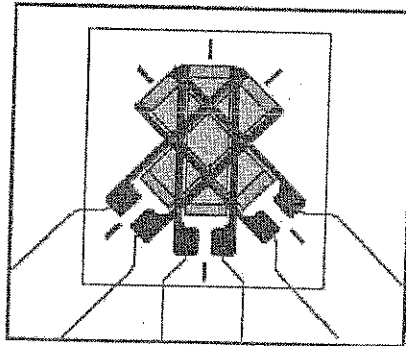


Figure 3.9 – Typical 45° Stacked Triaxial Rosette Strain Gage.

Where required, signal wires were secured to the box girder using 3/8 inch wide stainless steel strips. These strips were attached to the support bar by a resistance weld, similar to the method used to attach the weldable strain gages. Figure 3.10 is a photograph of a signal wire attached to a support bar of one of the girders tested in the laboratory at Lehigh University (note the beams were upside down during the laboratory testing). This method of attachment securely held the wires in place and was simple and efficient. Signal wires installed on the bottom flange were secured using "C" clamps and wire ties.

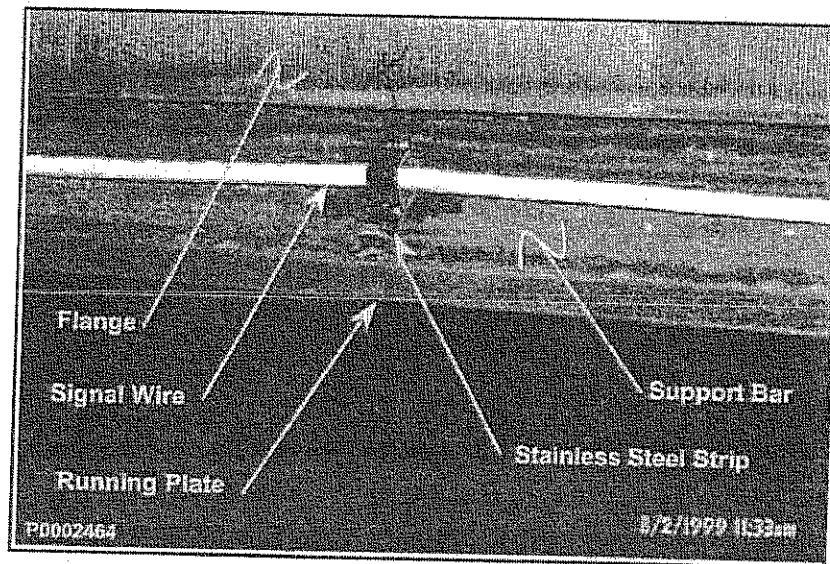


Figure 3.10 – Photograph of Method Used to Fasten the Signal Wires to the Support Bar of the Box Girders (Note, this Photograph was Taken of One of the Laboratory Specimens but is Identical to the Layout in the Field)

3.2 Data Acquisition System

All data were collected using a Campbell Scientific CR9000 Data Logger. The data logger was controlled and programmed using a laptop computer on site. Data were temporarily stored on 80Mb and 160Mb PCMCIA memory cards installed in the CR9000 and were subsequently copied to a laptop and backed-up on site. Data were converted to units of stress (ksi) in the logger and any selected channel(s) could be plotted in real-time during the testing. Vishay Model 2300 signal conditioners were used to ensure a stable, noise-free signal. The signal conditioners provided the excitation voltage, the remaining arms of the Wheatstone bridge and low-pass active analog filtering. After monitoring several trains, it was found that a 100Hz cut-off frequency removed all high frequency noise without attenuating the signal.

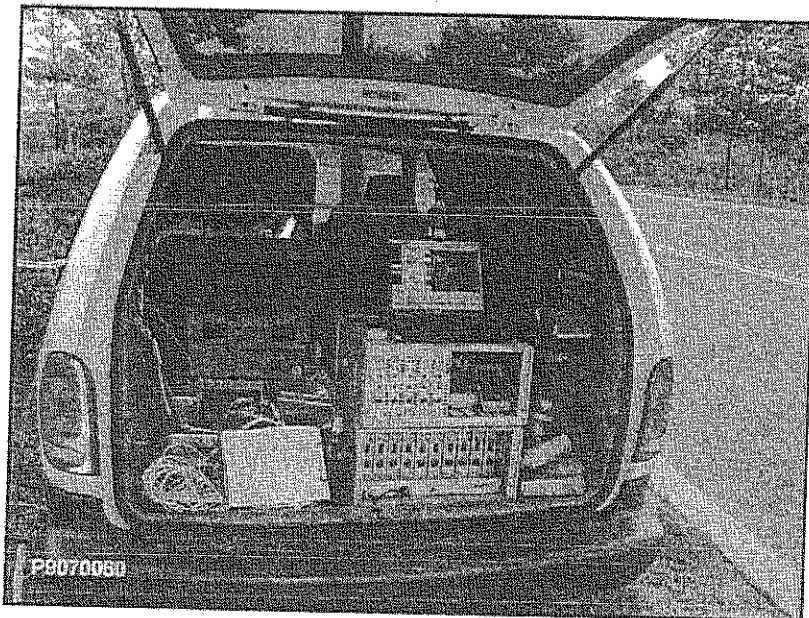


Figure 3.11 – Photograph of Data Acquisition System Used During Controlled Load Tests

For the controlled load tests, the data acquisition system was placed on tables or in the back of a van during testing, as illustrated in Figure 3.11. During the uncontrolled monitoring, the data acquisition system was stored on-site in a vented steel box and left unattended at all locations except at column 16. Figure 3.12 shows the steel box left at column 25 during the one week monitoring period. At column 16, the system was stored in a van and powered by a generator. However, at all other locations, power was provided from various Port Authority facilities. All power was passed through power conditioning devices to ensure a stable and noise free power source.

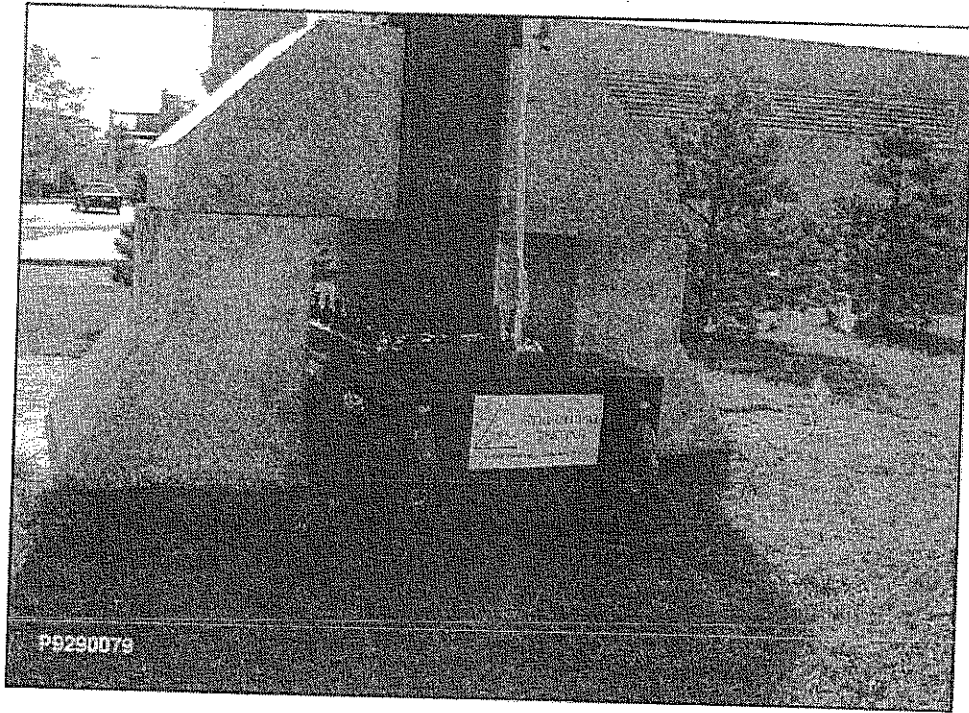


Figure 3.12 – Photograph of Steel Box Used to House the Data Acquisition System During Uncontrolled Monitoring (Photograph Taken at Column 25)

4.0 Results of Controlled Load Tests

4.1 Column 07 – Air Side Girders 209/211

This section of the girder is on a slight horizontal curve as the train approaches station D2 from D3 headed north. The spans on the south and north side of column 07 are relatively short, 91.2ft and 91.9ft respectively. The column is the middle support of the six-span continuous structure and has a fixed bearing. The girder is a Type I cross section. Strain gages were located adjacent to column 07 on the airside girder as shown in Figure 3.2. Crawl, intermediate (60% operating), and normal (100% operating) speed tests were conducted at this location.

4.1.1 Crawl and Dynamic Tests

Figure 4.1 illustrates the response during a northbound crawl run. The overall response of the girder to in-plane bending is consistent with the behavior of continuous beams. As expected, as the train approaches, both positive and negative moments are produced due to the continuity between the spans. Peak stresses occur as the train passes immediately over the instrumented section of the girder. However, after the train crossed the expansion joint at column DLT-05, live load stress levels at column 07 returned to zero.

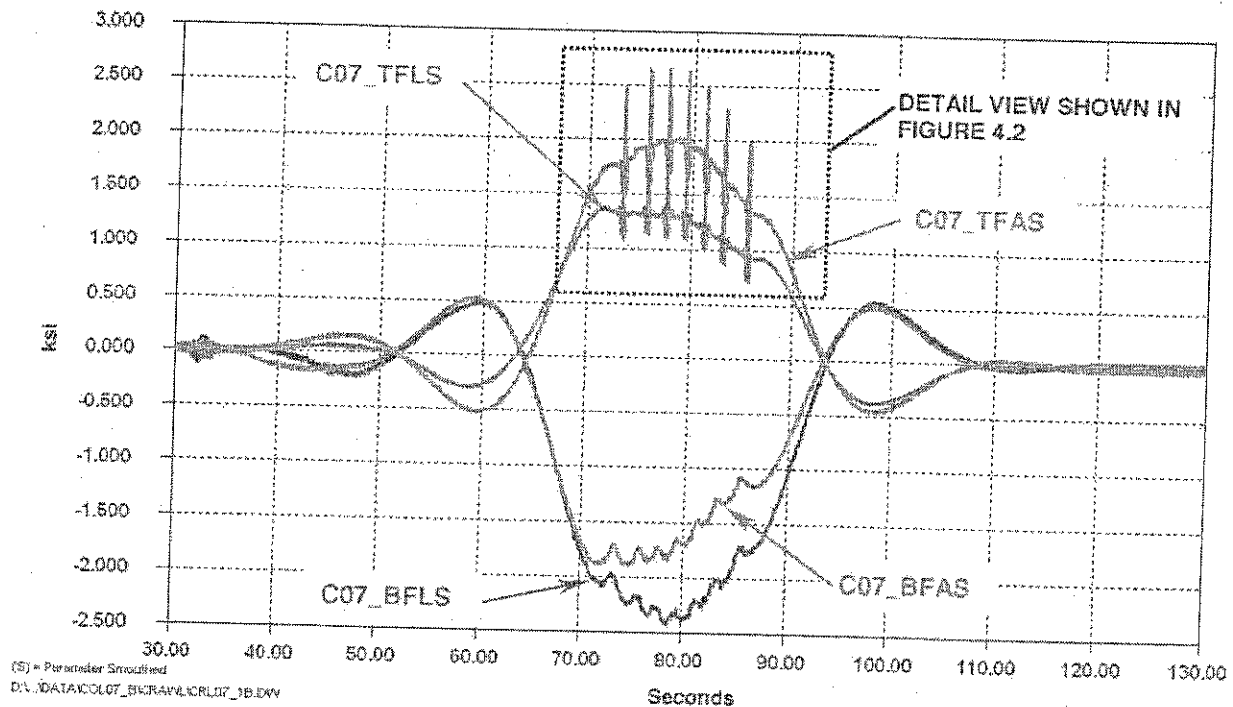


Figure 4.1 – Typical Response Adjacent to Column 07 During Passage of the Test Train (Crawl Speed Test Train Headed North)

Note that there is a difference in the response in the air side and land side gages which begins approximately at the 70 second mark. This was also observed in the dynamic tests. This is discussed more in Section 4.2.1.

Each of the wheels of the car produce local stresses in the top flange as they pass over the gage. Figure 4.2 is a detailed view of the response shown in Figure 4.1, but only for the gages on the top flange.

Nevertheless, ignoring the small cycles produced by each wheel in the top flange, each train produces a single dominant stress cycle.

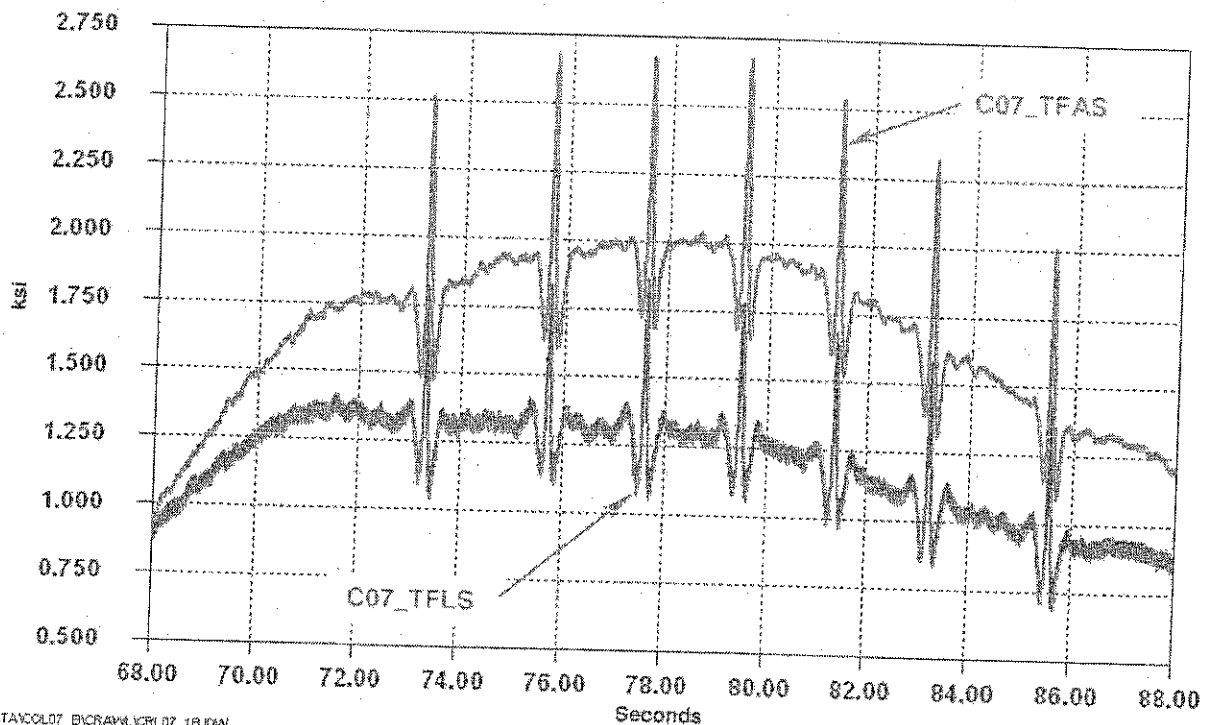


Figure 4.2 – Detailed View of Figure 4.1 for Top Flange Gages Adjacent to Column 07 During Passage of the Test Train (Crawl Speed, Test Train Headed Northbound)

The response in Figure 4.2 shows the effect of each wheel as it passes over the top flange gages in greater detail. Note that *locally*, stresses are slightly reduced as the wheel approaches and after it passes. However, while the wheel is directly over the gage, stresses are increased. This is due to local *longitudinal* vertical flange bending produced by the passing wheel load, as illustrated in Figure 4.3.

In terms of the local behavior, the running plate, support bar and top flange can be idealized as a built-up “beam”. The running plate, support bar, and top flange correspond to the top flange, web and bottom flange, respectively. As the wheel approaches and after it passes, compressive stresses are produced at the gage, as illustrated by the exaggerated deflected shape in Figure 4.3. When the wheel is directly over the gage, tension stresses are produced in the top flange plate at the gage. Obviously, a portion of the “local” stress is the result of membrane forces produced in the flange plate. However, the reversal in stress range suggests that the local longitudinal bending stresses dominate the local behavior. Similar behavior was observed at all other instrumented sections of the guideway.

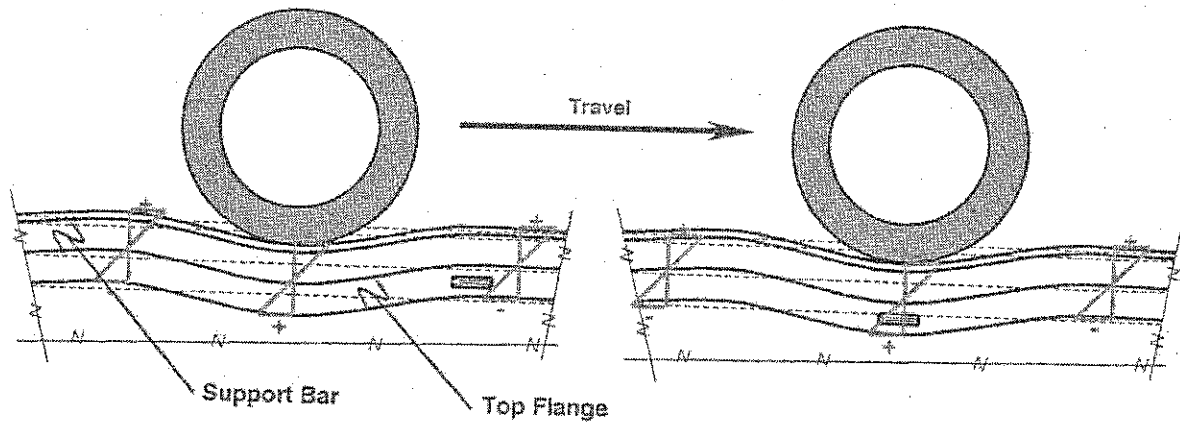


Figure 4.3 – Local Bending in Top Flange Due to Wheel Load

It should be noted that transverse stresses are also developed in the top flange from cantilever bending of the top flange and bending between the webs of the box. The longitudinal strain gages installed on the edges of the top flange are not capable of measuring these effects. Strain gages could not be positioned to measure the transverse stresses on the cantilevered portions of the flange since they would be damaged by the wheels of the car. However, transverse stresses were measured in the top flange near column 26 and midspan of span 148 where tri-axial rosettes were placed on the top flange in the "bath tub" region. The results of these measurements are discussed in Sections 4.5.3 and 4.6.3.

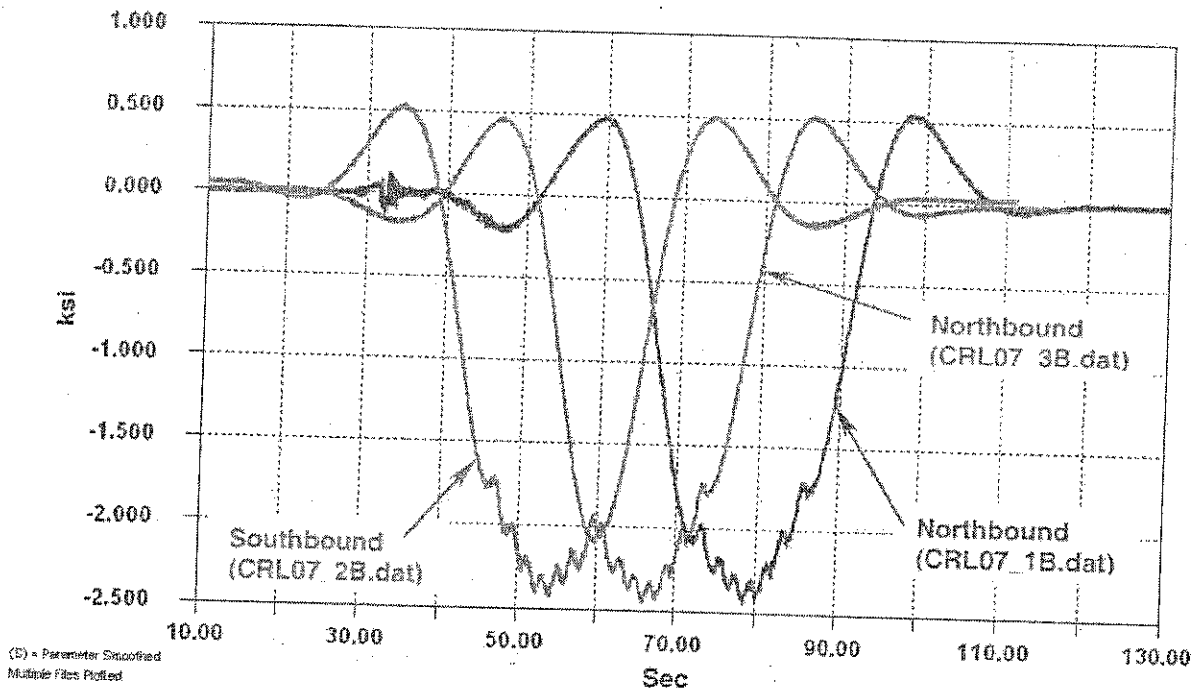


Figure 4.4 – Comparison of Northbound and Southbound Crawl Runs for Bottom Flange Land Side Gage Adjacent to Column 07

Figure 4.4 compares the measured response during the three crawl tests for C07_BFLS, located on the land side of the bottom flange. As can be seen, the two northbound crawl runs are consistent. Comparing the time histories from the single southbound test and the northbound runs demonstrates there is no change in behavior as the direction of the train is reversed.

Figure 4.5 Illustrates the response at column 07 as the test train traveled northbound at normal operating speed. The general response is identical to that shown in Figure 4.1 for the northbound crawl tests. Although, not shown, data collected during the intermediate speed tests are also consistent with the crawl and normal operating speed tests.

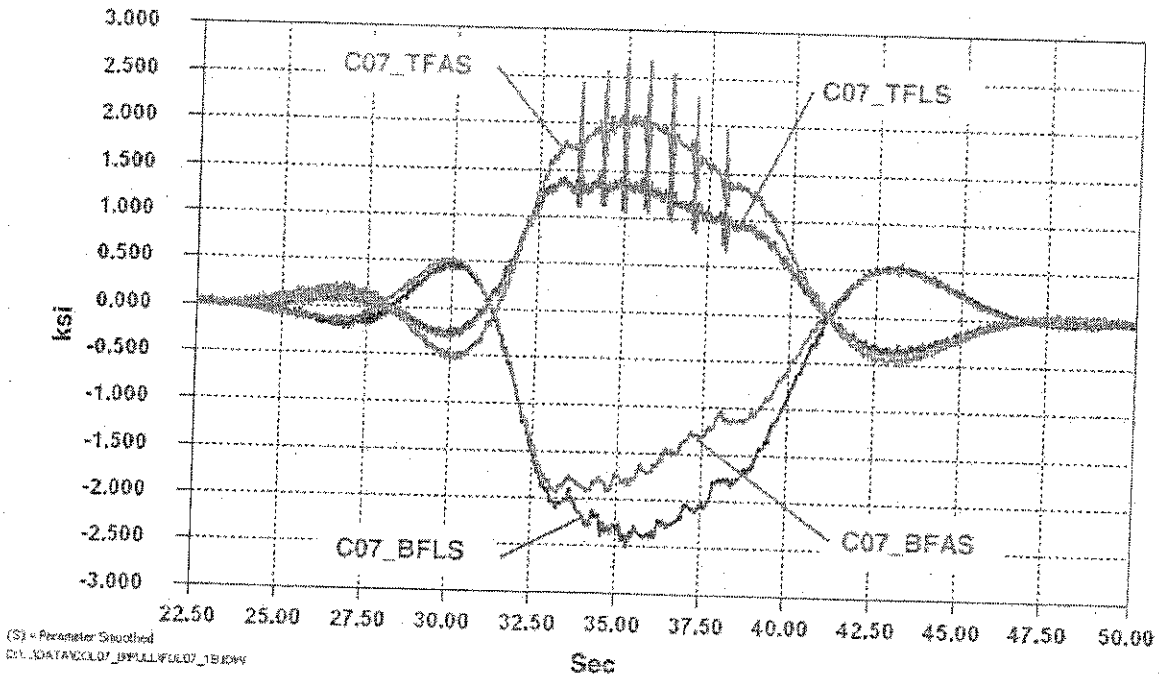


Figure 4.5 – Response Adjacent to Column 07 for a Test Train Traveling at Normal (100%) Operating Speed

Table 4.1 summarizes the data from all the controlled tests conducted at Column 07. The minimum stress (S_{min}), maximum stress (S_{max}) and the stress range (S_r) produced by the test train are listed. For the gages located on the top flange, the maximum stress (S_{max}) includes only the global response, and *not* the local effects produced by the individual wheels. The stress range (S_r) listed for the top flange gages is the *peak-to-peak* stress range and includes the effects of the wheels. (When determining the stress range, this is appropriate.) The minimum stress (S_{min}), maximum stress (S_{max}) and the stress range (S_r) are illustrated in Figure 4.6. The minimum and maximum stress data can be compared to finite element analysis results without being biased by the influence of local effects. This analysis is not part of this investigation program.

Table 4.1 indicates the vehicle speed has no measurable effect on the stresses developed in the box girder in this location. Because column 07 is located on a relatively straight segment of the guideway, the centrifugal forces generated by the moving vehicle should be small. This can be seen by considering the response of the top flange due to the passage of the individual wheels. The stress range produced by each wheel essentially remains unchanged as the speed of the vehicle is increased.

Location	Crawl Tests			60% Operating			100% Operating		
	S_{min}	S_{max}	S_r	S_{min}	S_{max}	S_r	S_{min}	S_{max}	S_r
C07_BFLS	-2.4	0.6	3.0	-2.5	0.5	3.0	-2.5	0.5	3.0
C07_BFAS	-1.9	0.5	2.4	-1.9	0.5	2.4	-1.9	0.5	2.4
C07_TFLS	-0.4	1.3	2.3 ¹	-0.4	1.4	2.4 ¹	-0.4	1.4	2.4 ¹
C07_TFAS	-0.5	2.0	3.2 ¹	-0.5	2.1	3.2 ¹	-0.5	2.0	3.2 ¹
C07_TFLS ²	-	-	0.8 ²	-	-	0.9 ²	-	-	0.8 ²
C07_TFAS ²	-	-	1.1 ²	-	-	1.0 ²	-	-	1.0 ²

Notes:

1. Includes local effects of wheel loads.
2. Stress range produced by local effects of wheel load only.
3. S_{min} = minimum stress, S_{max} = maximum stress, S_r = "peak to peak" stress range

Table 4.1 – Summary of Response Adjacent to Column 07 for Controlled Load Tests

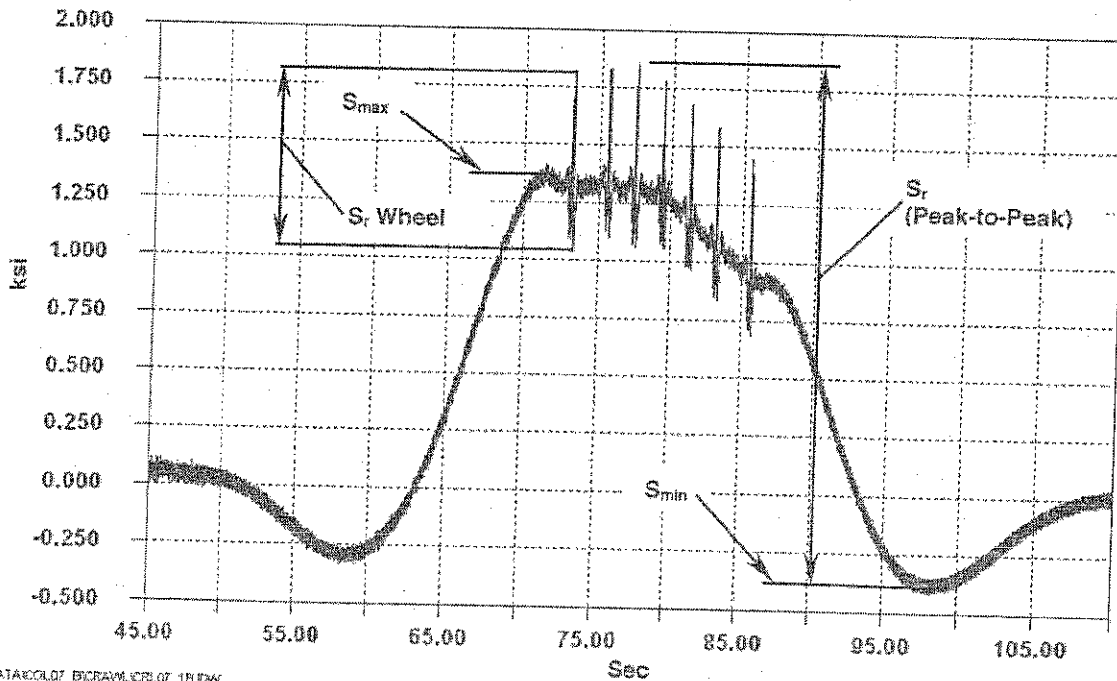


Figure 4.6 – Figure Illustrating Minimum Stress, Maximum Stress, and Stress Range Listed in Table 4.1 (Gage C07_TFLS Shown, Other Locations Similar)

4.1.2 Calculation of Forces

Using the data acquired at each corner of the box girder, the proportions of axial, vertical bending, lateral bending, and warping stresses were calculated. The girder resists torsional forces by a combination of warping stresses and pure or St. Venant's torsional stresses. The warping stresses were assumed to be uniformly distributed. (This was confirmed by a finite element analysis of a typical box girder subject to pure torsion.) The St. Venant's torsional stresses cannot be calculated since the gages were oriented longitudinally on the edges of the flanges. Note that in terms of fatigue, the St. Venant's stresses do not contribute to the stress field producing fatigue cracks in the support bars or flange.

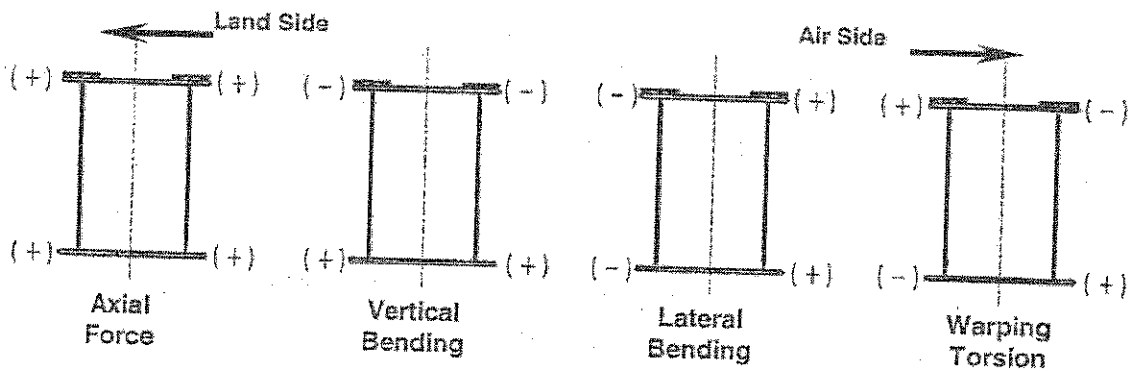


Figure 4.7 Assumed Positive Sign Convention in Box Girders.

Figure 4.7 illustrates the assumed positive sign convention in determining the proportions of stress components. The sign convention is oriented looking north on the girder (air side to the right). If a given stress or force component is plotted as negative, it means at that instant in time, the actual direction of the respective force component is opposite to the assumed direction. In addition, in the plots of stress vs. time, the data (stresses) are presented for the top flange gage locations but still consistent with the above sign convention. Thus, if a given stress component is plotted as negative, it simply indicates that the stress in the top flange is opposite to that assumed in Figure 4.7. These stresses were then used to compute the force effects (axial, vertical bending, lateral bending) in the box girder.

The stress components were determined by assuming that the only factors contributing to the measured stresses in the flanges were the result of axial, vertical bending, lateral bending, and warping stresses. Thus, the stress measured at each location is comprised of four components which are unknown. Assuming that distortion due to warping is relatively small and a linear strain distribution is produced during bending, four equations can be developed, i.e., one for each corner of the box. Using the section properties of the girder, the proportions between individual stress components can be determined and a set of four linear equations with four unknowns can be developed and solved.

It should be noted that the calculation of the axial, vertical bending, and lateral bending components is biased by any local effects if the "raw" data are used. For example, the calculation of the axial stress component is drastically altered if the local

effects produced by the wheels on the top flange are included in the calculation. To minimize any potential bias, all "local effects" were removed from the data.

Figure 4.8 is a plot of the axial, vertical bending, lateral bending and warping stresses produced as the test train passed over column 07 at crawl speed headed north. As expected, the vertical bending stress dominates the response. Lateral bending stresses are less than 0.5ksi, while the axial and warping stress components are negligible. (The negative stress indicates that vertical bending stresses are opposite of that assumed in Figure 4.7. Thus, a negative bending moment was observed, as expected.)

Figure 4.9 is a plot of the axial, vertical bending, lateral bending and warping stresses produced as the test train passed at normal operating speed headed north. As in Figure 4.8, the vertical bending stress dominates the response. This is because the girder essentially is straight in this region. Hence, the axial, lateral, and torsional stresses should be the smaller components. The other stress components remained relatively unchanged as the speed increased, indicating the dynamic lateral and centrifugal forces are negligible in this section of the guideway.

However, note that a lateral moment was produced at this section as the strain passed. Since the girder is essentially straight, the cause of this moment is not readily apparent. It may be the result of the support bent "leaning" as the train passes. It may also be the result of bearing moments. It must be noted that both of these explanations are speculation. Additional instrumentation would be required to determine the exact cause of this behavior. Although the exact cause of this behavior is unknown, the primary force component is the result of vertical bending, as expected.

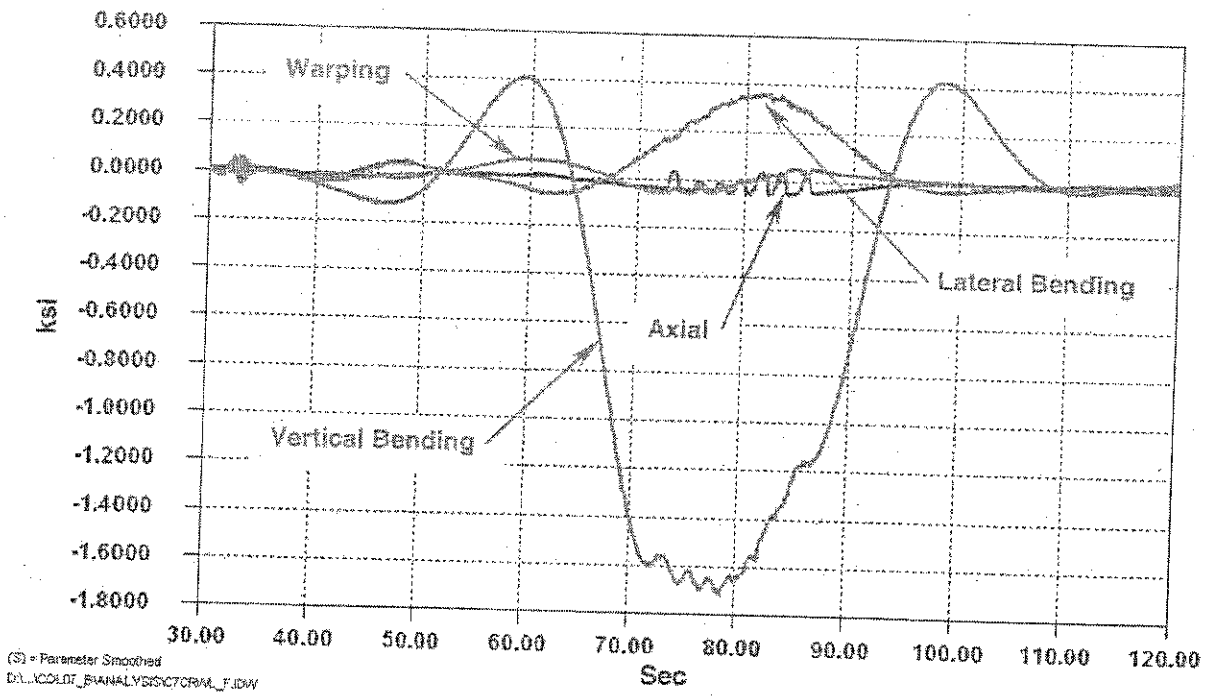


Figure 4.8 - Calculated Axial, Vertical Bending, Lateral Bending and Warping Stresses in the Girder Adjacent to Column 07 (Test Train Headed North at Crawl Speed)

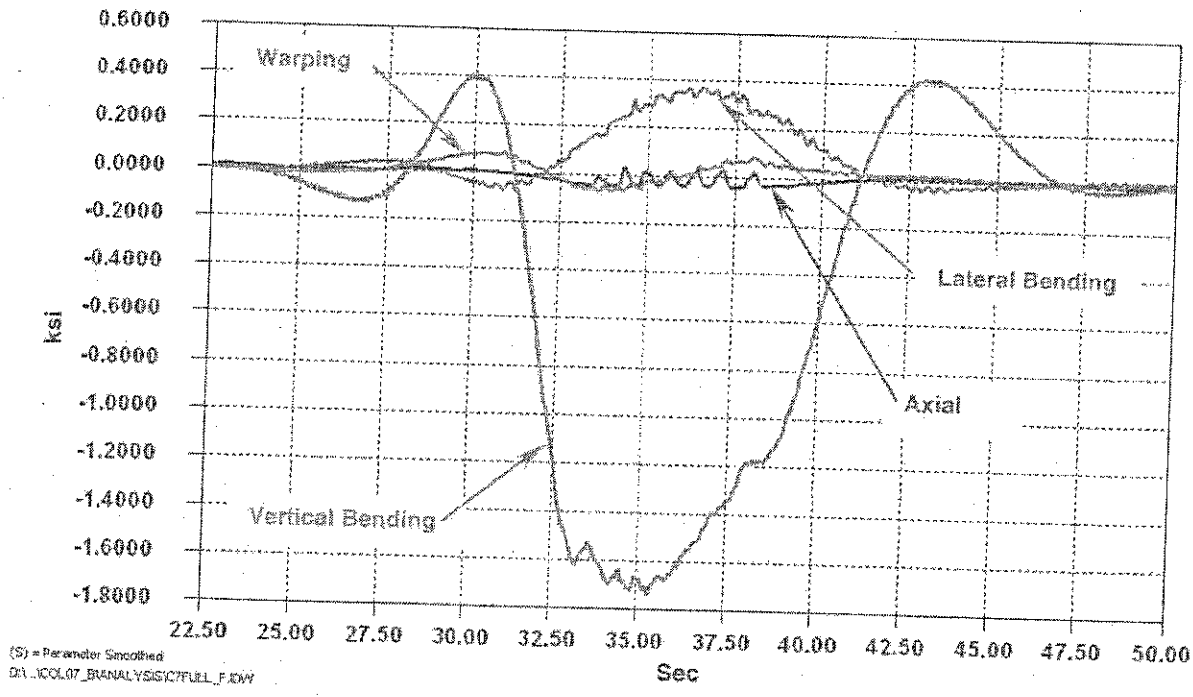


Figure 4.9 - Calculated Axial, Vertical Bending, Lateral Bending and Warping Stresses in the Girder Adjacent to Column 07 (Test Train Headed North at Normal Operating Speed)

Figure 4.10 presents the calculated *force* components for the test data shown in Figure 4.8. The total torsional moment is not shown since only the warping stresses are known. The warping torsional moment can't be calculated simply by knowing the stress components because it is a function of length. A detailed structural analysis would have to be performed to determine the warping torsional moment.

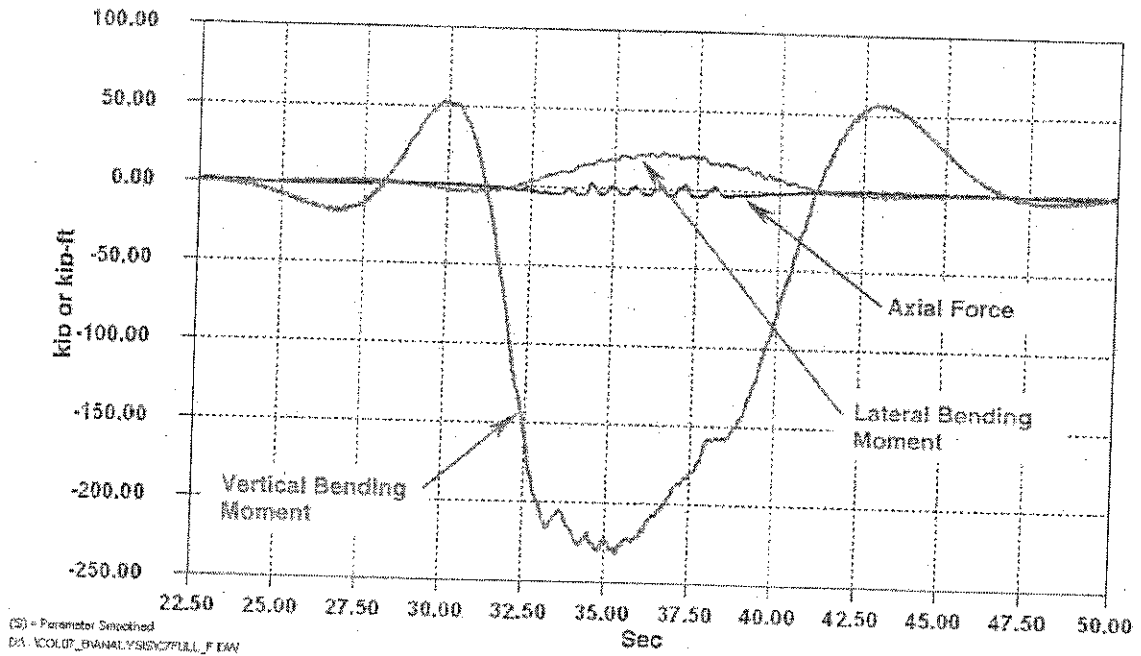


Figure 4.10 - Calculated Axial Force, Vertical Bending Moment, and Lateral Bending Moment in the Girder Adjacent to Column 07 (Test Train Headed North at Crawl Speed)

4.2 Column DLT-10 – Land Side Girders 218/220

This section of the girder is on a slight reverse curve where the guideway separates for trains coming into Station D2. It is a three span continuous structure with column DLT-10 being the northern first interior column. The spans on the south and north sides of column DLT-10 are relatively short, about 91ft and 92.8ft respectively and the bearing is fixed. The girder is a Type I cross section. In this area, the trains typically approach station D2 from D1 headed south. Only crawl and normal operating (100% operating) speed tests were conducted at this location.

4.2.1 Crawl and Dynamic Tests

Figure 4.11 illustrates the response at column DLT-10 as the test train headed south at crawl speed. There is an expansion joint at column 10, which is the next column north of DLT-10. As expected, the train has very little influence at column DLT-10 while it is north of column 10. However, as soon as it crosses the expansion joint and begins to cross onto span 220, negative moments are produced in the girder near DLT-10. As the train passes over the gages, the effect of each wheel is observed in the top flange. This is similar to that observed at column 07. As the train passes into span 218, positive moments are produced at DLT-10 due to continuity of the girder. The data were found to be consistent and repeatable.

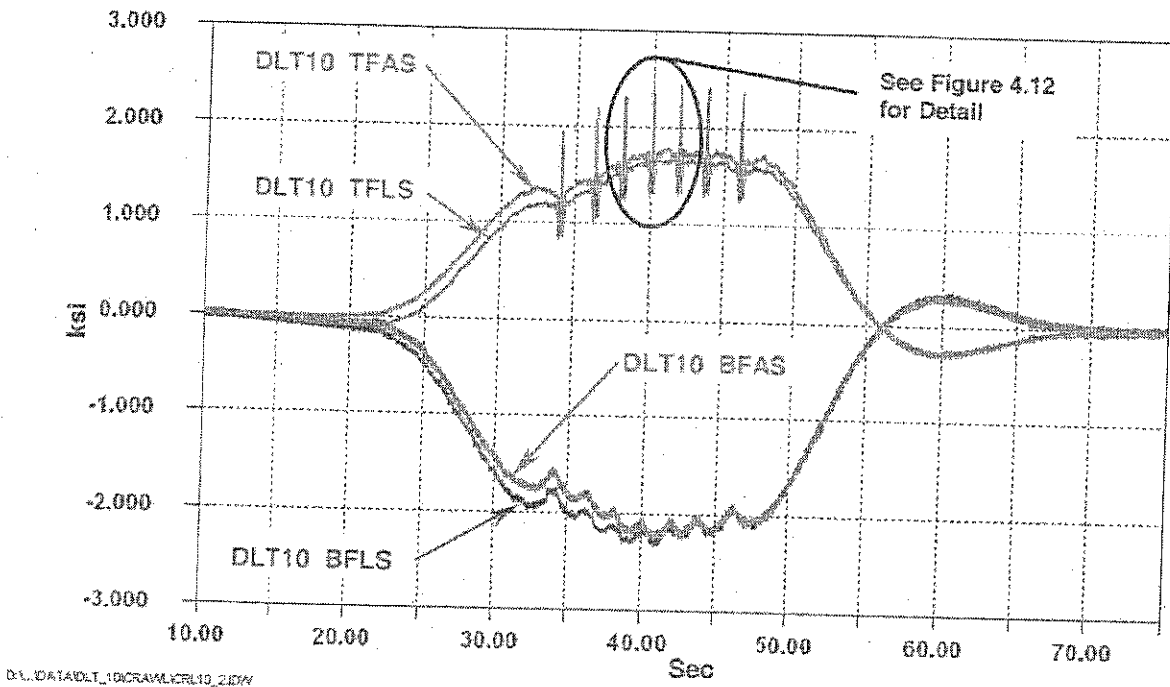


Figure 4.11 – Typical Response Adjacent to Column DLT 10 During Passage of the Test Train (Test Train Headed South at Crawl Speed)

Figure 4.12 is a close-up of the top flange response at column DLT 10 as the train passes over the gages at crawl speed. For clarity, only the response produced by the middle three wheels in the top flange gages is shown. The behavior is essentially identical to that observed at column 07. As the wheel approaches and after it passes, stresses are reduced due to the local effect of the wheel. However, while the wheel is directly over the gage, peak tension stresses are produced. This is due to the same local vertical flange bending as was illustrated in Figure 4.3.

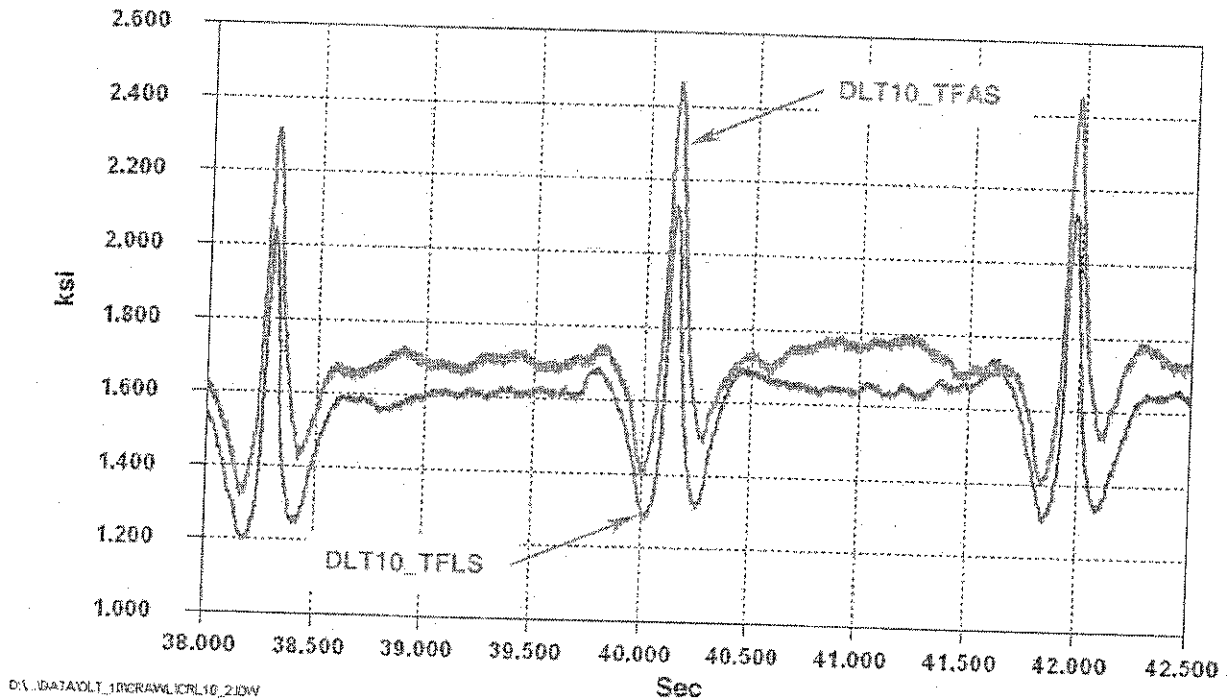


Figure 4.12 – Detail of Response Measured in the Top Flange at Column DLT 10 During Passage of the Test Train Shown in Figure 4.11. Only the Three Interior Wheels are Shown (Test Train Headed South at Crawl Speed)

During the crawl tests, the test train was run in both directions. Figure 4.13 compares the response of gage DLT10_BFLS, which is located on the land side of the bottom flange, for the test train headed north and south. The minimum stress, maximum stress, and peak stress range are all identical. These tests demonstrate that the direction of travel has no unexpected effects on the behavior of the box girder in this region.

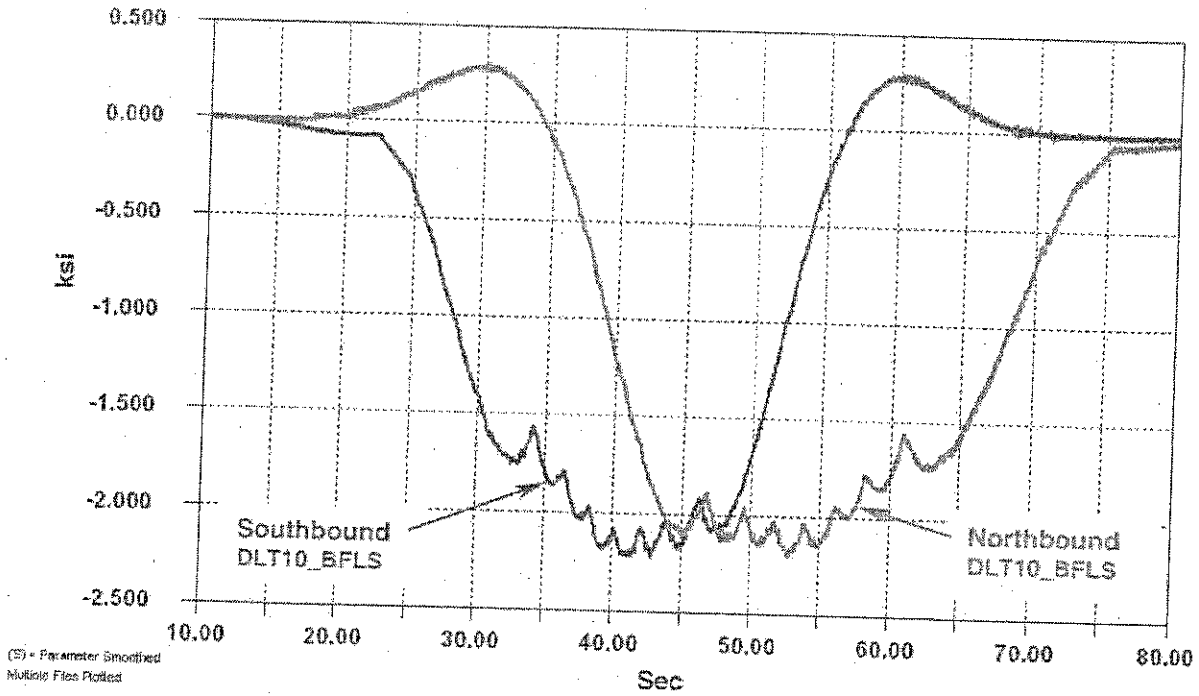


Figure 4.13 – Comparison of Northbound and Southbound Crawl Runs at Column DLT-10 for Bottom Flange Land Side Gage

Only normal operating speeds were considered for the dynamic speed runs at column DLT-10. There was little difference between the dynamic and crawl tests. Some dynamic amplification appeared to occur directly under the wheel itself. However, global stresses were not significantly influenced. The results of the controlled test are summarized in Table 4.3.

Location	Crawl Tests			60% Operating			100% Operating		
	S_{min}	S_{max}	S_r	S_{min}	S_{max}	S_r	S_{min}	S_{max}	S_r
C07_BFLS	-2.3	0.3	2.6	N/A	N/A	N/A	-2.4	0.3	2.7
C07_BFAS	-2.2	0.3	2.5	N/A	N/A	N/A	-2.2	0.3	2.5
C07_TFLS	-0.3	1.7	2.4 ¹	N/A	N/A	N/A	-0.2	1.7	2.6 ¹
C07_TFAS	-0.3	1.7	2.8 ¹	N/A	N/A	N/A	-0.3	1.8	2.8 ¹
C07_TFLS ²	-	-	0.9 ²	-	-	N/A	-	-	1.0 ²
C07_TFAS ²	-	-	1.1 ²	-	-	N/A	-	-	1.0 ²

Notes:

1. Includes local effects of wheel loads.
2. Stress range produced by local effects of wheel load only.
3. S_{min} = minimum stress, S_{max} = maximum stress, S_r = "peak to peak" stress range

Table 4.3 – Summary of Response at Column DLT-10 for Controlled Load Tests

The data in Table 4.3 suggests that speed has little influence on the minimum stress, maximum stress and stress range. This is not surprising since the girder is relatively straight and the speed of the train is rather slow as it approaches the station.

4.2.2 Calculation of Forces

Using the data acquired at each corner of the box girder, axial, vertical bending, lateral bending, and warping stresses were calculated adjacent to column DLT-10. The assumed positive sign convention in determining the proportions of stress components is shown in Figure 4.7. The sign convention is oriented looking north on the girder (air side to right). To minimize any bias in the calculations, local effects were removed from the data.

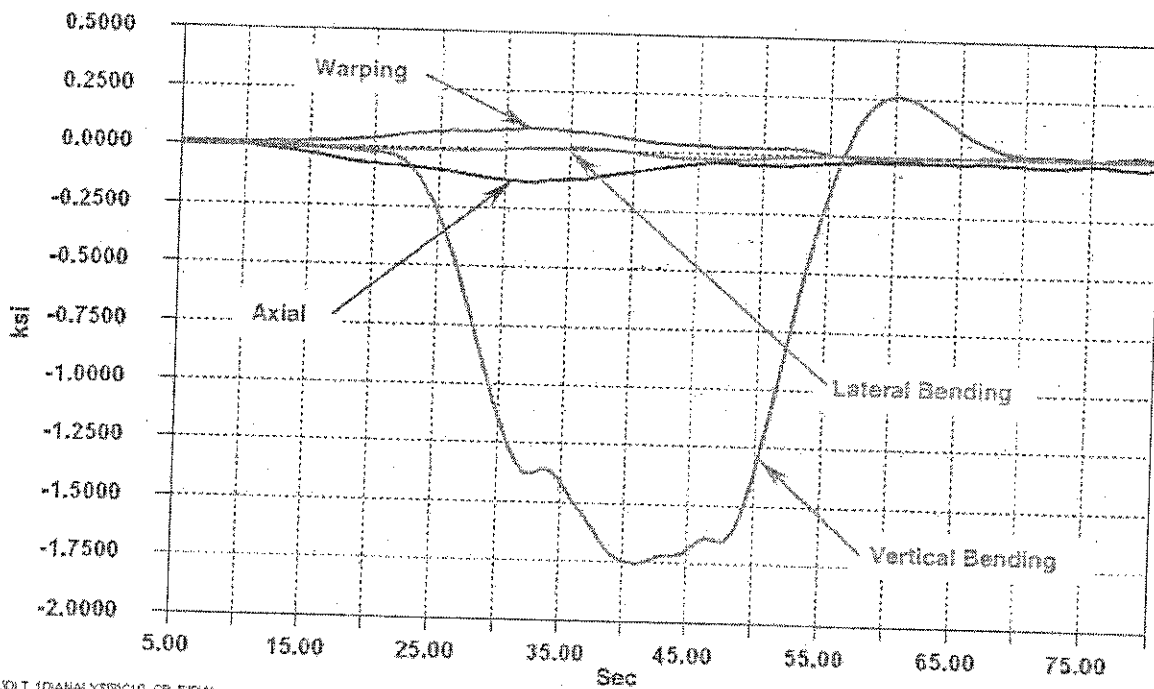


Figure 4.14 - Calculated Axial, Vertical Bending, Lateral Bending and Warping Stresses in the Girder Adjacent to Column DLT-10 (Test Train Headed South at Crawl Speed)

Figure 4.14 is a plot of the calculated axial, vertical bending, lateral bending and warping stresses produced as the test train passed at crawl speed. The train was headed south. The vertical bending stress dominates the response and lateral bending stresses are very small. The contributions of the axial and warping stress components are negligible.

Figure 4.15 presents the calculated *force* components for the test data shown in Figure 4.14. The total torsional moment is not shown since only the warping stresses are known. As stated above, there was little difference between the crawl and dynamic speed runs.

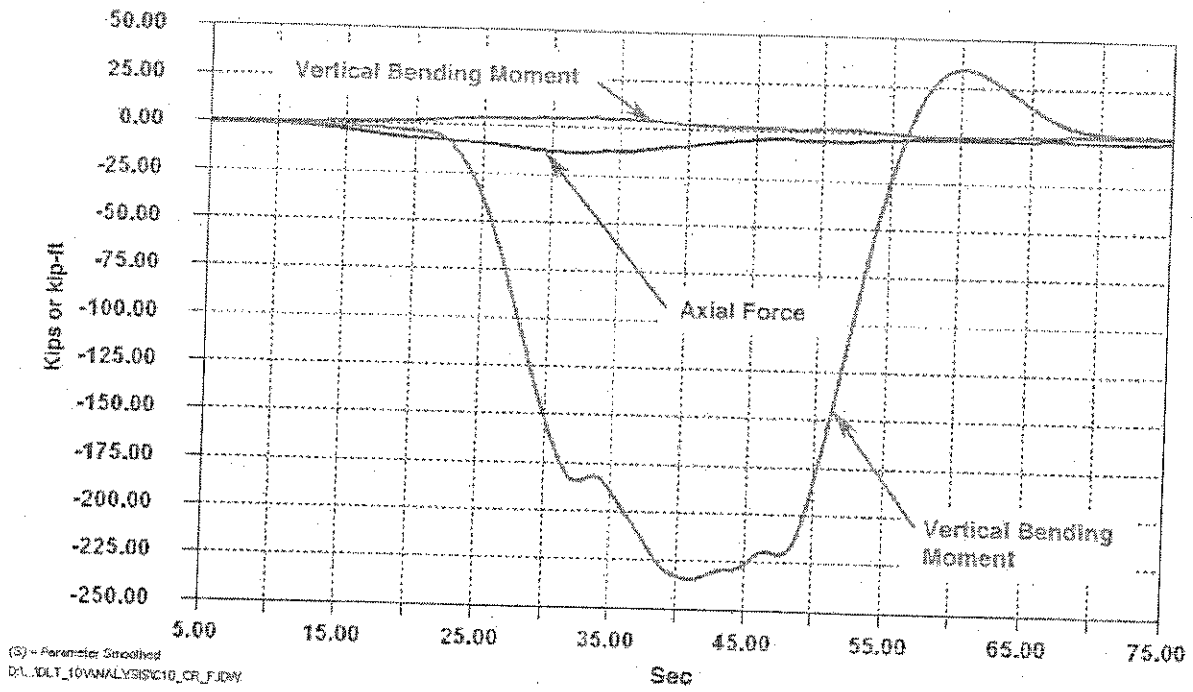


Figure 4.15 - Calculated Axial Force, Vertical Bending Moment, and Lateral Bending Moment in the Girder Adjacent to Column DLT-10 (Test Train Headed South at Crawl Speed)

4.3 Column 12 – Air Side Girders 225/227

This section of the girder is on a horizontal curve approximately 300ft north of Station D2. It is a 3-span continuous unit with column 12 the northern interior column. The spans on the south and north sides of column 12 are about 99.4ft and 99.1ft respectively and the bearing is fixed. In this area, the trains typically approach station D1 from D2 headed north. The girder is a type IV cross section and the gages were located adjacent to the column area as shown in the gage plan.

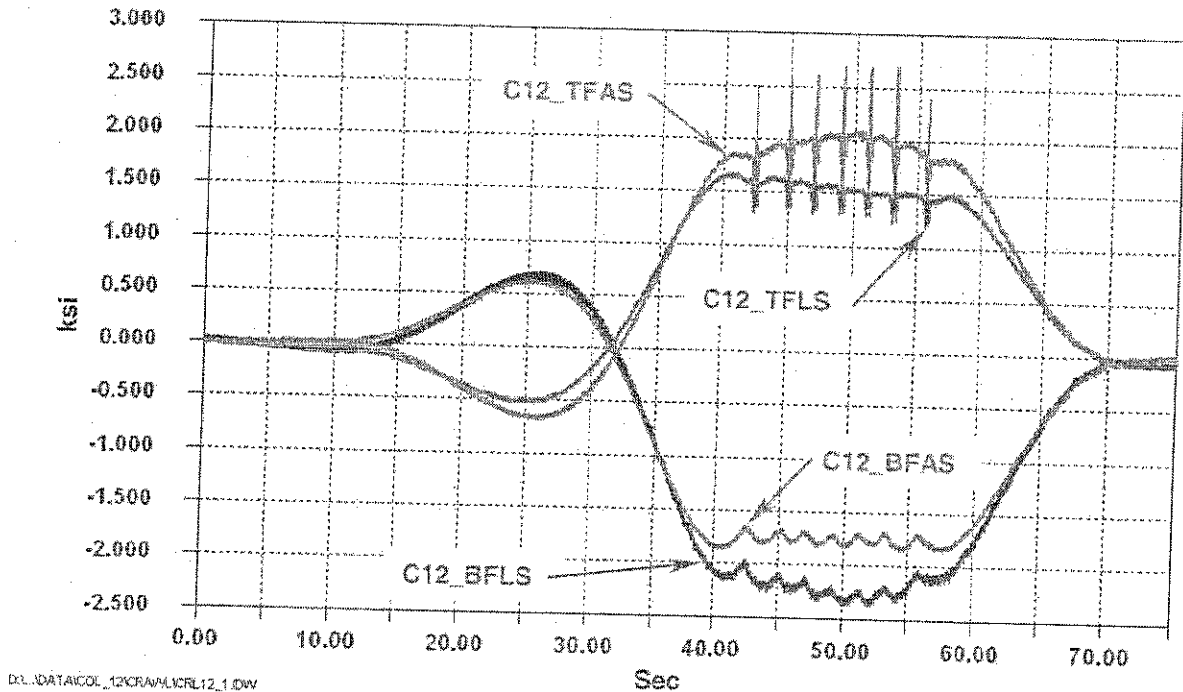


Figure 4.16 – Typical Response Adjacent to Column 12 During Passage of the Test Train (Test Train Headed North at Crawl Speed)

4.3.1 Crawl and Dynamic Tests

Figure 4.16 illustrates the response of the girder during a crawl test as the test train headed north. The response is as expected for a 3-span continuous beam under moving live load. While the train is between columns 10 and 11, small positive moments are produced at column 12 due to continuity. Once the train is north of pier 11 a large negative moment is produced and remains until the train leaves the span. Although not shown in detail, the local wheel effects are evident, especially at the top flange. The data from test runs in both directions were consistent and repeatable, indicating the direction of travel has no effect on the behavior of the box girder at this location. The data are summarized in Table 4.4.

Location	Crawl Tests			60% Operating			100% Operating		
	S_{min}	S_{max}	S_r	S_{min}	S_{max}	S_r	S_{min}	S_{max}	S_r
C12_BFLS	-2.3	0.7	3.0	-2.4	0.7	3.1	-2.6	0.7	3.2
C12_BFAS	-1.9	0.6	2.5	-1.8	0.6	2.4	-1.8	0.7	2.4
C12_TFLS	-0.5	1.7	2.8 ¹	-0.5	1.7	2.8 ¹	-0.5	1.7	3.0 ¹
C12_TFAS	-0.7	2.1	3.4 ¹	-0.7	2.1	3.3 ¹	-0.7	2.3	3.3 ¹
C12_TFLS ²	-	-	0.9 ²	-	-	1.0 ²	-	-	1.2 ²
C12_TFAS ²	-	-	1.0 ²	-	-	0.8 ²	-	-	0.6 ²

Notes:

1. Includes local effects of wheel loads.
2. Stress range produced by local effects of wheel load only.
3. S_{min} = minimum stress, S_{max} = maximum stress, S_r = "peak to peak" stress range

Table 4.4 – Summary of Response at Column 12
for Controlled Load Tests

Dynamic tests at intermediate (60%) and normal (100%) operating speed revealed the horizontal curve has an effect on the girder response under intermediate and normal operating speed. The local stresses due to the wheel loads on the top flange exhibit this effect. Figure 4.17 compares the results of crawl, intermediate, and normal speed runs for gage C12_TFLS, located on the land side of the top flange for the train heading north. Traveling in this direction, the girder curves toward the right (air side) causing the train to lean to the left (land side). Thus, the downward forces applied by the wheels on the left (land side) of the train increase. The local stress range produced by each wheel is about 0.9, 1.0 and 1.2ksi for the crawl, intermediate and normal operating speed tests, respectively. However, on the girder air side, the applied wheel loads appear to decrease. The local stress range produced by each wheel on the air side is about 1.0, 0.8 and 0.6ksi for the crawl, intermediate and normal operating speed tests, respectively, as shown in Figure 4.17b. Although the overall stress range on the girder air side is greater than the land side stress range, the difference is relatively small. There is a small effect on the peak-to-peak stress range due to train speed.

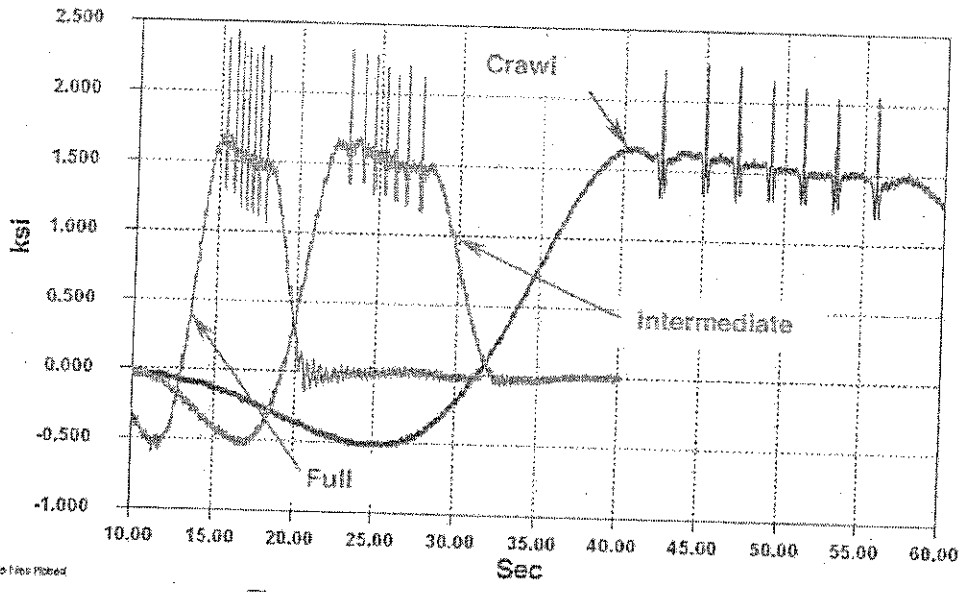


Figure 4.17a - Land Side of Top Flange (C12_TFLS)

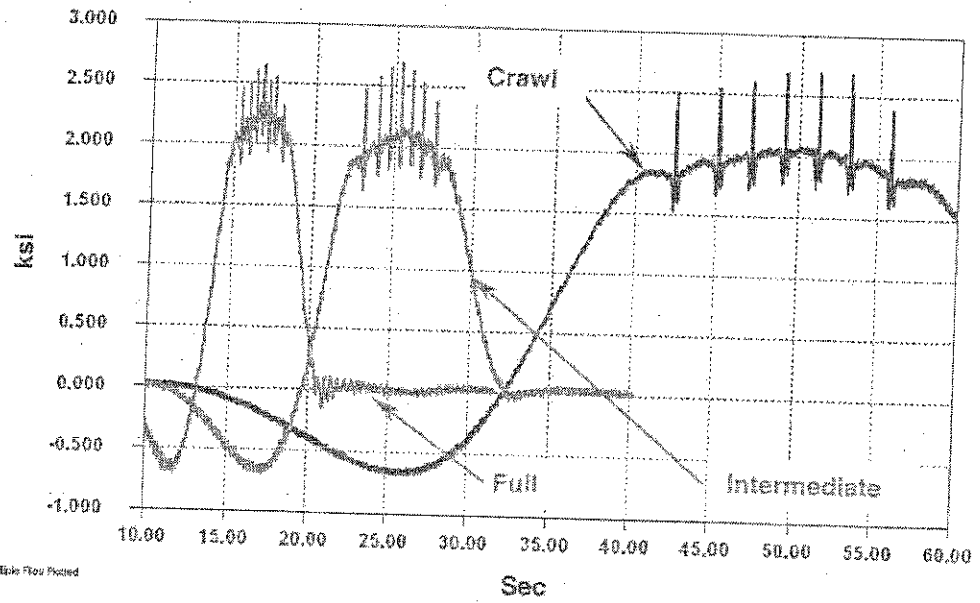


Figure 4.17b - Air Side of Top Flange (C12_TFAS)

Figure 4.17a and b - Effect of Travel Speed and Girder Curvature on Local Stresses in the Top Flange (Test Train Headed North)

4.3.2 Calculation of Forces

Using the data acquired at each corner of the box girder, axial, vertical bending, lateral bending, and warping stresses were calculated. The assumed positive sign convention is the same as the previous locations. Local effects were removed from the data so as not to bias the calculations.

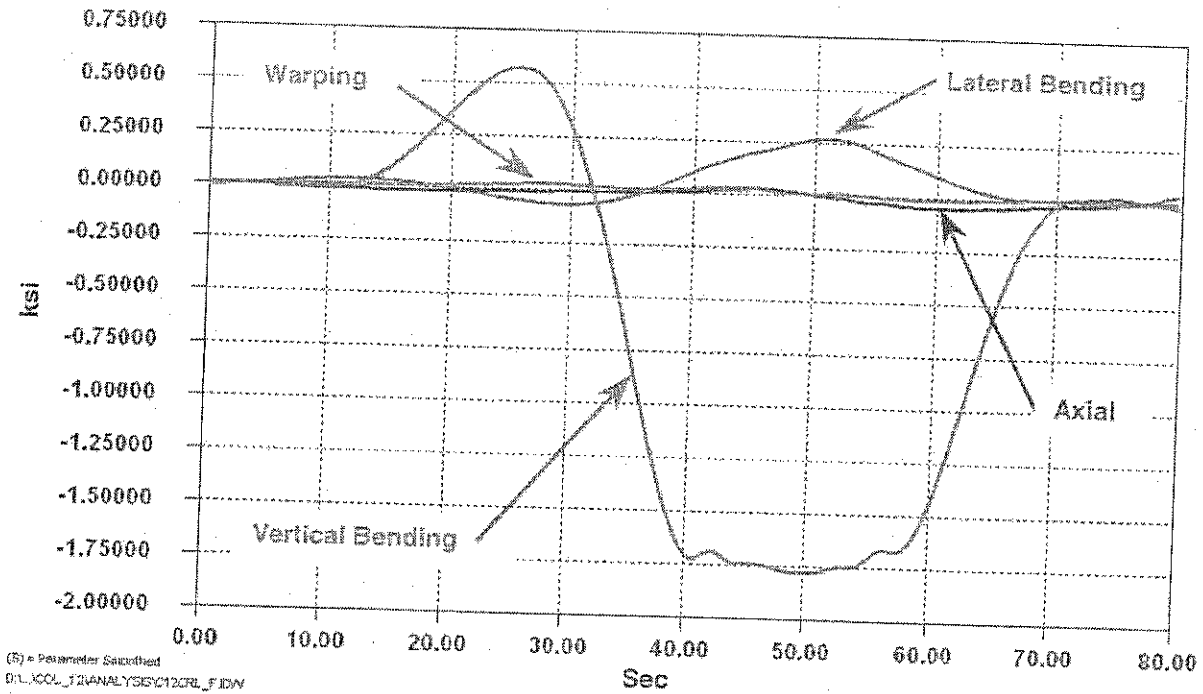


Figure 4.18 - Calculated Axial, Vertical Bending, Lateral Bending and Warping Stresses in the Girder Adjacent to Column 12 (Test Train Headed North at Crawl Speed)

Figures 4.18 and 4.19 compare the calculated stress components for crawl and normal operating speed tests. The calculations reveal that there is a small increase in the lateral stress produced as the train speed increases. This would be expected as the box girder is curved at this location.

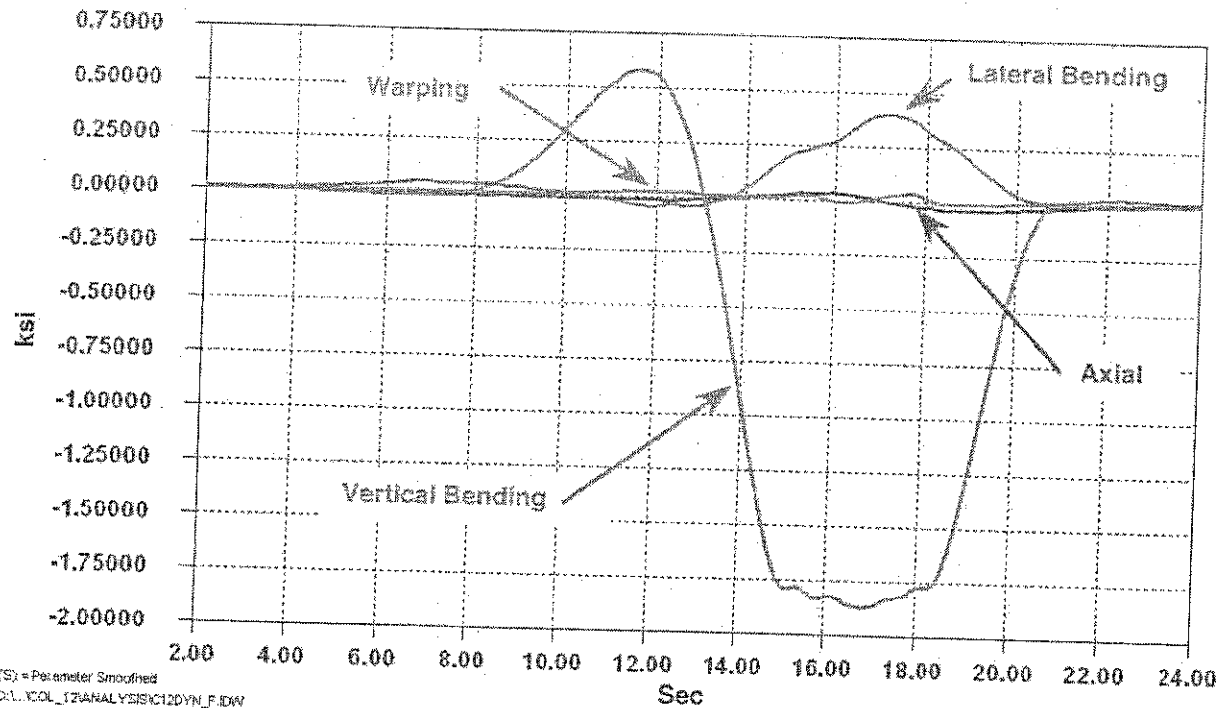
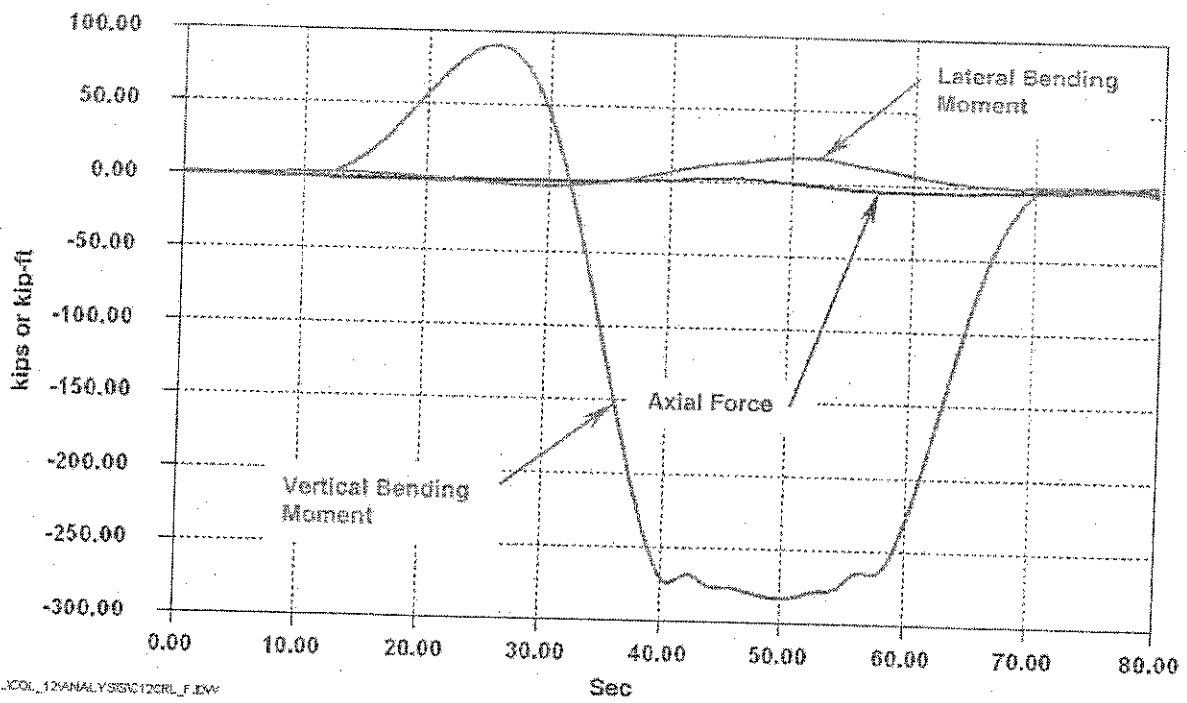


Figure 4.19 - Calculated Axial, Vertical Bending, Lateral Bending and Warping Stresses in the Girder Adjacent to Column 12 (Test Train Headed North at Normal Operating Speed)



D:\V\COL_12\ANALYSIS\12COL_F.EDW

Figure 4.20 - Calculated Axial Force, Vertical Bending Moment, and Lateral Bending Moment in the Girder Adjacent to Column 12 (Test Train Headed North at Crawl Speed)

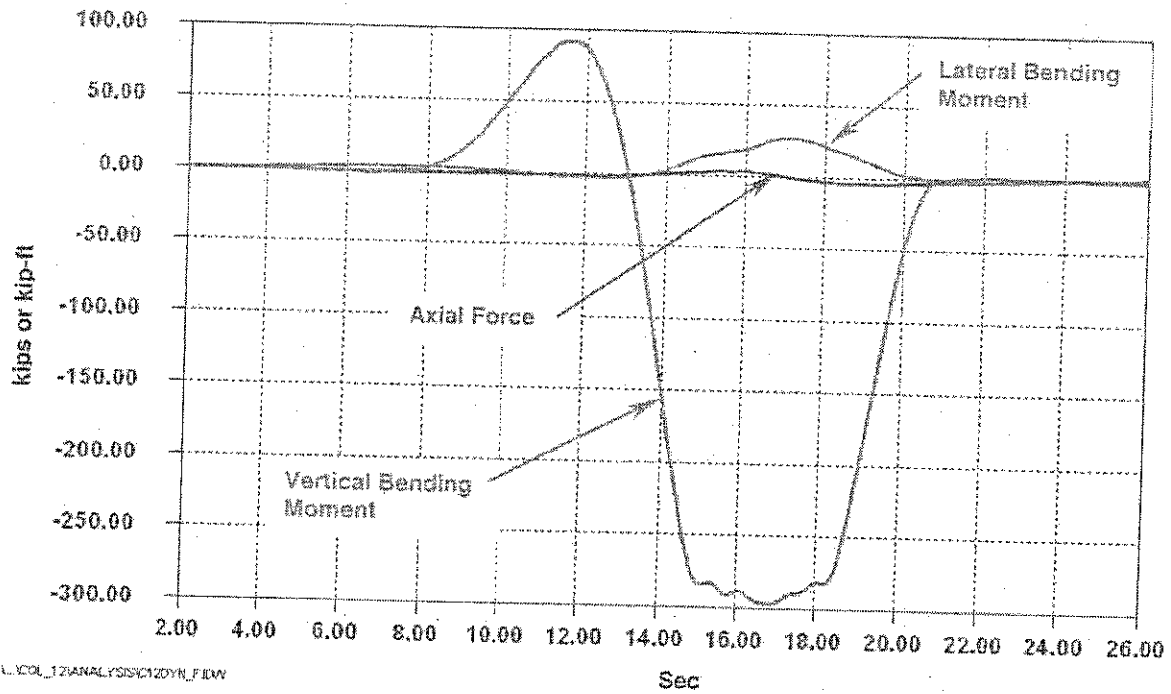


Figure 4.21 - Calculated Axial Force, Vertical Bending Moment, and Lateral Bending Moment in the Girder Adjacent to Column 12 (Test Train Headed North at Normal Operating Speed)

Figure 4.20 is a plot of the calculated axial force vertical bending moment, and lateral bending moment produced as the test train passed at crawl speed. The train was headed north. The vertical bending moment (and thus stress) dominates the response while the axial force and lateral bending moment are very small. The contributions of the warping stress component was found to be negligible.

Figure 4.20 presents the calculated force components for dynamic speed run. There is little difference in the response, although there is slight increase in the lateral bending moment.

4.4 Column 16 – Land Side Girders 234/236

This section of the girder is on a tangent at the end of a horizontal curve approximately 500ft south of Station D1. It is a 3-span continuous structure with column 16 being the first interior column on the south end. The spans on the south and north sides of column 16 are about 131.3ft and 150.3ft respectively and the bearing is fixed. In this area, the trains typically approach station D2 from D1 headed south. The girder is a type IV cross section.

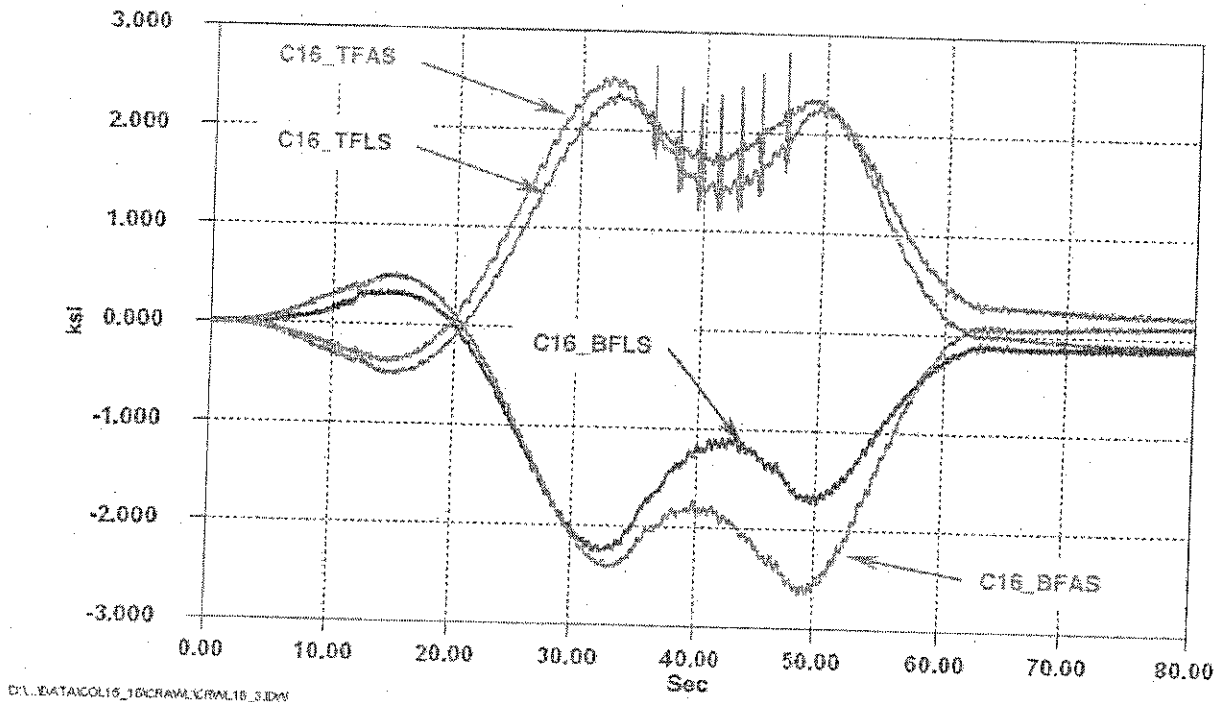


Figure 4.22 – Typical Response Adjacent to Column 16 During Passage of the Test Train (Test Train Headed South at Crawl Speed)

4.4.1 Crawl and Dynamic Tests

The global response at column 16 is slightly different than that observed at the other locations. This change in behavior is related to the length of span vs. the length of the test train. The span lengths of girders 234/236 on either side of column 16 are considerably longer than the 90ft long test train. Thus, maximum negative moments are not produced when the train is directly over the column, but rather when the train is at some point within either span. As a result, two negative moment peaks are produced, leading to the "camelback" type response shown in Figure 4.22.

Knowing the axle spacing of the wheels and assuming a constant speed, the location of the train can be calculated at any point of the test. Calculations show that, for a southbound train, the first peak in negative moment occurs when the front axle of the train is about 22ft-9in north of centerline of bearing column 16. The second peak in negative moment occurs when the rear axle of the train is about 26ft-0in south of centerline of bearing column 16. Although there are two peaks (or valleys) at each gage, the train still only produces *one* dominant stress cycle per passage.

The time history shown in Figure 4.22 was collected as the test train headed south. As the train leaves span 236 and crosses over column 16 into span 234, the measured stresses on each side of the bottom flange become quite different. This is attributed to the fact that lateral bending of the girder is more pronounced with the longer spans (see Section 4.4.2 *Calculation of Forces* for more information).

Regardless of travel direction or speed, the gages did not completely return to zero after the train passed. This is shown in the time history from 70 to 80 seconds (see Figure 4.22). The gages on the land side remained in compression while the gages on the air side remained in tension. This implies a small lateral moment is being "locked" into the girder. This distribution of stress (compression on the land side, tension on the air side) was always observed, regardless of travel direction or speed. The exact cause for this is unknown, however it is likely related to the curvature of the girder and the bearings (boundary conditions). Consideration should be given to field inspection of the bearings supporting this 3-span unit of the guideway under normal operating conditions.

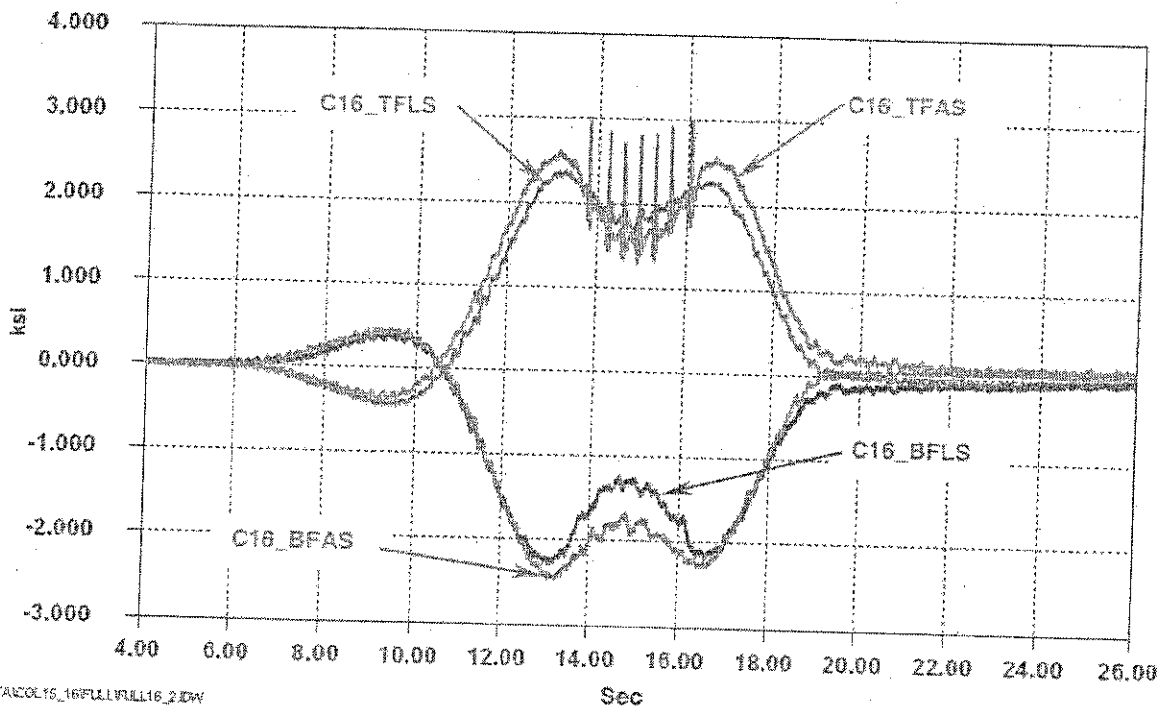


Figure 4.23 – Typical Response Adjacent to Column 16 During Passage of the Test Train (Test Train Headed South at Normal Operating Speed)

Measurements made during a typical southbound test with the train at normal operating speed (100% operating) is presented in Figure 4.23. At the increased speed, the local stresses on the land side of the top flange have increased, while on the air side, local stresses decreased. This is consistent with the behavior observed at other locations on a horizontal curve (e.g., column 12). The results of the intermediate and normal operating speed tests conducted at column 16 are summarized in Table 4.6.

As the train leaves span 236 at normal operating speed and crosses over column 16 into span 234, the stresses measured on each side of the bottom flange do not differ by the same magnitude as observed during the crawl tests. Apparently, the centrifugal and overturning forces applied by the faster moving train combine such that vertical bending dominates the stress cycle. This response does not alter the total stress range.

Location	Crawl Tests			60% Operating			100% Operating		
	S_{min}	S_{max}	S_r	S_{min}	S_{max}	S_r	S_{min}	S_{max}	S_r
C16 BFLS	-2.2	0.3	2.5	-2.2	0.3	2.5	-2.2	0.4	2.6
C16 BFAS	-2.6	0.5	3.1	-2.5	0.5	3.0	-2.4	0.5	2.9
C16 TFLS	-0.5	2.3	3.3 ¹	-0.5	2.3	3.4 ¹	-0.4	2.3	3.4 ¹
C16 TFAS	-0.4	2.5	2.9 ¹	-0.4	2.5	2.9 ¹	-0.4	2.6	2.9 ¹
C16 TFLS ²	-	-	1.0 ²	-	-	1.1 ²	-	-	1.3 ²
C16 TFAS ²	-	-	0.9 ²	-	-	0.7 ²	-	-	0.6 ²

Notes:

1. Includes local effects of wheel loads.
2. Stress range produced by local effects of wheel load only.
3. S_{min} = minimum stress, S_{max} = maximum stress, S_r = "peak to peak" stress range

Table 4.6 – Summary of Response at Column 16
for Controlled Load Tests

4.4.2 Calculation of Forces

Using the data acquired at each corner of the box girder, the axial, vertical bending, lateral bending, and warping stress components were calculated. The assumed positive sign convention is the same as the previous locations. Local effects were removed from the data so as not to bias the calculations.

Figures 4.24 & 4.25 present the calculated stress and force components for a typical test run conducted at crawl speed. As mentioned above, a small amount of stress is locked into the girder as the train passes. However, Figure 4.25 clearly indicates that the locked force components are a rather small percentage of the live-load effects.

As can be seen from Table 4.6, there was little difference in the stress range produced during crawl and normal operating speed tests. Although not shown here, the force components calculated for the normal operating speed tests are essentially identical to those calculated for the crawl tests.

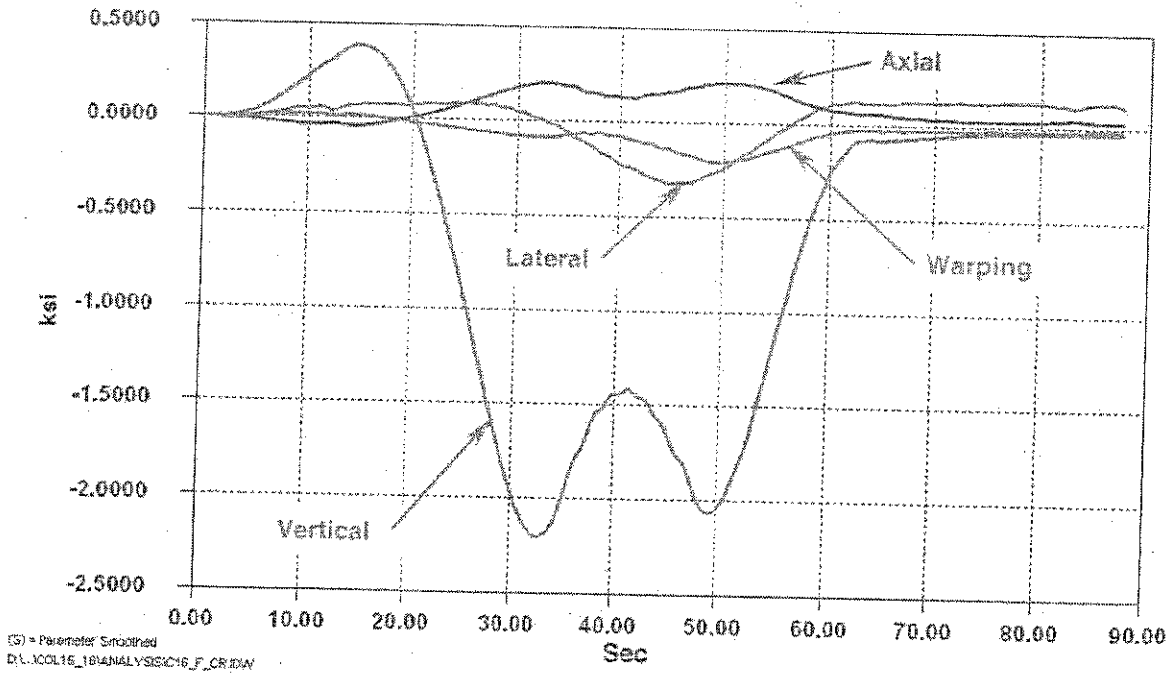


Figure 4.24 - Calculated Axial, Vertical Bending, Lateral Bending, and Warping Stress Components in the Girder Adjacent to Column 16 (Test Train Headed South at Crawl Speed)

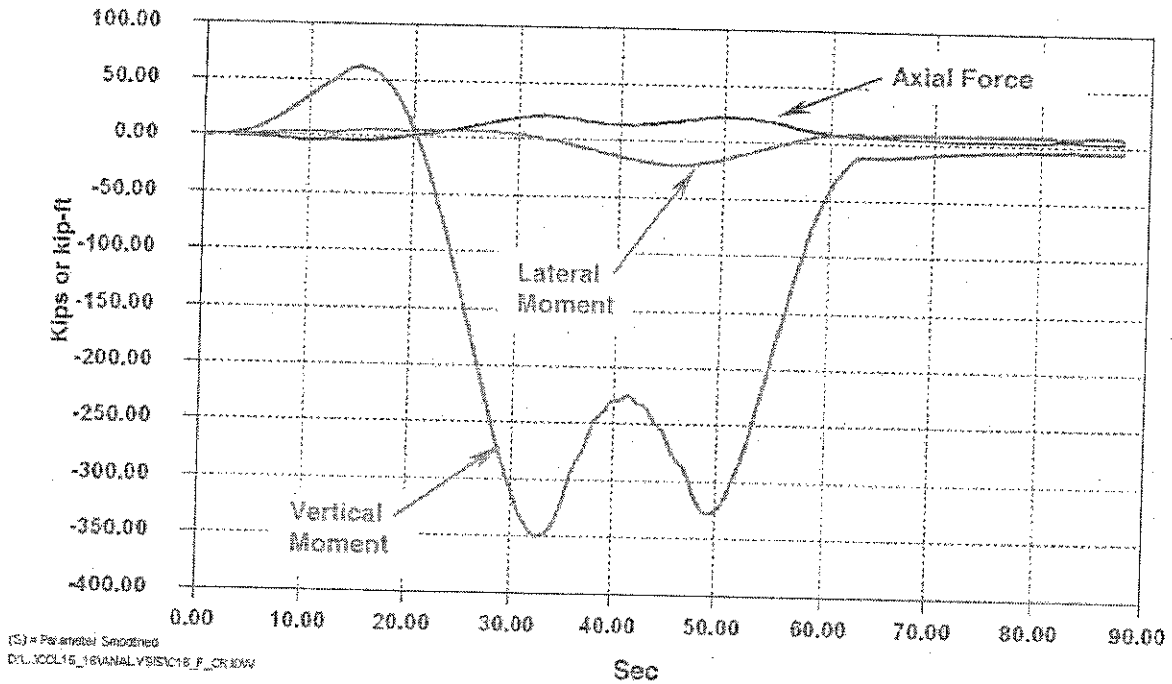


Figure 4.25 - Calculated Axial Force, Vertical Bending Moment, and Lateral Bending Moment in the Girder Adjacent to Column 16 (Test Train Headed South at Crawl Speed)

4.5 Column 26 – Land Side Girders 148/150

This section of the girder is on a horizontal curve approximately 700ft north of Station D1. It is a 3-span continuous structure with column 26 the first interior column on the south end. The spans on the south and north sides of column 26 are about 101.5ft and 155.4ft respectively and the bearing is fixed. In this area, the trains typically approach station D1 from Terminal A headed south. The girder is a type VI cross section. Because of lockout arrangements, only crawl tests could be conducted. Random empty trains were recorded and used for the dynamic data. The gages at this section are located 5ft-4in south of column 26. The data obtained from the triaxial rosettes mounted on the top flange are discussed in Section 4.5.3.

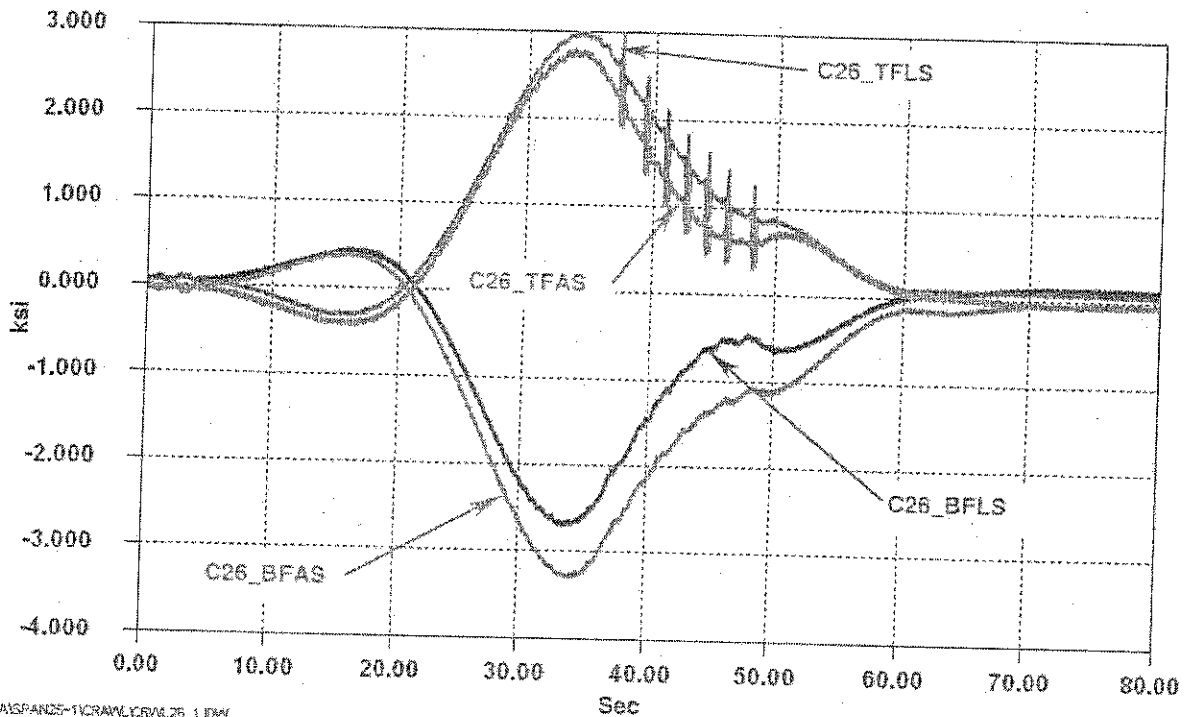


Figure 4.26 – Typical Response Adjacent to Column 26 During Passage of the Test Train (Test Train Headed South at Crawl Speed)

4.5.1 Crawl and Dynamic Tests

The results of the crawl and dynamic tests are summarized in Table 4.7. Figure 4.26 illustrates the response at column 26 for the gages installed on the edges of the top and bottom flanges. For this test, the train was headed south at crawl speed. The maximum negative moment at the instrumented section occurred before the train reached the gages. Only one major peak is produced because span 148 is relatively short compared to span 150 and the length of the train (span 148 is about 55ft shorter than span 150 and about 11ft longer than the train). When the last set of wheels are crossing the gages, the front of the train is only about five feet from the expansion joint at column 25. Based on the measurements, calculations indicate the peak negative moment occurs when

the front axle of the train is about 20ft north of centerline of column 26. The passage of each train produces only one primary stress cycle.

As the train passes over column 26, the global stresses begin to decrease rapidly and the increases due to local stresses produced by the wheels do not increase the peak stress range (S_{rmax}). This phenomenon only occurred at column 26. At other instrumented locations, the stress ranges produced by the individual wheels increased the total stress range.

Location	Crawl Tests			60% Operating			100% Operating		
	S_{min}	S_{max}	S_r	S_{min}	S_{max}	S_r	S_{min}	S_{max}	S_r
C26_BFLS	-2.7	0.4	3.1	N/A	N/A	N/A	-2.9	0.4	3.3
C26_BFAS	-3.3	0.4	3.7	N/A	N/A	N/A	-3.2	0.5	3.7
C26_TFLS	-0.3	3.0	3.3 ¹	N/A	N/A	N/A	-0.4	2.9	3.3 ¹
C26_TFAS	-0.4	2.8	3.2 ¹	N/A	N/A	N/A	-0.4	3.1	3.5 ¹
C26_TFLS ²	-	-	0.7 ²	-	-	N/A	-	-	1.0 ²
C26_TFAS ²	-	-	0.9 ²	-	-	N/A	-	-	0.7 ²

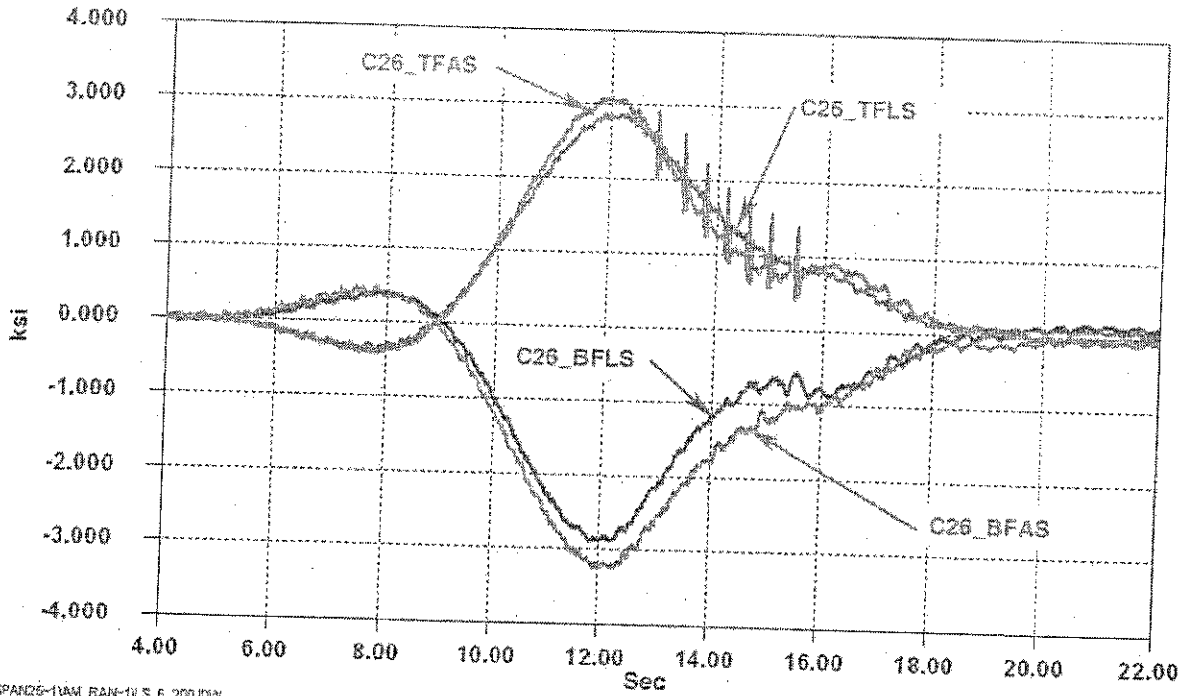
Notes:

1. Includes local effects of wheel loads.
2. Stress range produced by local effects of wheel load only.
3. S_{min} = minimum stress, S_{max} = maximum stress, S_r = "peak to peak" stress range

Table 4.7 – Summary of Response at Column 26
for Controlled Load Tests

Figure 4.27 illustrates the dynamic response at column 26 as a random empty train crossed. Measurements were made during the passage of several random southbound trains.

Comparing the data in Table 4.7, and Figures 4.26 and 4.27, it is apparent that there is only a slight difference between the crawl and dynamic response. Overall, the measurements were consistent and the behavior was as expected. The direction of travel had no unexpected influence on behavior.



D:\L\SPAN26-11\W\RAIN-1LS_6_200.D\W

Figure 4.27 – Typical Response Adjacent to Column 26 During Passage of a Random Train (Random Southbound Train at Normal Operating Speed, 6:33AM, September 2, 1999)

4.5.2 Calculation of Forces

Axial, vertical bending, lateral bending, and warping stresses calculated for a southbound crawl run are plotted in Figure 4.28. The dominant component of the stress cycle is the vertical bending stress. The other three components are small in comparison. The stress components from a random southbound train traveling at 100% operating speed are presented in Figure 4.29. Overall, there was little difference between the crawl and dynamic test results.

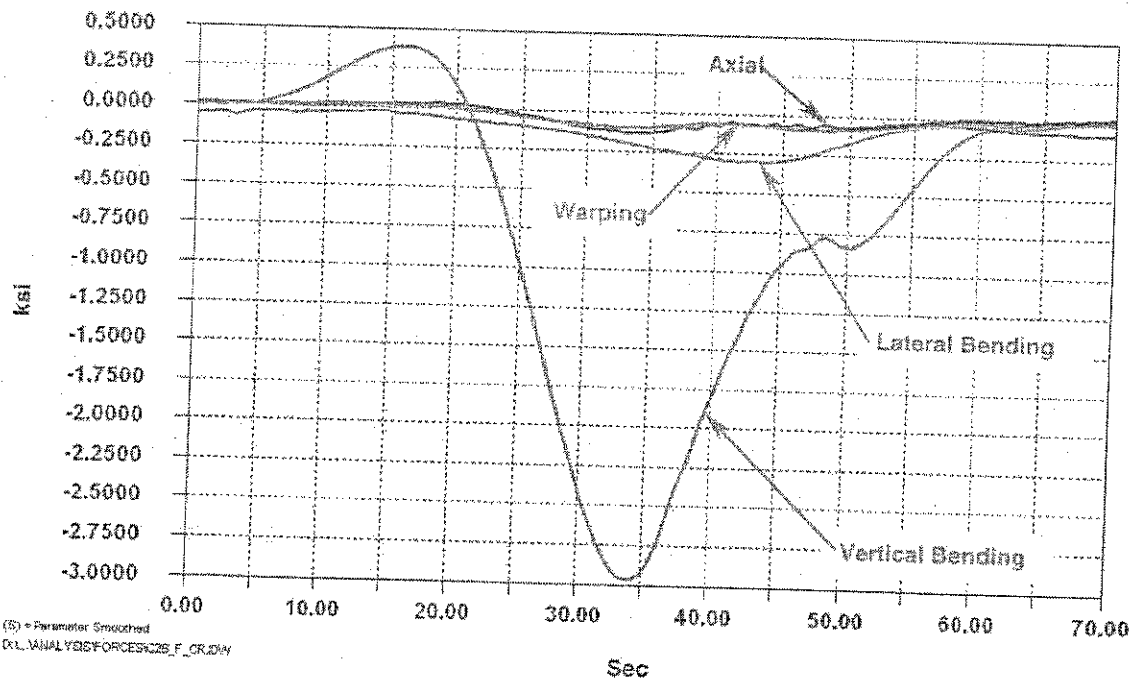


Figure 4.28 - Calculated Axial, Vertical Bending, Lateral Bending, and Warping Stress Components at Column 26 (Test Train Headed South at Crawl Speed)

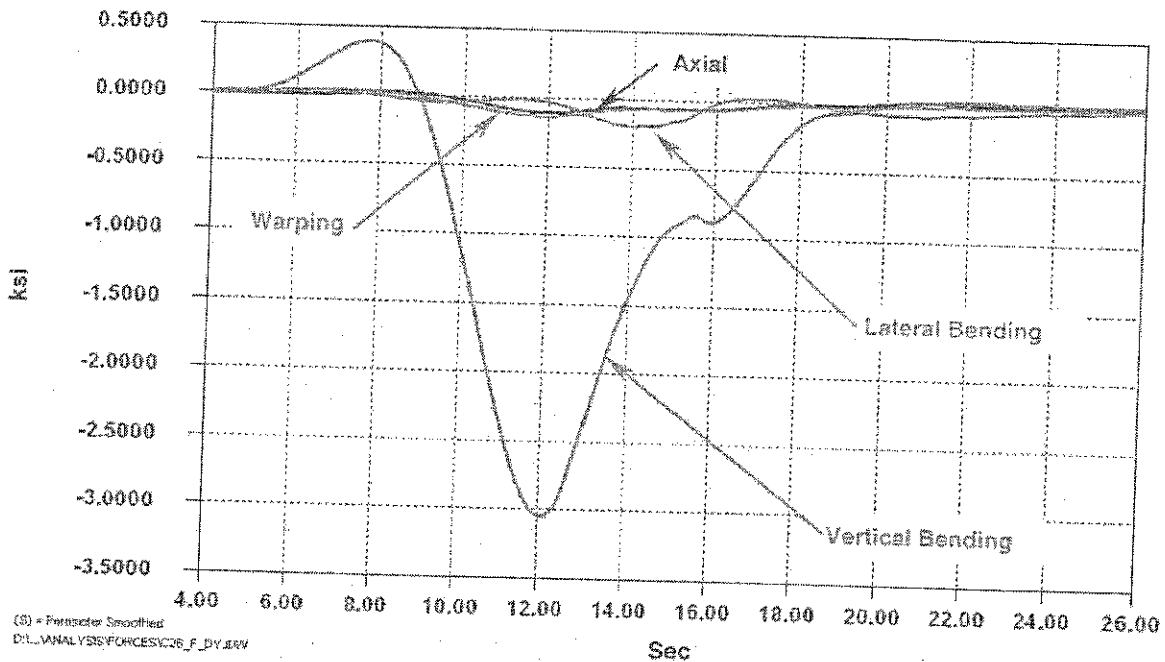


Figure 4.29 - Calculated Axial, Vertical Bending, Lateral Bending, and Warping Stress Components at Column 26 (Random Train Traveling at Normal Operating Speed Headed South)

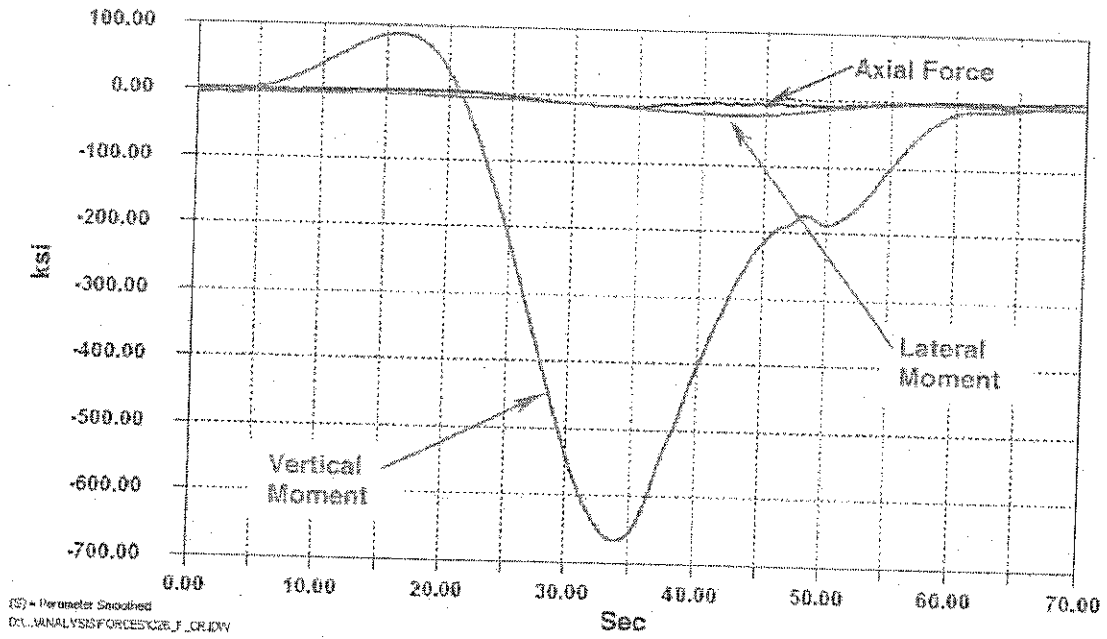


Figure 4.30 - Calculated Axial Force, Vertical Bending Moment, and Lateral Bending Moment in the Girder Adjacent to Column 26 (Test Train Headed South at Crawl Speed)

Figure 4.30 presents the calculated force components at Column 26 as the test train passed at a crawl speed. As expected, the dominant force component is the vertical moment. Although not shown, the force components were calculated for a typical empty train running at normal operating speed. The force components were relatively unchanged, as shown in the plots of the stress components (compare Figures 4.28 and 4.29).

4.5.3 Tri-axial Rosettes

Tri-axial stacked rosettes were installed on the top flange of the box girder at the same cross section as the other instrumentation adjacent to column 26. The gages were placed in the "bath tub" region of the guideway and approximately one inch from the support bar weld toe, as shown in Figure 3.7. The center "leg" of each gage was oriented perpendicular to the weld toe in order to determine the transverse stress range at the weld toe. Transverse membrane and/or plate bending stresses in the top flange could produce longitudinal weld toe cracking at the top flange. Similar cracking has been observed on some thin orthotropic steel decks used in highway bridges.

Figure 4.31 presents the response of gages located on the land side and air side of the bath tub oriented perpendicular to the support bar weld toe for a crawl test. Similar to the gages placed on the edges of the top flange, the effect of each wheel is apparent in the response. The stress range is about 2.6ksi and 1.6ksi on the land side and air side gages respectively. During the passage of a random train carrying about 50 passengers (estimated), the maximum stress range at the land side gage was just less than 3.0ksi. This may also be attributed to the increased speed of the train and the additional downward forces induced by the train "leaning" toward the land side.

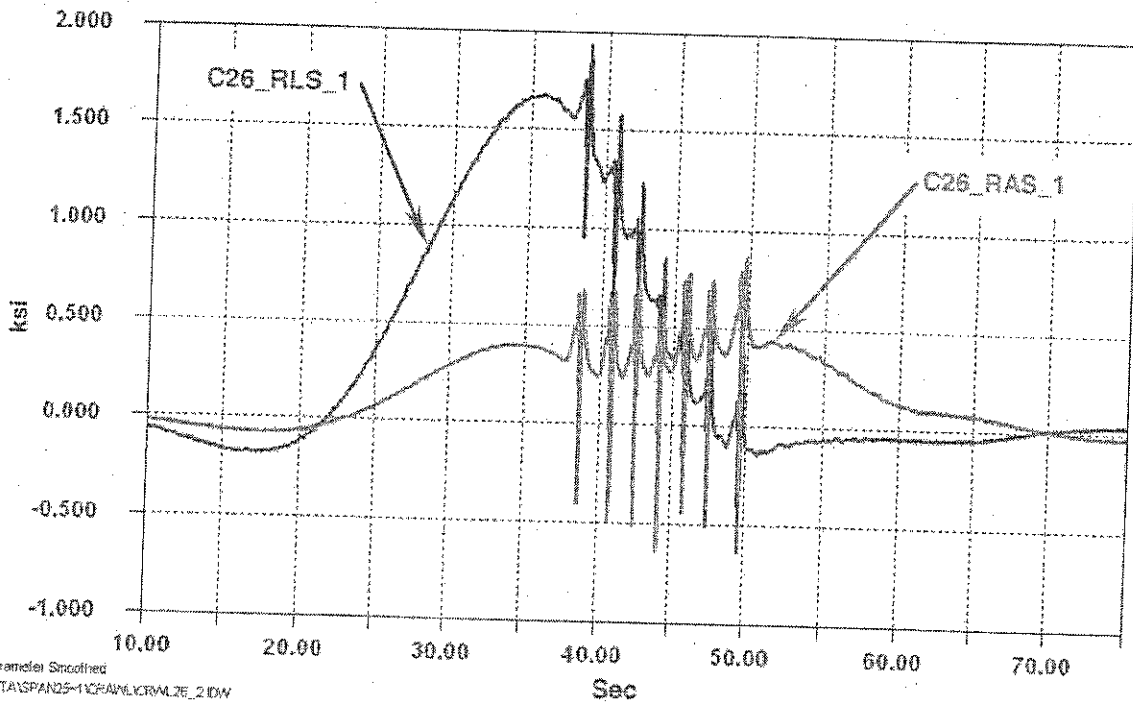


Figure 4.31 - Measured Stresses on Top Flange Perpendicular to Support Bar Weld Toe in Bath Tub Region Adjacent to Column 26. (Test Train Passing at Crawl Speed Headed South)

Principle strains ($\mu\epsilon$) were calculated for a typical crawl test and are presented in Figure 4.32 for both the land side and air side gages respectively. Also shown in Figure 4.32 is the strain ($\mu\epsilon$, (i.e., C26_RLS_1 or C26_RAS_1)) measured perpendicular to the support bar weld toe. As expected, the principal strain is larger than the strain perpendicular to the weld toe. The principal axis was typically oriented within 10 to 15 degrees of being perpendicular to weld toe.

Note that the data are presented in units of micro-strain instead of stress. These units were selected in order to provide some information on the magnitude of the surface strains produced in the "as-built" top flange. Although these data are only valid for this location, it is likely that they reasonably represent the behavior of other girders and that the magnitude of strains elsewhere are of the same order of magnitude.

Overall, the rosettes did not reveal any unexpected behavior at this location. Relatively small transverse strains are produced in the bathtub and adjacent to the support bar weld toe as each train passes.

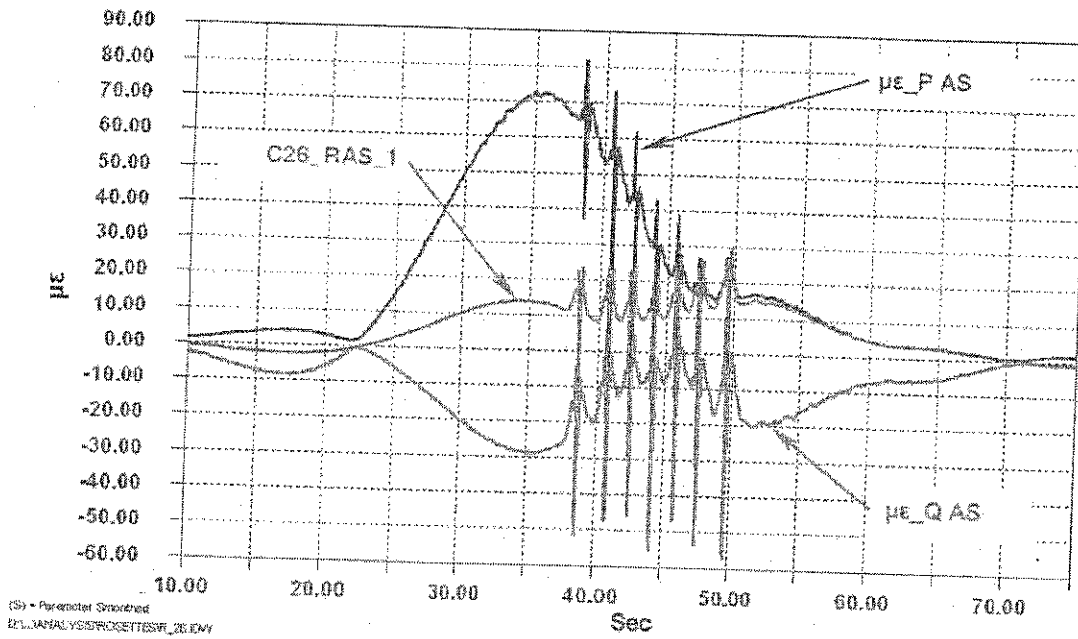
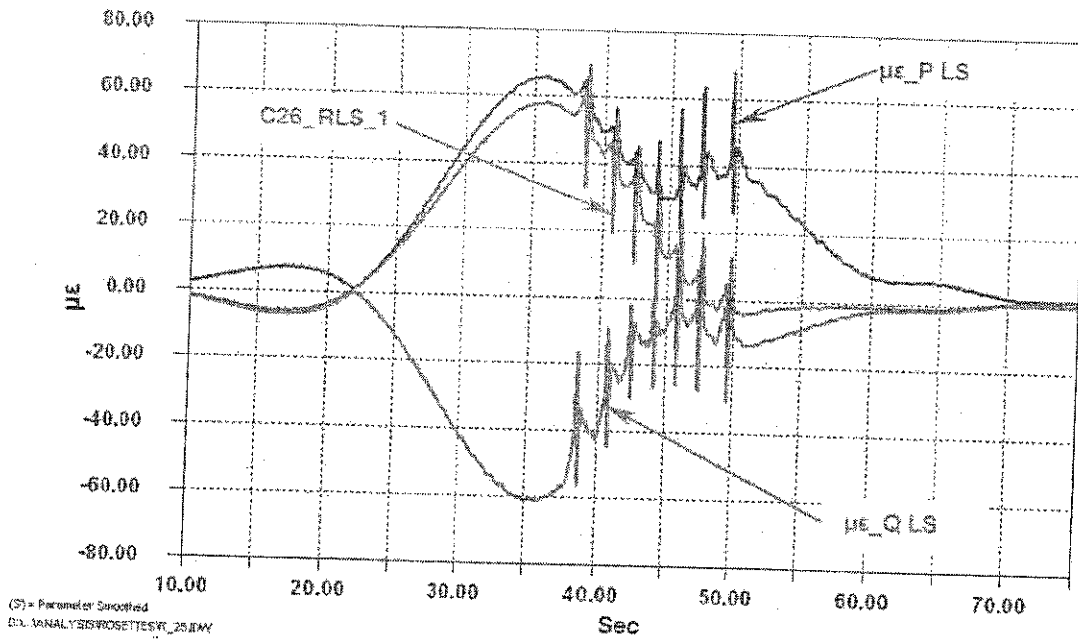


Figure 4.32 - Calculated Principle Strains on the Land Side and Air Side of the Top Flange in the Bath Tub Region Adjacent C26 and Measured Strains Adjacent to the Support Bar (Test Train Passing at Crawl Speed Headed South)

4.6 Span 148 – Land Side Girder

This section of the girder is on a horizontal curve approximately 700ft north of Station D1. It is the south end span of a 3-span continuous structure. Span 148 is 155.4ft long. In this area, the trains typically approach station D1 from Terminal A headed south. The girder is a type VI cross section. Because of lockout arrangements, only crawl tests could be conducted with the test train. Random empty trains were recorded and used for the dynamic data. The data obtained from the triaxial rosettes mounted on the top flange are discuss in Section 4.6.3.

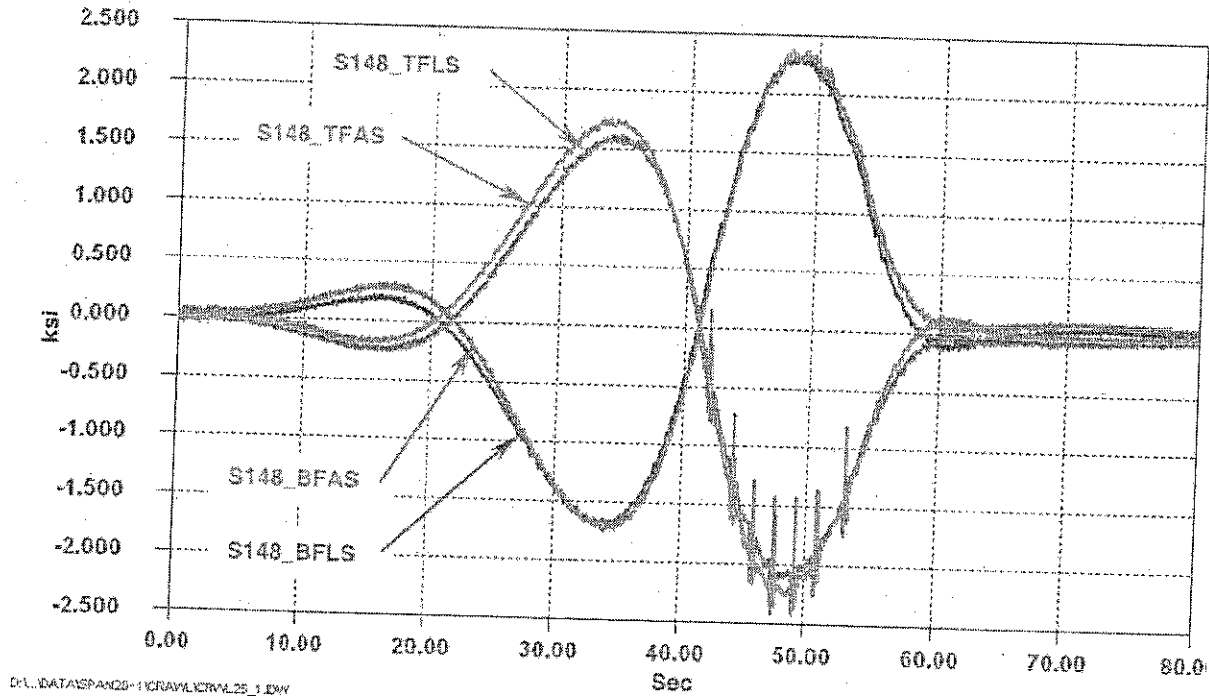


Figure 4.33 – Typical Response Adjacent to Span 148 During Passage of the Test Train (Test Train Headed South at Crawl Speed)

4.6.1 Crawl and Dynamic Tests

The results of the crawl and dynamic tests are summarized in Table 4.8. Figure 4.33 illustrates the response at span 148 for the gages installed on the edges of the top and bottom flanges. As expected, the response at midspan is considerably different than that observed adjacent to column 26 (see Section 4.5). Note the significant reversal in stress as the train leaves span 150 and passes into span 148. A negative moment is produced in span 148 when the train is located in span 150.

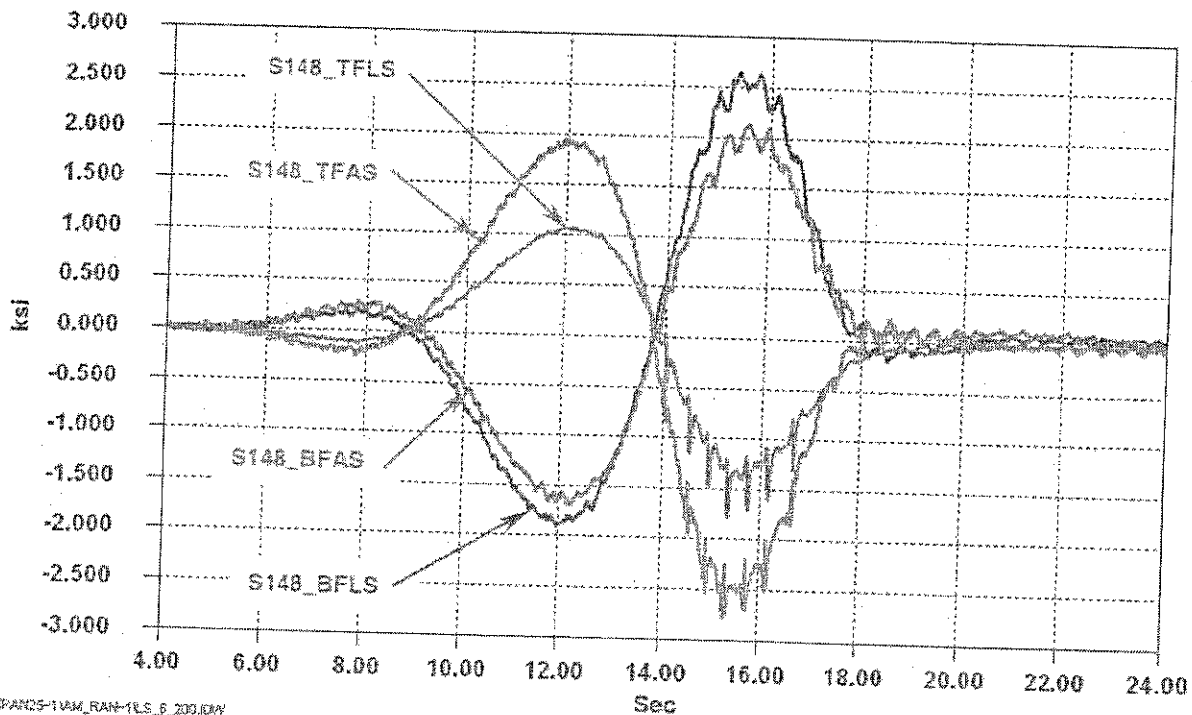
The global bending stresses overshadow the local stress range produced by the individual wheel loads in the top flange and the flange remains in compression as the wheels pass.

Location	Crawl Tests			60% Operating			100% Operating		
	S_{min}	S_{max}	S_r	S_{min}	S_{max}	S_r	S_{min}	S_{max}	S_r
C26 BFLS	-1.7	2.3	4.0	N/A	N/A	N/A	-1.9	2.7	4.6
C26 BFAS	-1.7	2.4	4.1	N/A	N/A	N/A	-1.6	2.2	3.8
C26 TFLS	-2.1	1.6	4.0 ¹	N/A	N/A	N/A	-1.4	1.1	2.9 ¹
C26 TFAS	-2.2	1.7	4.2 ¹	N/A	N/A	N/A	-2.5	1.9	4.7 ¹
C26 TFLS ²	-	-	1.0 ²	-	-	N/A	-	-	0.6 ²
C26 TFAS ²	-	-	0.7 ²	-	-	N/A	-	-	0.5 ²

Notes:

1. Includes local effects of wheel loads.
2. Stress range produced by local effects of wheel load only.
3. S_{min} = minimum stress, S_{max} = maximum stress, S_r = "peak to peak" stress range

Table 4.8 – Summary of Response at Span 148
for Controlled Load Tests



DA...SPAN25-1VAM_RAN-1LS_6_200.DWG

Figure 4.34 – Typical Response Adjacent to Span 148 During Passage of a Random Train
(Random Empty Southbound 6:33AM, September 2, 1999, Normal Operating Speed)

Figure 4.34 illustrates the dynamic response at Span 148 as a random empty train crossed at 6:33AM on September 2nd. There is a noticeable difference in the time history data from the crawl and dynamic tests. Figure 4.35 compares the response of the top flange for crawl and dynamic runs. During the crawl run, the top flange gages track about the same as the test train passes. However, when the train passes at normal operating speed, the minimum and maximum stresses are different. The peak stresses on the air side of the top flange increase while decreasing on the land side. A review of Figures 4.33 & 4.34 indicates the opposite is true on the bottom flange. This suggests that there is an increase in *lateral* moments as the train passes at operating speed. If the change was the result of an increase in torsional warping moments, stresses would increase (or decrease) on diagonally opposite corners of the box (see Figure 4.7). This observation was subsequently verified by calculations of the force components.

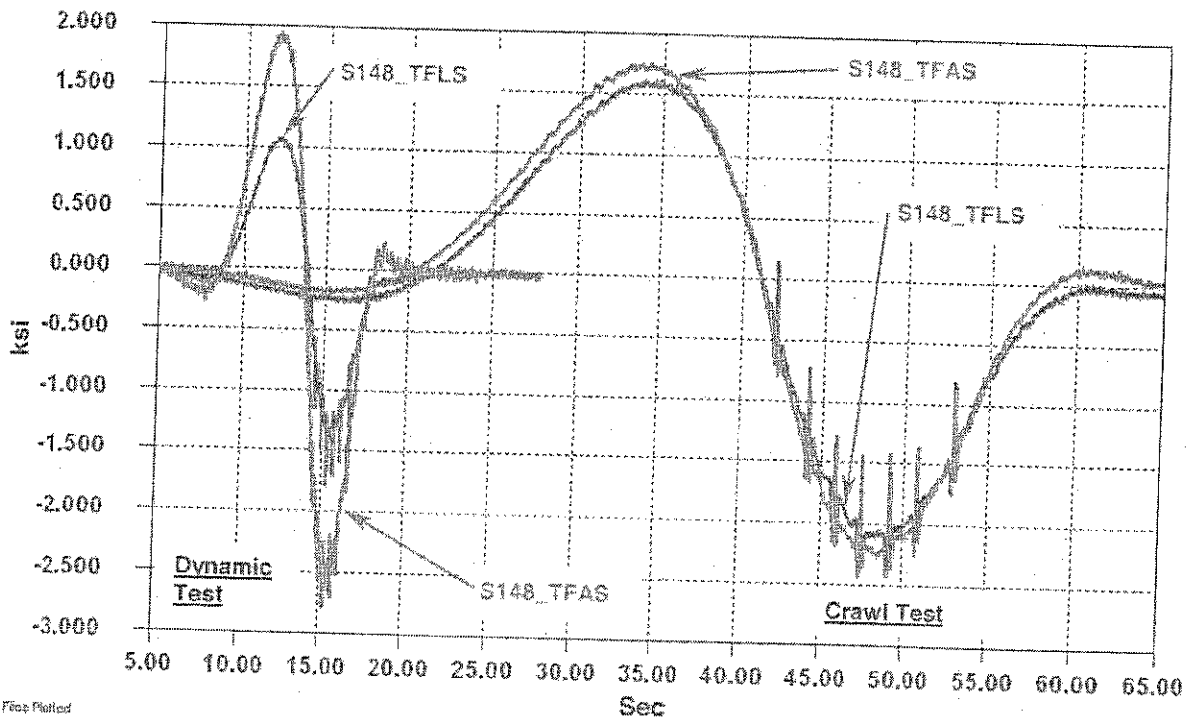


Figure 4.35 – Response of Top Flange for Crawl and Dynamic (100% Operating) Speed Tests (Note the Increase and Decrease in Peak Stress Values)

4.6.2 Calculation of Forces

Calculated axial, vertical bending, lateral bending, and warping stress components are plotted in Figure 4.36 for a southbound crawl run. The vertical bending component clearly dominates the stress cycle. The other three components are negligible. As stated above, under dynamic loading, the response of the girder was quite different.

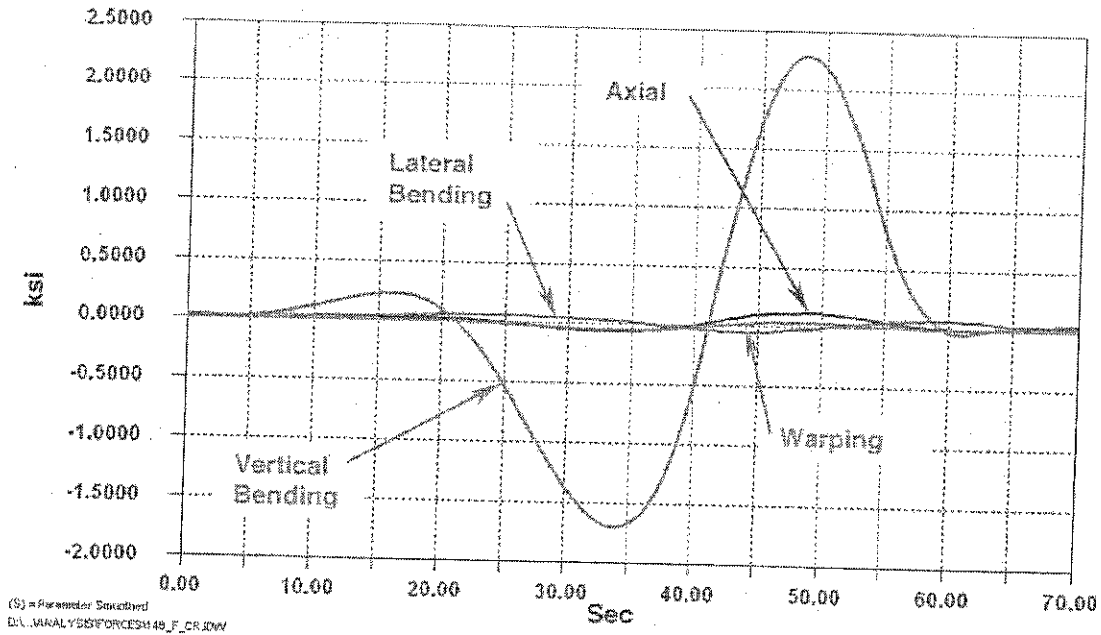


Figure 4.36 - Calculated Axial, Vertical Bending, Lateral Bending, and Warping Stress Components in Span 148
(Test Train Passed at Crawl Speed Headed South)

The calculated stress components are presented in Figure 4.37 for a random southbound train traveling at 100% operating speed. Note the increase in the lateral bending stress component for the dynamic test as compared to the crawl test. This observation is consistent with the data shown in Figures 4.33 and 4.34. The axial and warping stresses also increase slightly.

Figure 4.38 presents the calculated axial force, vertical bending moment, and lateral bending moments for the train shown in Figure 4.37. Although the lateral moment increased, the vertical bending moment again dominates the response of the girder.

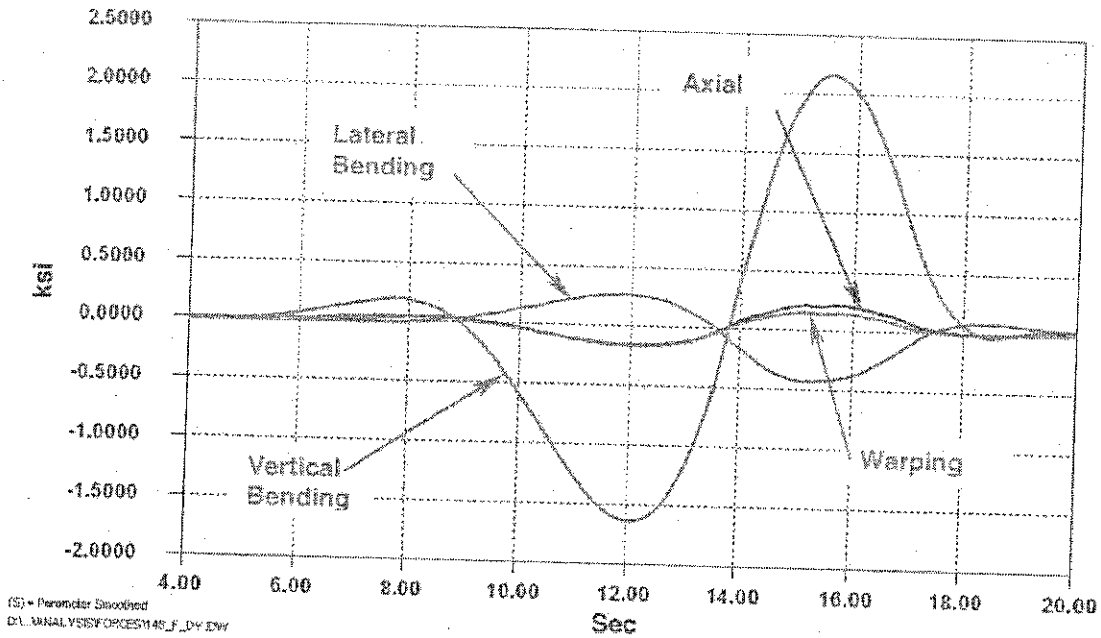


Figure 4.37 - Calculated Axial, Vertical Bending, Lateral Bending, and Warping Stress Components in Span 148
 (Random Train Traveling at Normal Operating Speed Headed South)

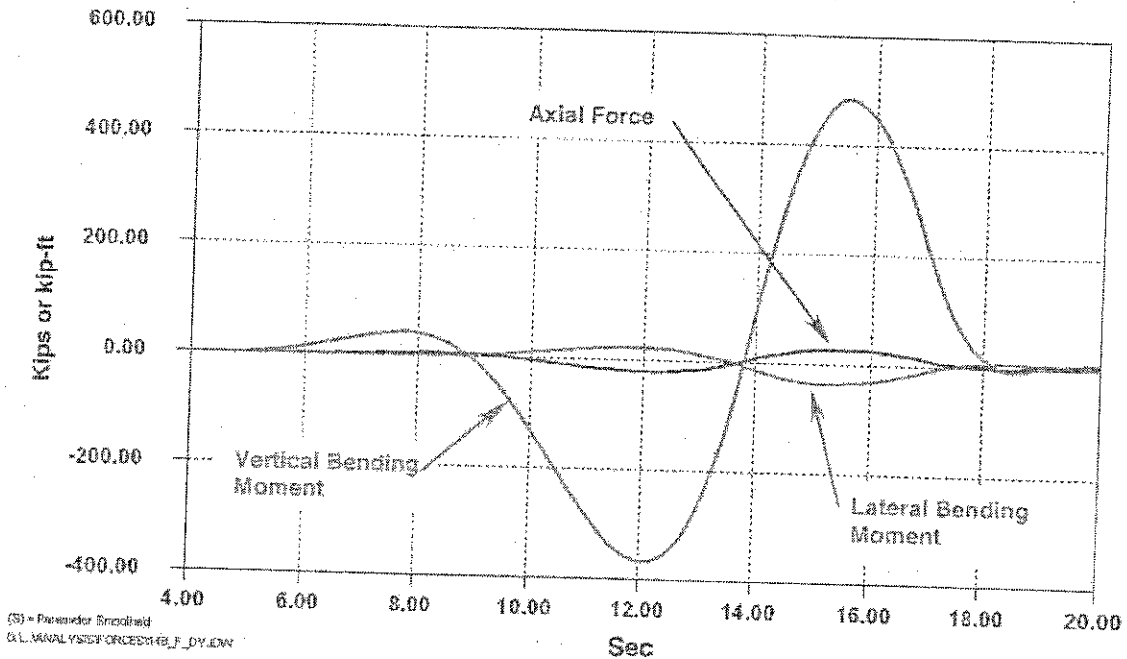


Figure 4.38 - Calculated Axial Forces, Vertical Bending Moments, and Lateral Bending Moments in Span 148
 (Random Train Passing at Normal Operating Speed Headed South)

4.6.3 Tri-axial Rosettes

Tri-axial rosettes were installed on the top flange of the box girder at the same cross section as the other instrumentation located near midspan of span 148. The gages were placed in the "bath tub" region of the guideway and approximately one inch from the support bar weld toe, as shown in Figure 3.6. The center "leg" was oriented perpendicular to the longitudinal support bar weld toe in order to measure transverse membrane and/or plate bending stresses in the top flange adjacent to the support bar weld toe.

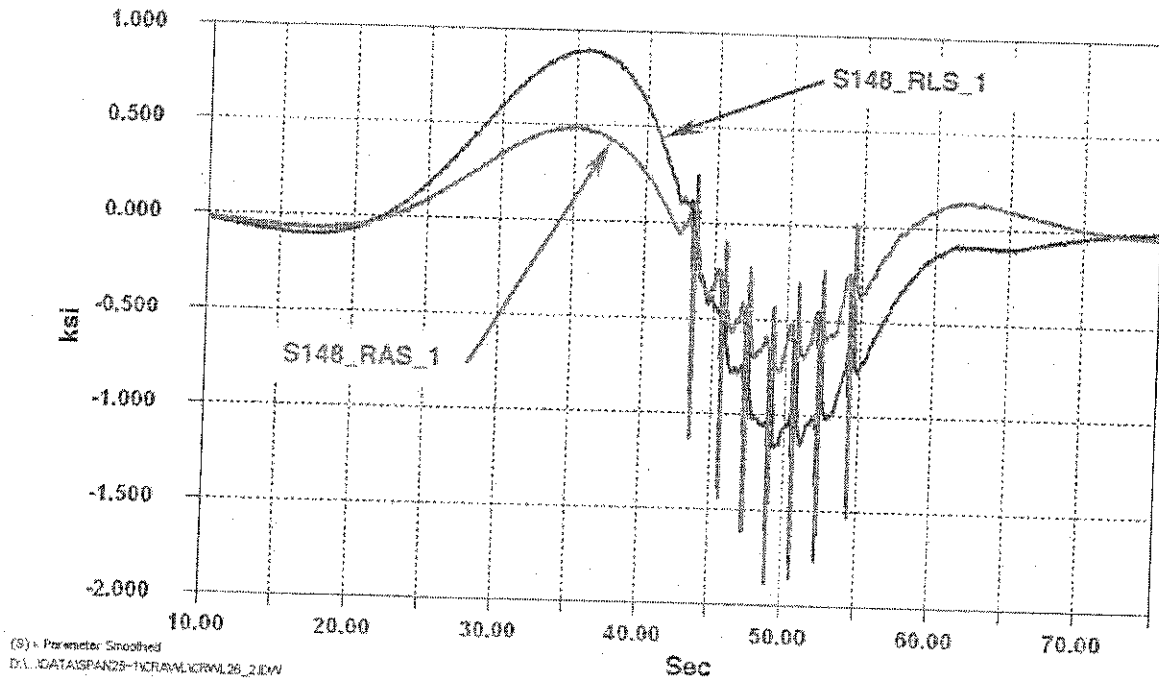


Figure 4.39 - Measured Stresses on Top Flange Perpendicular to Support Bar Weld Toe in Bath Tub Region in Span 148 (Test Train Passing at Crawl Speed Headed South)

Figure 4.39 presents the response of gages located on the land side and air side of the bath tub oriented perpendicular to the support bar weld toe for a crawl test. The response of these rosettes is similar to those located adjacent to column 26. The effect of each wheel is apparent in the response. The stress range is about 2.8ksi and 2.4ksi on the land side and air side gages respectively. Dynamic tests were not conducted during the controlled tests at this location. However, during the passage of random trains carrying about 50 passengers (estimated), the maximum stress range at the land side gage was 3.0ksi. This may also be attributed to the increased speed of the train and the additional downward forces induced by the train "leaning" toward the land side.

Figure 4.40 presents the calculated principle strains along with the strain measured perpendicular to the support bar weld toe for both rosettes. As expected, the principal strain is larger than the strain perpendicular to the weld toe. Though not shown on the plot for clarity, the principal axis was typically oriented within 10 to 20 degrees of being perpendicular to weld toe.

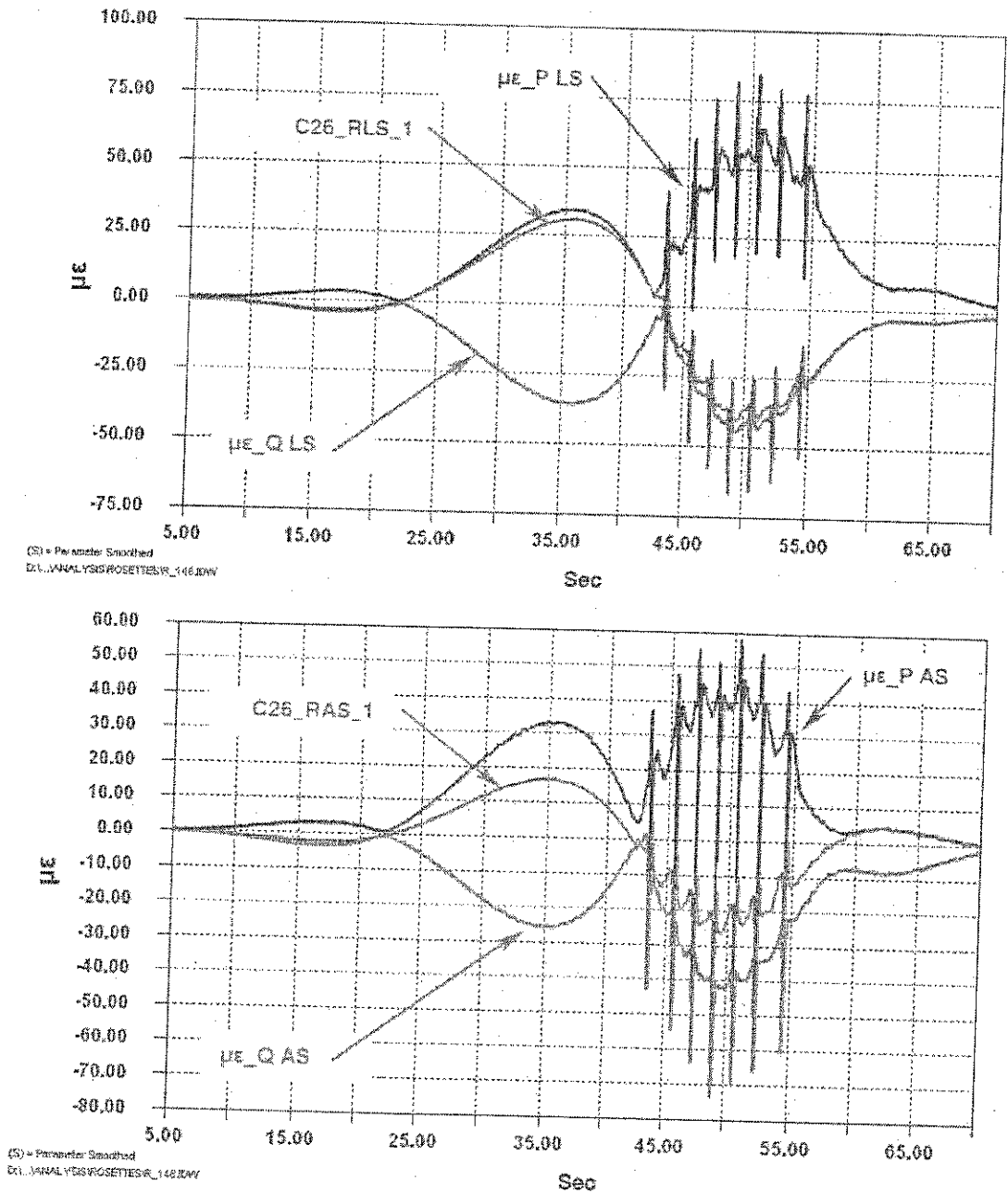


Figure 4.40 - Calculated Principle Strains on the Land Side and Air Side of the Top Flange in the Bath Tub Region adjacent Span 148 and Measured Strains Adjacent to the Support Bar (Test Train Passing at Crawl Speed Headed South)

The data are presented in units of micro-strain instead of stress to provide information on the magnitude of surface strains produced in the "as-built" top flange. Although these data are only valid for this location, it is likely that they reasonably represent the behavior of other girders and that the magnitude of strains elsewhere are of the same order of magnitude.

Overall, the rosettes did not reveal any unexpected behavior. Relatively small transverse strains are produced in the bathtub and adjacent to the support bar weld toe as the train passes.

5.0 Results of Uncontrolled Monitoring

5.1 Results of 24 Hour Monitoring at Column 07

All four gages installed at column 07 were monitored for a period of 24 hours beginning at 12:00AM on September 27, 1999. Triggered time histories and stress-range histograms were collected during the period.

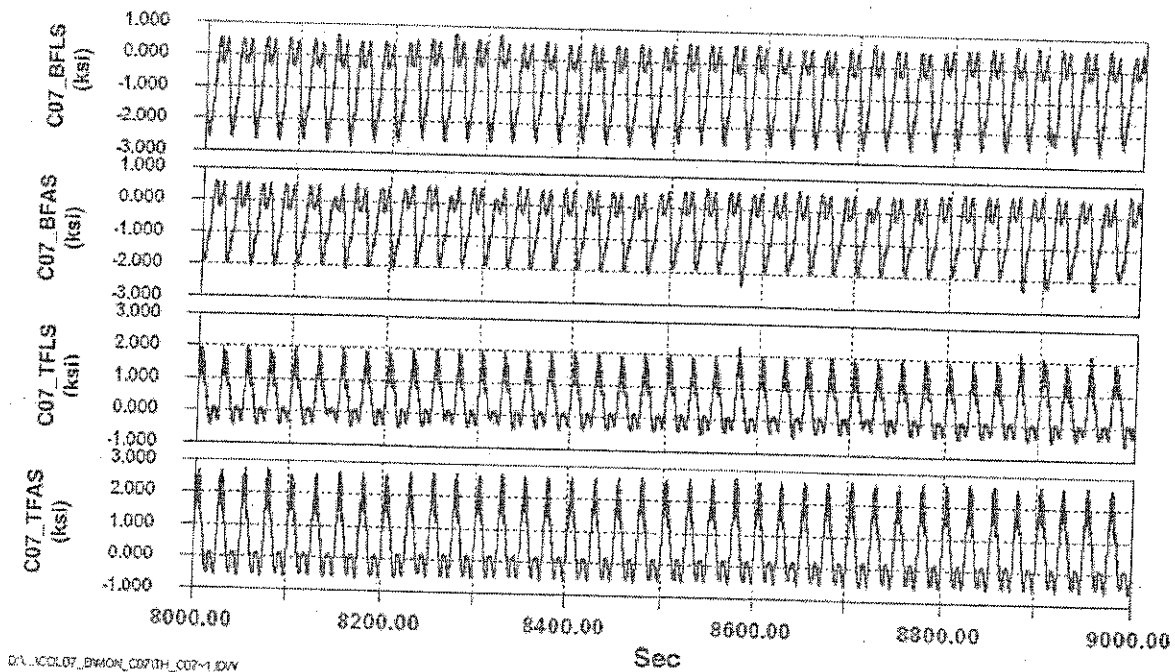


Figure 5.1 – Portion of Triggered Time History Collected at Column 07 During the 24 Hour Uncontrolled Monitoring Period

Figure 5.1 is a small portion of the triggered time history data for the channels installed at column 07 and is typical for the entire 24 hours. There is little variation in stress range or peak stress values. The data are also consistent with the controlled load tests.

The histogram data for channel C07_BFLS is presented at 3 hour intervals in Table 5.1. (The table begins at 3:00AM since there are zero cycles in all bins for the 12:00AM interval.) Recall that in Table 4.1, each train produced a single, dominant stress cycle of about 3.0ksi at gage C07_BFLS. Thus, it is possible to estimate the number of trains by counting only the number of cycles greater than 2.5ksi. For example, between 6:00AM and 9:00AM, it is estimated that 41 trains passed over column 07 ($101 - 60 = 41$). Considering all data listed in Table 5.1, it is estimated that 415 trains producing stresses exceeding 2.5ksi crossed the span during the 24 hour monitoring period. This works out to about one train every 3½ minutes.

Bin (ksi)	Time of Day (September 27 th , 1999)							
	3:00AM	6:00AM	9:00AM	12:00PM	3:00PM	6:00PM	9:00PM	12:00AM
	Cumulative Number of Cycles in Each Bin							
0.5-1.0	26	72	140	257	390	488	562	617
1.0-1.5	0	0	1	3	5	5	5	5
1.5-2.0	0	0	0	0	1	1	1	1
2.0-2.5	0	0	0	0	0	0	0	0
2.5-3.0	1	2	2	2	2	3	3	3
3.0-3.5	25	58	99	162	237	304	366	406
3.5-4.0	0	0	0	2	4	5	5	5
4.0-4.5	0	0	0	0	1	1	1	1

Figure 5.1 – Stress-Range Histogram Presented at Three Hour Intervals
Data Collected at Column 07 During the 24 Hour Uncontrolled Monitoring Period
(Channel C07_BFLS Shown)

Table 5.1 also indicates that the peak stress range produced by random trains was around 3.0ksi to 3.5ksi for this strain gage and does not vary significantly. This also implies that empty and loaded trains produce similar stress ranges (3.0ksi to 3.5ksi) throughout the day at this location. Similar results were obtained at all four gages.

Stress-range histograms for all four channels are summarized in Table 5.2 for the entire 24 hour monitoring period. Also listed in Table 5.2 are the effective stress range (S_{eff}) and the maximum stress range (S_{max}) measured during the 24 hour period. The effective stress range was calculated by ignoring all cycles less than 0.5ksi. As noted previously, it is estimated that 415 trains passed over column 07. Note the large number of cycles between 0.5ksi and 1.0ksi for the gages mounted on the top flange as compared to the bottom flange gages. Most of the additional cycles are produced by the individual wheels of the train. This can be verified by multiplying the number of trains per day (415) by the number of axles per train (7). For both top flange gages, this works out to about 2,900 wheels/day (cycles/day), which is in very good agreement with the number listed in the 0.5ksi to 1.0ksi bin. The remaining cycles were produced as part of the random-amplitude stress-range spectrum.

Bin (ksi)	Avg. of Bin (ksi)	Summary of 24 Hour Monitoring at Column 07 (September 27 th , 1999)			
		C07_BFLS	C07_BFAS	C07_TFLS	C07_TFAS
		Total Number of Cycles in Each Bin			
0.5-1.0	0.75	617	193	2895	2505
1.0-1.5	1.25	5	252	2	526
1.5-2.0	1.75	1	1	0	0
2.0-2.5	2.25	0	28	328	0
2.5-3.0	2.75	3	376	83	0
3.0-3.5	3.25	406	5	1	419
3.5-4.0	3.75	5	0	0	0
4.0-4.5	4.25	1	1	0	0
Total # Cycles		1038	856	3309	3450
S_{reff}		2.4	2.2	1.3	1.7
S_{max}		4.5	4.5	3.5	3.5

Table 5.2 – Summary of Stress-Range Histograms for all Channels Collected at Column 07 During the 24 Hour Uncontrolled Monitoring

5.2 Results of 24 Hour Monitoring at Column DLT-10

Only gages installed on the top flange at column DLT-10 were monitored for a period of 24 hours beginning at 12:00AM on October 18, 1999. Both triggered time histories and stress-range histograms were collected during the period.

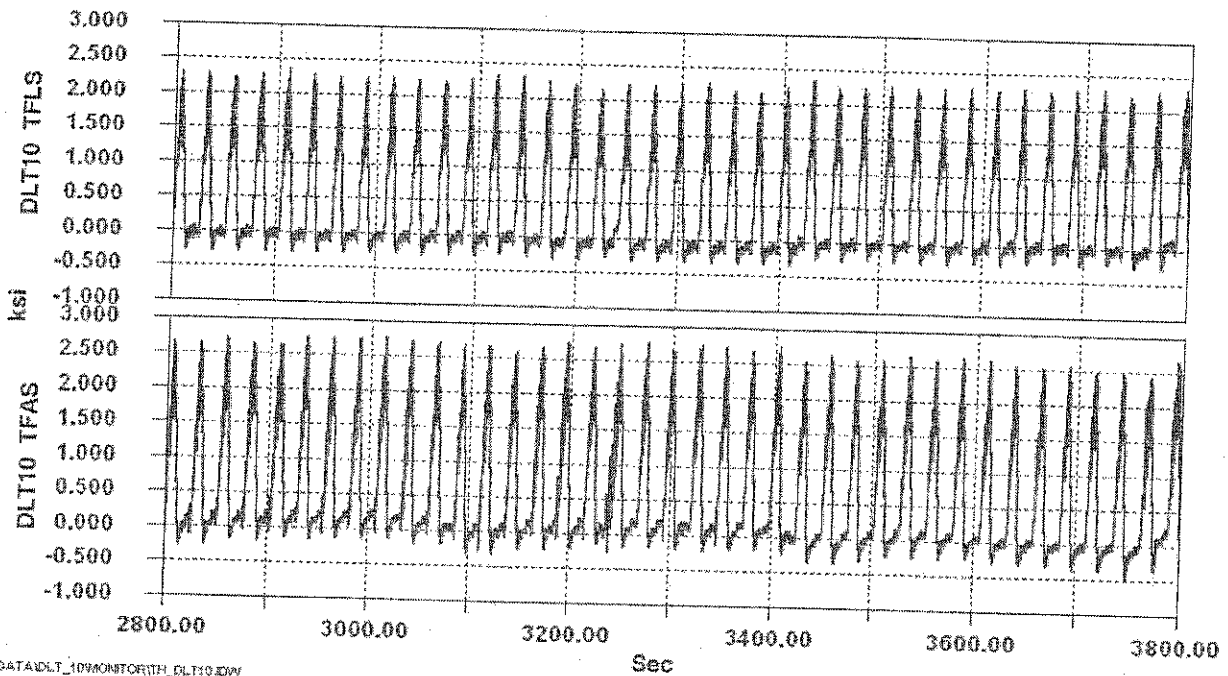


Figure 5.2 – Portion of Triggered Time History Collected at Column DLT-10 During the 24 Hour Uncontrolled Monitoring Period

Figure 5.2 is a small portion of the triggered time history data for channels DLT10_TFLS and DLT10_TFAS, installed on the top flange of column DLT-10. The data are typical for the entire 24 hours and there was little variation in stress range or peak stress values. The data are also consistent with the controlled load tests.

Stress-range histograms, the effective stress range (S_{reff}) and the maximum stress range (S_{rmax}) measured during the 24 hour period are presented in Table 5.3. Cycles less than 0.5ksi were ignored in the effective stress range. The large number of cycles between 0.5ksi and 1.5ksi are attributed to the individual wheels of the train.

Bin (ksi)	Avg. of Bin (ksi)	Summary of 24 Hour Monitoring at Column DLT-10 (October 18 th , 1999)			
		DLT10_BFLS	DLT10_BFAS	DLT10_TFLS	DLT10_TFAS
Total Number of Cycles in Each Bin					
0.5-1.0	0.75	Not Monitored	Not Monitored	2546	2408 ¹
1.0-1.5	1.25			461	161 ¹
1.5-2.0	1.75			0	0
2.0-2.5	2.25			67	0
2.5-3.0	2.75			303	191
3.0-3.5	3.25			0	174
3.5-4.0	3.75			0	3
Total # Cycles				-	-
S_{reff}		-	-	1.4	1.6
S_{rmax}		-	-	3.0	4.0

Notes:

1. Data Adjusted to Remove Random "Noise" Spikes

Table 5.3 – Summary of Stress-Range Histograms for all Channels Collected at Column DLT-10 During the 24 Hour Uncontrolled Monitoring

About 370 trains passed over column DLT-10 during the 24 hour monitoring period. The triggered time histories revealed that no trains passed over column DLT-10 between 12:00AM and 4:50AM on Monday monitoring. Maintenance records indicate that this girder was "locked out" during the early morning hours of the monitoring. Data was obtained simultaneously at column DLT-10 land side and column 12 air side. It is interesting to note that the data acquired at column 12 indicate 34 more trains crossed column 12 than column DLT-10. Thus, only 17 trains were "missed" (34train/2sides=17 trains per side) due to the lockout.

Occasional random noise spikes were observed in the histogram and recorded in the triggered time histories for channel DLT10_TFAS. The source of this noise is unknown. However, it is speculated that the noise was produced by an outside electrical source since an FFT of the data revealed a frequency of 60Hz. The artificial noise cycles were removed from the test data.

5.3 Results of 24 Hour Monitoring at Column 12

Both gages installed on the top flange at column 12 were monitored for a period of 24 hours beginning at 12:00AM on October 18, 1999. Triggered time histories and stress-range histograms were collected during the period. Although not shown, the triggered time histories were consistent with the controlled load tests and little variation in peak stress range was observed.

Stress-range histograms for Column 12 are summarized in Table 5.4 for the 24 hour monitoring period. Also listed in Table 5.4 are the effective stress range (S_{reff}) and the maximum stress range (S_{rmax}).

Bin (ksi)	Avg. of Bin (ksi)	Summary of 24 Hour Monitoring at Column 12 (October 18 th , 1999)			
		C12_BFLS	C12_BFAS	C12_TFLS	C12_TFAS
Total Number of Cycles in Each Bin					
0.5-1.0	0.75	Not Monitored	Not Monitored	103 ¹	2387
1.0-1.5	1.25			2723 ¹	7
1.5-2.0	1.75			0 ¹	0
2.0-2.5	2.25			0 ¹	0
2.5-3.0	2.75			120	5
3.0-3.5	3.25			206	353
3.5-4.0	3.75			92	31
Total # Cycles		-	-	3244	2783
S_{reff}		-	-	1.9	1.8
S_{rmax}		-	-	4.0	4.0

Notes:

1. Data Adjusted to Remove Random "Noise" Spikes

Table 5.4 – Summary of Stress-Range Histograms for all Channels Collected at Column DLT-10 During the 24 Hour Uncontrolled Monitoring

Several noise spikes were observed in the histogram and recorded in the triggered time histories collected at column 12 for channel C12_TFLS. These artificial cycles were removed from the test data.

5.4 Results of 24 Hour Monitoring at Column 16

All four gages installed at column 16 were monitored for a period of 24 hours beginning at 5:55AM 9/6/99 to 6:05AM 9/7/99. Triggered time histories and stress-range histograms were collected. Stress-range histograms for Column 16 are summarized in Table 5.5 along with the effective stress range (S_{ref}) and the maximum stress range (S_{rmax}) measured during the 24 hour period. Figure 5.3 is a typical portion of the triggered time history data for the gages installed at column 16. The data were consistent with the controlled load tests and little variation in stress range or peak stress was observed.

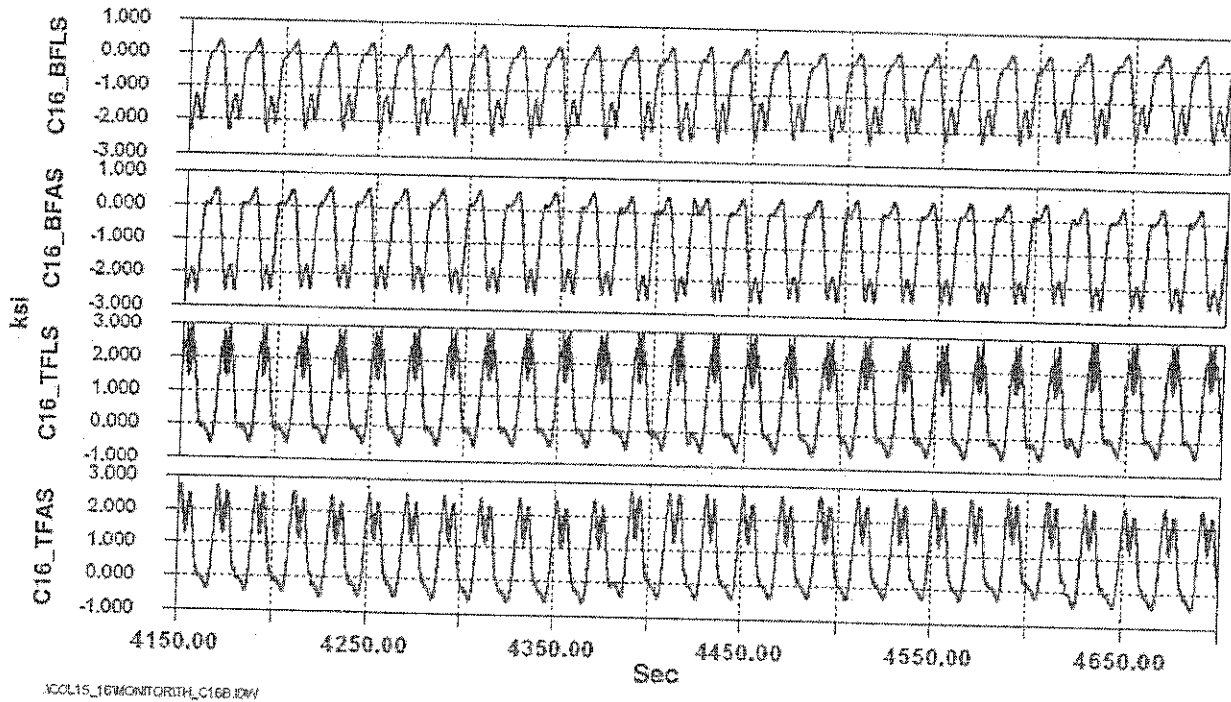


Figure 5.3 – Portion of Triggered Time History Collected at Column 16 During the 24 Hour Uncontrolled Monitoring Period

An estimated 380 trains passed over column 16 during the monitoring period. As before, the large number of cycles between 0.5ksi and 1.0ksi for the gages mounted on the top flange are produced by the individual wheels of the train.

Bin (ksi)	Avg. of Bin (ksi)	Summary of 24 Hour Monitoring at Column 16 (5:55AM 9/6/99 to 6:05AM 9/7/99)			
		C16_BFLS	C16_BFAS	C16_TFLS	C16_TFAS
		Total Number of Cycles in Each Bin			
0.5-1.0	0.75	676	661	897	2970
1.0-1.5	1.25	61	36	2115	388
1.5-2.0	1.75	1	1	133	0
2.0-2.5	2.25	17	1	0	2
2.5-3.0	2.75	356	21	0	57
3.0-3.5	3.25	8	326	117	308
3.5-4.0	3.75	0	21	266	9
4.0-4.5	4.25	0	0	1	0
4.5-5.0	4.75	0	0	0	0
Total # Cycles		1119	1067	3529	3734
S_{reff}		2.0	2.3	1.9	1.6
S_{rmax}		3.5	4.0	4.5	4.0

Table 5.5 – Summary of Stress-Range Histograms for all Channels at Column 16 During the 24 Hour Uncontrolled Monitoring

5.5 Results of 24 Hour Monitoring at Column 26

Gages installed on the edges of the top and bottom flanges at column 26 were monitored for a period of 1 week beginning at 12:00AM 9/27/99 to 10:20AM 10/3/99. Triggered time histories and stress-range histograms were collected during the period. Stress-range histograms for Column 26 are summarized in Table 5.6 with the effective stress range (S_{reff}) and the maximum stress range (S_{rmax}).

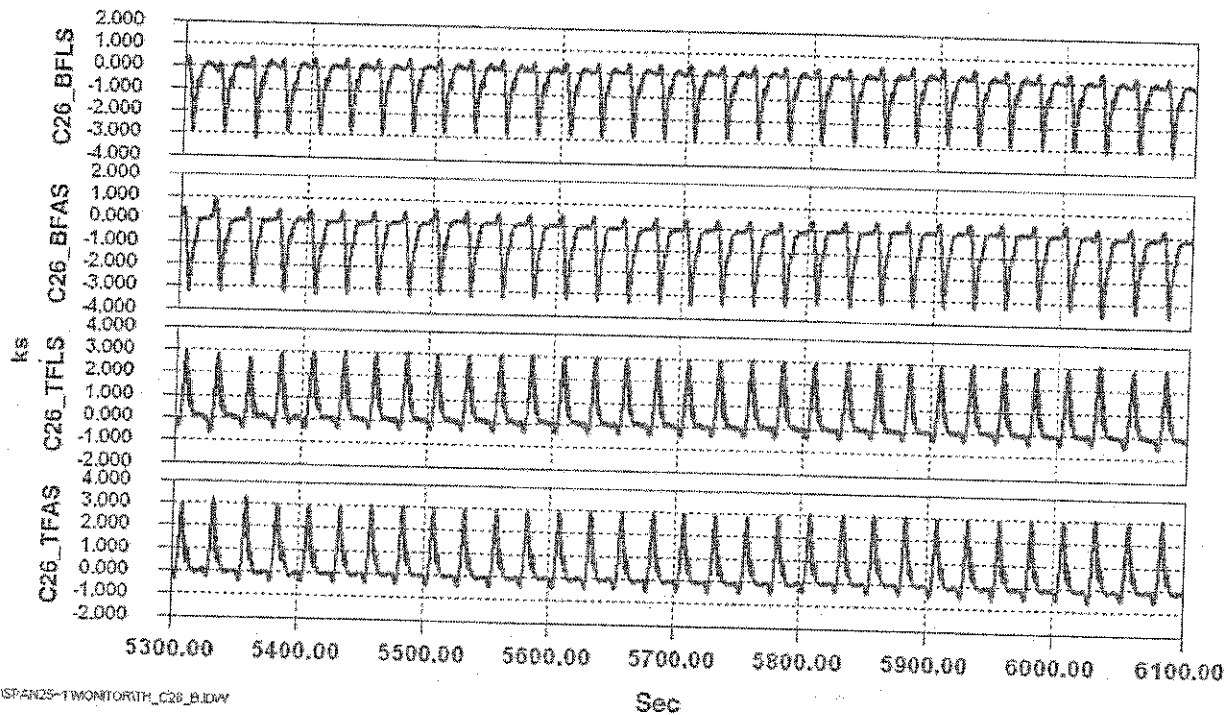


Figure 5.4 – Portion of Triggered Time History Collected at Column 26 During the 24 Hour Uncontrolled Monitoring Period

Figure 5.4 is a typical portion of the triggered time history data for all four channels installed at column 26. The data were consistent with the controlled load tests and little variation in stress range or peak stress was observed.

Occasional short bursts of EMF "noise" were observed in the histogram and triggered time histories for channel C26_BFAS. An FFT of the triggered time histories revealed a frequency of 60Hz. Unfortunately, the artificial cycles could not be easily removed since they randomly affected all stress-range bins. Therefore, to provide meaningful histogram data, it was decided to select 24 hours of "clean" data for channel C26_BFAS. The interval selected was from 3:40PM on Wednesday, September 29th to 3:40PM on Thursday, September 30th, 1999. These data were compared to "clean" histogram data for other parts of the week and found to be in very good agreement. Thus, the histogram data presented for channel C26_BFAS accurately represents a typical 24 hour period for any weekday. To obtain a reasonable and conservative estimate of the number of cycles for one week, the number of cycles counted in 24 hours can simply be multiplied by seven.

Roughly 2,400 trains passed over column 26 during the week-long monitoring period (about 375 every 24 hours). This is reasonably consistent with the other 24 hour measurements. The number of cycles produced by the individual wheels between 0.5ksi and 1.5ksi is also consistent for the gages mounted on the top flange as compared to the bottom flange gages. Overall, the trends observed in the stress-range histograms collected at column 26 are consistent and similar to other locations.

Bin (ksi)	Avg. of Bin (ksi)	Summary of 1 Week Monitoring at Column 26 (12:00AM 9/27/99 to 10:20AM 10/3/99) ²			
		C26_BFLS	C26_BFAS ¹	C26_TFLS	C26_TFAS
Total Number of Cycles in Each Bin					
0.5-1.0	0.75	1693	293	11908	18959
1.0-1.5	1.25	29	2	10327	50
1.5-2.0	1.75	14	0	12	16
2.0-2.5	2.25	11	1	9	6
2.5-3.0	2.75	12	0	29	32
3.0-3.5	3.25	1730	1	570	653
3.5-4.0	3.75	666	286	1744	1672
4.0-4.5	4.25	16	128	70	64
4.5-5.0	4.75	0	2	1	9
5.0-5.5	5.25	0	0	2	5
5.5-6.0	5.75	0	0	0	1
6.0-6.5	6.25	0	0	0	1
Total # Cycles		4171 ²	713 ^{1,2}	24672 ²	21468 ²
S _{reff}		2.9	3.3 ¹	1.8	1.8
S _{rmax}		6.0	5.0 ¹	6.0	6.5

Notes:

1. Due to noise in channel C26_BFAS, only 24hrs of data is presented. The data are from 3:40PM Wednesday, September 30th to 3:40 PM Thursday, Sep. 30th, 1999.
2. The total period monitored was 154.33 hours. The equivalent number of cycles per day can be obtained by multiplying the total number of cycles listed by 0.155 (24hr/154.33hr).

Table 5.6 – Summary of Stress-Range Histograms for all Channels at Column 26 During the Week Long Uncontrolled Monitoring

5.6 Results of Week-Long Monitoring at Span 148 Mid-Span

Gages installed on the edges of the top and bottom flanges at the mid-span of Span 148 were monitored for a period of one week, beginning at 12:00AM 9/27/99 until 10:20AM 10/3/99. Triggered time histories and stress-range histograms were collected during the period. Stress-range histograms, the effective stress range (S_{eff}) and the maximum stress range (S_{max}) are summarized in Table 5.7. Figure 5.5 is a typical portion of the triggered time history data for all four channels installed at span 148. The data were consistent with the controlled load tests and little variation in stress range or peak stress was observed.

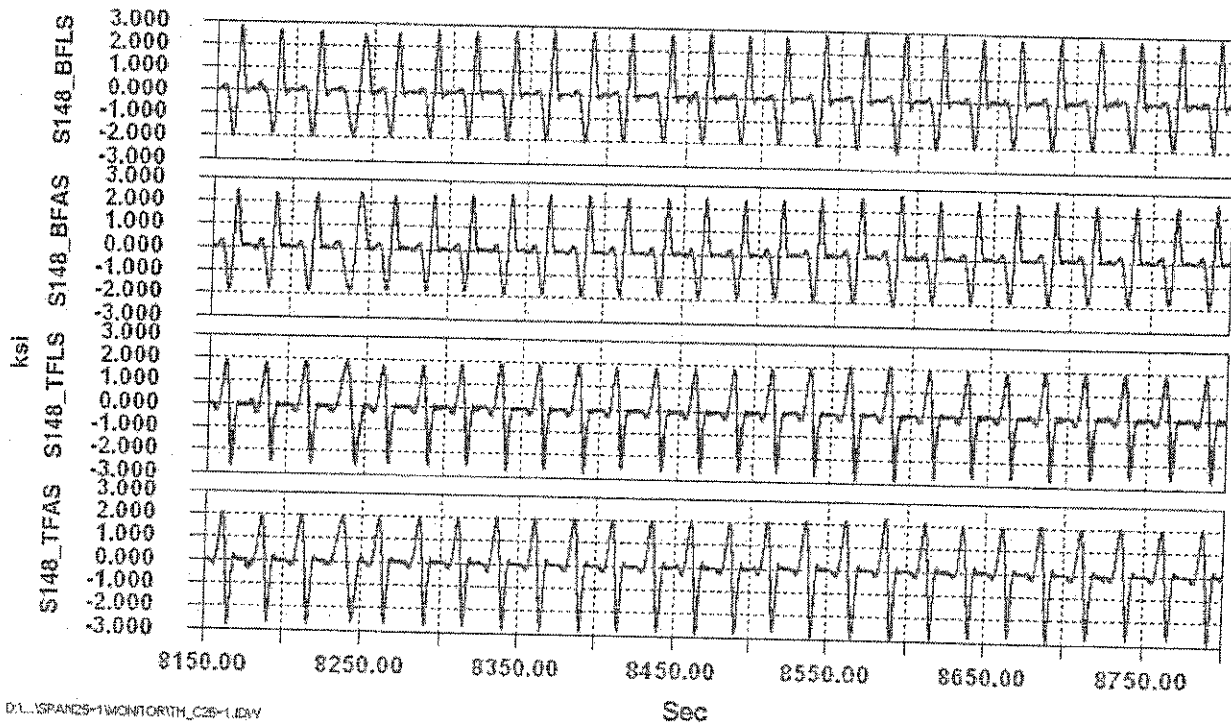


Figure 5.5 – Portion of Triggered Time History Collected at Span 148 During the 24 Hour Uncontrolled Monitoring Period

Random short bursts of EMF “noise” were observed in the histogram and triggered time histories for all channels after 3:00PM on Wednesday, September 29th. An FFT of the triggered time histories revealed a frequency of 60Hz. The artificial cycles were easily removed from all channels except S148_BFLS. To provide meaningful histogram data, it was decided to only use the “clean” histogram data from 12:00AM September 27th 1999 to 3:00PM September 29th 1999. The data were compared to “clean” histogram data for other parts of the week and found to be in very good agreement. All cycles in the 0.5 to 1.0ksi stress-range bin were ignored for channel S148_TFLS since it was determined that most of these cycles were produced by the random 60Hz noise signal. Removing these cycles has little effect on the calculated effective stress range, as will be discussed later.

The stress-range histograms from Span 148 suggest that about 2,300 trains crossed during the monitoring period or about 360 trains every 24 hours. Note the inconsistency in the estimated number of trains which passed over column 26 (≈ 2400) compared to the estimated number which crossed span 148 (≈ 2300). Some cycles in the histograms counted as trains were actually cycles from separate events. (This is explained more fully in Section 7.) Nevertheless, the estimated number of trains are within about 5% of each other and are also consistent with the data from the 24 hour monitoring at other locations. The individual wheels produced cycles between 0.5ksi and 1.5ksi in the top flange, which is also consistent with the other locations and the controlled test data.

Bin (ksi)	Avg. of Bin (ksi)	Summary of 1 Week Monitoring at Span 148 (12:00AM 9/27/99 to 10:20AM 10/3/99) ³			
		S148_BFLS	S148_BFAS	S148_TFLS	S148_TFAS
Total Number of Cycles in Each Bin					
0.5-1.0	0.75	1851	1508	Cycles Removed Due to Noise ²	12179
1.0-1.5	1.25	61	67	16738	141
1.5-2.0	1.75	24	41	336	37
2.0-2.5	2.25	30	111	57	48
2.5-3.0	2.75	4	11	38	52
3.0-3.5	3.25	6	7	12	20
3.5-4.0	3.75	0	436	150	3
4.0-4.5	4.25	79	1708	1642	91
4.5-5.0	4.75	788	80	476	1892
5.0-5.5	5.25	69	3	19	288
5.5-6.0	5.75	10	1	1	10
Total # Cycles		2922 ^{1,4}	3973 ⁴	19469 ²	14761 ⁵
S_{ref}		3.3	3.5	2.3	2.6
S_{rmax}		6.0	6.0	6.0	6.0

Notes:

1. Due to noise in channel S148_BFLS all histogram data collected after 3PM on Wednesday, September 29th was ignored. Thus, the histogram data for this channel is from 12:00AM 9/27/99 to 3:00PM 9/29/99.
2. A review of the data in the 0.5 to 1.0ksi stress-range bin indicated that almost all of these cycles were produced by an occasional 60Hz noise signal and were subsequently deleted.
3. The total period monitored was 154.33 hours. The equivalent number of cycles per day can be obtained by multiplying the total number of cycles listed by 0.155 (24hr/154.33hr).

Table 5.7 – Summary of Stress-Range Histograms for all Channels Collected at Span 148 During the Week-Long Uncontrolled Monitoring

6.0 Variability in Measurements and Development of Stress-Range Histograms

6.1 Variability in Strain Gage Measurements

Prior to discussing the interpretation of the measurements, a few comments regarding variability and strain gage measurements are appropriate.

Some variability in test data, especially that collected during field testing, is expected and not uncommon. In fact, it is not unreasonable to observe variability as high as 20% or greater during field testing. Factors contributing to these deviations include variations in vehicle position as well as variations in fabrication and material tolerances. On the monorail, the transverse position of the test vehicle is restricted and is not an issue.

In light of the above, caution and judgment must be exercised when using strain gage data to establish if a specific parameter, for example vehicle speed, has an influence on the measured stresses. A quantitative comparison of individual channels is not necessarily appropriate. It is more reasonable to establish if, on the whole or average, measured stress ranges are different than at other locations *and* if these difference can be attributed to that parameter.

The magnitude of the measured stresses must also be considered. This is best illustrated in the following example. Assume that for a certain gage, measured stress ranges were 0.5ksi for a crawl test. However, for the same location during a dynamic test, measured stress ranges were 0.75ksi. This apparent increase in stress range of 50% is not of great concern because the magnitude of both measurements is insignificant with respect to the fatigue life of even the worst details. In addition, the accuracy of very small measurements is questionable due to the resolution of the system.

6.2 Development of the Stress-Range Histograms

The stress-range histogram data collected during the uncontrolled monitoring yields a random variable-amplitude stress-range spectrum for each gage. A convenient way to use the measured spectrum in a fatigue evaluation is to determine the effective-stress range. Traditionally, fatigue designs and evaluations compare calculated (or measured) stress ranges to the constant amplitude fatigue exponential relationship for the applicable detail. It has been shown that a variable-amplitude stress-range spectrum can be represented by an equivalent constant-amplitude stress range equal to the cube root of the mean cube (r_{mc}) of all stress ranges (Miner's rule: $S_{\text{eff}} = [\sum \alpha_i S_i^3]^{1/3}$) [1, 2].

Several methods can be used to convert a random-amplitude stress-range response into a stress-range histogram. For the monorail field data, stress-range histograms were developed using the rainflow cycle counting method [3]. The rainflow cycle counting method is well accepted and widely used in many civil engineering applications. The rainflow analysis algorithm was programmed to ignore any stress range less than 0.2ksi (7με). In addition, stress-range measurements less than this are questionable, since it is difficult to distinguish between real data and background "noise".

The effective stress ranges presented in Section 5 were calculated by ignoring all stress-range cycles less than 0.5ksi. Previous research has shown that small stress ranges ($< 1/4$ the constant-amplitude fatigue limit (CAFL)) have little effect on the cumulative damage at the detail [4, 5]. It has also been demonstrated that as the number of random variable cycles of lower stress range levels are considered, the predicted cumulative damage provided by the calculated effective stress range becomes asymptotic to the applicable S-N curve. For most components of typical highway or railroad bridges, a cut-off such as this is appropriate and necessary.

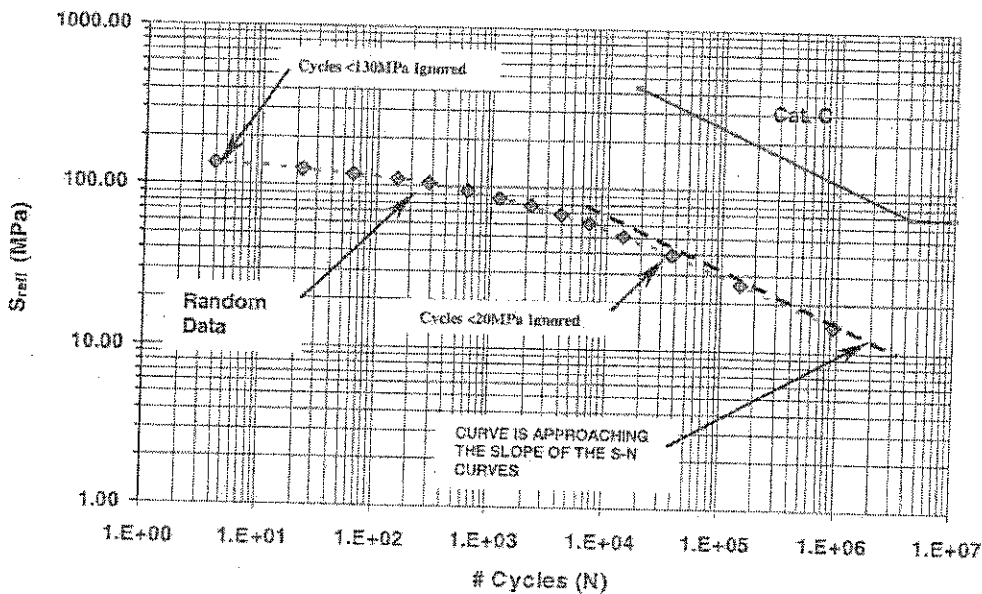


Figure 6.1 – Effect of Truncating Cycles at Different Stress Range Cut-Off Levels (Data is Taken from a Long-Term Monitoring Program Conducted on a Highway Bridge Recently Completed by Lehigh University)

Figure 6.1 shows the effect of calculating the effective stress range for several levels of truncation using field test data. These data were collected during a long-term monitoring program of a highway bridge, recently completed by Lehigh University [5]. The data were collected over a period of two months. Although the units of stress are MPa, and not ksi, the point is the same.

As the truncation level decreases, the effective stress range and corresponding number of cycles plotted approaches the slope of the S-N curves (a slope of -3 on a log-log plot). The AASHTO Category C fatigue resistance curve is plotted in Figure 6.1 for comparison. As long as the cut-off level selected is consistent with the slope of the fatigue resistance curve, including additional stress cycles at lower truncation levels does not improve the damage assessment.

The maximum stress ranges reported for the uncontrolled monitoring in Section 5 were determined from the rainflow count. According to the rainflow cycle counting procedure, the peak and valley which comprise the maximum stress range may not be the

result of a single loading event and, depending on the computer algorithm used, may occur a considerable amount of time apart. In other words, an individual train did not necessarily generate the maximum stress range shown in the tables. In the guideway structure, the stress range-range spectrum is not as variable as is observed in typical highway bridges. As a result, in several cases it was possible to identify the maximum stress range with a specific vehicle passage in the triggered time histories. However, there were cases for which the maximum rainflow stress range slightly exceeded the maximum stress range from any individual vehicle. This could be the result of a multiple presence effect or stress reversals produced by a train on the other box girder. It is worth noting that the interval was set at ten minutes for the guideway monitoring which minimized the possibility of combining peaks and valleys from unrelated loading events.

7.0 Summary of Field Measurements Made on the Guideway

Field testing of selected portions of the Newark Airport Monorail structure have been completed. The testing program included controlled-load crawl and dynamic tests and uncontrolled monitoring. The data collected included time histories and stress-range histograms. Several key observations are summarized below:

1. General Behavior of the Guideway - Overall, the global behavior of the structure is as expected and no unusual behavior was observed during the controlled tests or uncontrolled monitoring. The field measurements should be used to calibrate analysis models as required.
2. Effect of Vehicle Speed - Tests were conducted at crawl and normal operating speed at all locations. Comparison of the crawl and dynamic test data revealed dynamic effects are not significant. In fact, at some locations there was no difference in the minimum stress, maximum stress, and stress range. However, at locations where the guideway was curved, local bending stresses in the top flange were influenced by the speed of the vehicle. As the train travels around a curve, an overturning moment due to centrifugal forces is developed. This results in both increases and decreases in the vertical load applied by the wheels located on the outside and inside of the curve, respectively.
3. Effect of Travel Direction - The measurements did not reveal any change in behavior with change in travel direction.
4. Effect of Vehicle Weight - Controlled tests were not conducted using the AW-1 or AW-2 loading. However random trains were monitored and the number of passengers estimated. It was found that the empty test train and random trains produced comparable stress ranges.
5. Local Bending in the Top Flange Due to Wheel Loads - It was shown that the individual wheels of the train apply concentrated loads to the top flange through the running plate/support bar assembly. Local bending of the top flange was observed at every location where instrumentation was installed. Figure 4.2 described and illustrated this effect as the wheel passes over the top flange.

6. Top Flange Stress-Range Histograms - The effective stress range (S_{reff}) and maximum stress ranges (S_{rmax}) obtained from the histograms are summarized in Table 7.1. Also shown in the table are the cycles per day and the equivalent number of cycles per year. The columns titled S_{reff} , S_{rmax} , and Number of Cycles per Day (N) are taken directly from the summary stress-range histogram tables for all locations except span 148 and column 26. For these locations, the total number of cycles listed in the tables are for 6.43 days (154.33hrs) and must be multiplied by 24hr/154.33hr to obtain the cycles per day shown in Table 7.1. Assuming 365 days per year, the number of cycles produced per year was estimated and is also listed in Table 7.1. With the exception of gages installed at midspan of span 148, all of the histogram data were reasonably consistent.

Location	S_{reff} (ksi)	S_{rmax} (ksi)	Number of Cycles per Day (N)	Equivalent Cycles per Year
C07_TFLS	1.3	3.5	3,309	1,207,785
C07_TFAS	1.7	3.5	3,450	1,259,250
DLT10_TFLS	1.4	3.0	3,337	1,218,005
DLT10_TFAS	1.6	4.0	2,937	1,072,005
C12_TFLS	1.9	4.0	3,244	1,184,060
C12_TFAS	1.8	4.0	2,783	1,015,795
C16_TFLS	1.9	4.5	3,529	1,288,085
C16_TFAS	1.6	4.0	3,734	1,362,910
S148_TFLS	2.3	6.0	3,028	1,015,169
S148_TFAS	2.6	6.0	2,296	769,681
C26_TFLS	1.8	6.0	3,837	1,286,469
C26_TFAS	1.8	6.5	3,339	1,119,403

Table 7.1 – Summary of Stress-Range Histogram Data and Fatigue Life Estimates for Top Flange at Strain Gages

Note, the histogram data presented in Table 7.1 are only applicable to the instrumented locations. The stress range at fatigue sensitive details, like a support bar splice, will be different away from the instrumentation. It should also be noted that the stress range at the support bar is most likely larger than on the edge of the flange where the gages were installed. Thus, engineering judgment must be used when using the field data for a fatigue evaluation.

In locations where the maximum stress range (S_{rmax}) exceeds the CAFL of the detail, a finite-life approach should be used to estimate the fatigue life. In this case, the fatigue life may be estimated by using the effective stress range (S_{reff}), the number of cycles per year (or day) and the appropriate S-N curve established by the laboratory test program. Again, note that the data in Table 7.1 are only valid at the location of the gages. Using a calibrated analysis, the stress ranges at other locations can be calculated and similar fatigue evaluations made.

References:

1. Moses, F., Schilling, C.G., Raju, K.S., *Fatigue Evaluation Procedures for Steel Bridges*, NCHRP Report 299, National Cooperative Highway Research Program, 1987 American Association of State Highway and Transportation Officials.
2. Miner, M.A., *Cumulative Damage in Fatigue*, Journal of Applied Mechanics, Vol. 1, No.1, Sept., 1945.
3. Downing S.D., Socie D.F., *Simple Rainflow Counting Algorithms*, International Journal of Fatigue, January 1982.
4. Fisher, J.W., Nussbaumer, A., Keating, P.B., and Yen, B.T., *Resistance of Welded Details Under Variable Amplitude Long-Life Fatigue Loading*, NCHRP Report 354, National Cooperative Highway Research Program, 1993.
5. Connor, R.J., Fisher, J.W., *Results of Field Measurements on the Williamsburg Bridge Orthotropic Deck – Final Report on Phase III*, ATLSS Report No. 00-___, Department of Civil and Environmental Engineering, Lehigh University, Bethlehem PA, 2000. (*In progress at time of this writing*)

Acknowledgments

This work was sponsored by ADTranz NA. The authors greatly appreciate the constructive comments and suggestions of engineers from Modjeski & Masters, HDR, and the Port Authority during the preparation of this report. Mr. Robert Shusko (*Formerly with ADTranz*) provided invaluable assistance during the field testing program.

The authors also wish to recognize Lehigh University ATLSS Technical Staff, Mr. Russ Longenback, Mr. Ed Tomlinson, Mr. Dan Zeroka, and Mr. Walter "Wally" Clouse whose efforts and support during the field testing activities made this work possible.